The clinical relevance of structural changes of the optic nerve head and retinal nerve fibre layer in glaucomatous optic neuropathy

Thesis submitted for the degree of

MD (Res) at University College London

Andrew John Tatham, MBChB FRCOphth FRCSEd FEBO

Supervisors:

Professor David Garway-Heath

Professor Roger Anderson

Institutions:

Hamilton Glaucoma Centre, University of California, San Diego, USA

Institute of Ophthalmology, University College London, UK (Non-resident)

Word Count: 35,603

1 SECTION I: OVERVIEW

1.1. Declaration

I, Andrew John Tatham confirm that the work presented in this thesis is my own. Where information has been derived from other sources, I confirm that this has been indicated in the thesis.

Andrew John Tatham 18/03/2018

1.2. Abstract

Background: Imaging is widely used to quantify glaucomatous structural changes. Although previous studies have examined the relationship between structure and function, measured using standard automated perimetry (SAP), the true relevance of structural changes remains poorly understood.

Aim: The aim of this body of work was to explore the structure-function relationship and to ascertain the point at which structural changes become associated with impaired ability to perform vision-dependent tasks.

Plan of research: After critically appraising previously described structure-function models, an investigation was conducted progressively evaluating the relationship between glaucomatous structural changes and 1) estimated loss of retinal ganglion cells (RGCs), 2) an objective measure of visual function (the pupil response), and 3) a vision-related task relevant to quality of life (driving).

Results: Localised RNFL defects visible on photographs, a common manifestation of glaucoma, were associated with large estimated RGC losses. However, problems were identified with the published method of RGC estimation. Asymmetric RNFL thinning was also found to be associated with asymmetry of the pupil response, and the magnitude of asymmetry required for a clinically detectable relative afferent pupillary defect (RAPD) was calculated. Finally, loss of RNFL was associated with worse ability to perform a simulated driving task, providing additional information to SAP alone.

Significance: Glaucomatous structural defects may be associated with significant functional impairment. Incorporating information from both structure

and function may improve our ability to predict patients at risk of developing problems with vision-related tasks of daily living.

1.3. Table of contents

1.4. List of Figures

1.5. List of Tables

1.6. List of Abbreviations

ADAGES	African Descent and Glaucoma Evaluation Study
ARVO	Association for Research in Vision and Ophthalmology
AUC	Area under receiver operating characteristic curve
BMO-MRW	Bruch's membrane opening - minimum rim width
CCT	Central corneal thickness
CDR	Cup to disc ratio
cpRNFL	Circumpapillary retinal nerve fibre layer
CSFI	Combined structure function index
CSLO	Confocal Scanning Laser Ophthalmoscope
DIGS	Diagnostic Innovations in Glaucoma Study
DLS	Differential Light Sensitivity
DRI-OCT	Deep range imaging Optical Coherence Tomography
EDI	Enhanced Depth Imaging
EMGT	Early Manifest Glaucoma Trial
FDF	Flicker Defined Form
FDT	Frequency Doubling Technology

GCC	Ganglion cell complex
GON	Glaucomatous optic neuropathy
HEP	Heidelberg Edge Perimeter
HGC	Hamilton Glaucoma Centre
HRT	Heidelberg Retina Tomography
IOP	Intraocular Pressure
LC	Lamina Cribrosa
mGCC	Macular ganglion cell complex
mGCIPL	Macular ganglion cell-inner plexiform layer
OCT	Optical coherence tomography
OHTS	Ocular Hypertension Treatment Study
ONH	Optic nerve head
MD	Mean deviation
NICE	National Institute of Health and Clinical Excellence
POAG	Primary open angle glaucoma
PSD	Pattern standard deviation
RAPD	Relative Afferent Pupillary Defect
RGC	Retinal ganglion cell

RNFL	Retinal Nerve Fibre Layer
ROC	Receiver operating characteristic
SAP	Standard automated perimetry
SDOCT	Spectral domain optical coherence tomography
SLP	Scanning laser polarimetry
SSOCT	Swept Source optical coherence tomography
SWAP	Short Wave Automated Perimetry
TDOCT	Time domain optical coherence tomography
VFI	Visual field index
VPL	Visual Performance Laboratory
UCL	University College London
UCSD	University of California San Diego

1.7. Supporting Publications

1. Tatham AJ, Weinreb RN, Zangwill LM, Liebmann JM, Girkin CA, Medeiros FA. Estimated retinal ganglion cell counts in glaucomatous eyes with localized retinal nerve fibre layer defects. Am J Ophthalmol. 2013 Sep;156(3):578-87.

2. Tatham AJ, Meira-Freitas D, Weinreb RN, Marvasti AH, Zangwill LM, Medeiros FA. Estimation of retinal ganglion cell loss in glaucomatous eyes with a relative afferent pupillary defect. Invest Ophthalmol Vis Sci. 2014 Jan 29;55(1):513-22.

3. Tatham AJ, Boer ER, Rosen PN, Della Penna M, Meira-Freitas D, Weinreb RN, Zangwill LM, Medeiros FA. Glaucomatous retinal nerve fibre layer thickness loss is associated with slower reaction times under a divided attention task. Am J Ophthalmol. 2014 Nov;158(5):1008-17.

4. Medeiros FA, Tatham AJ. Structure versus function in glaucoma: the debate that doesn't need to be. Ophthalmology 2016 Jun;123(6):1170-2.

1.8. Acknowledgements

I wish to thank all the staff at Hamilton Glaucoma Center, UCSD for their encouragement and support during my time in San Diego. Dr Weinreb has established a team of skilled, highly motivated and enthusiastic people, and the infrastructure for a thriving research environment. I was afforded every opportunity to thrive and I am grateful to Dr Weinreb for his mentorship and teaching and for being an inspirational figure in my career development. I am also grateful for his continued support since my return to the United Kingdom.

Special thanks for Dr Felipe Medeiros for his guidance and friendship and for showing me that statistics can be fun. I am grateful for the time him devoted to teaching and for his interest in exploring the patient's perspective of glaucoma, an often-overlooked area of research. I am also appreciative of Dr Linda Zangwill whose kindness and insightful input into my research was irreplaceable. She made each of the glaucoma fellows feel very welcome at UCSD.

I also wish to thank my supervisors at UCL, Professors Garway-Heath and Anderson. I am especially grateful for them agreeing to act as mentors, considering much of my work took place abroad. I first worked with Professor Garway-Heath, albeit too briefly, as a clinical fellow at Moorfields. He has been an inspiration to me in my career so far and his insightful critique of this work has been invaluable.

The work at Hamilton Glaucoma Center would not be possible without the team of highly skilled technicians, including Eunice Williams-Steppe, Tess Acera, Eric Cabezas and Joy McDonald, who were responsible for imaging and

obtaining visual field tests from participants, and conducting driving simulator testing. Also, Keri Dirkes and Suzanne Vega who run the Visual Field Analysis and Imaging Reading Center deserve special thanks for their kindness and for the welcome I received as a foreigner on their shores.

I also wish to thank Dan Auerbach and Manny Acera for their countless assistance and technical support. Dan leads the programmers and built the servers for exporting and maintaining the Hamilton Glaucoma Center research database. Special thanks should also be reserved for Dr Erwin Boer and Dr Peter Rosen for their expertise and assistance with the driving simulator and for Dr Chris Bowd and Dr Akram Belghith for their assistance with computations that required the use of Matlab.

Finally, I wish to acknowledge the team of research fellows I had the pleasure working with during my time in San Diego including Renato Lisboa, Daniel Meira-Freitas, Carolina Gracitelli, Na'amma Hammel and Chunwei Zhang. It was a pleasure to work with such a diverse group of ophthalmologists and scientists from around the world. I am grateful for the chance to be involved with the research work taking place at UCSD and for the guidance and mentorship I have received from friends and colleagues at UCL, without which I would have been unable to complete this body of work.

2 SECTION II: INTRODUCTION

2.1. Glaucoma

Glaucoma is a leading cause of blindness, affecting more than 70 million people worldwide, of whom approximately 10% are blind in both eyes (Quigley, & Broman 2006). Treatment is often effective at slowing progression but as glaucoma does not usually produce symptoms until the later stages, a large proportion of individuals affected remain undiagnosed. Population-based surveys suggest only 10% to 50% of people with glaucoma are aware they are affected and consequently there are many people losing vision without receiving appropriate treatment (Rotchford et al 2003; Hennis et al 2007; Budenz et al 2013).

Histologically, glaucoma is characterized by loss of RGCs with resultant structural changes to the ONH and inner retina. Dysfunction and loss of RGCs is accompanied by loss of visual field, which can be quantified using automated perimetry (Weinreb et al 2014). Although the pathophysiology of glaucoma is not fully understood, elevated IOP, which is related to the balance between aqueous humour secretion by the ciliary body and outflow through the trabecular meshwork and uveoscleral outflow pathway, is the major risk factor. Raised IOP results in mechanical stress and strain to the ONH, which is believed to lead to disruption of axonal transport and interruption of retrograde supply of neurotrophic factors essential for RGC survival (Burgoyne et al 2005).

Detection of glaucoma has relied historically on detection of raised IOP, however IOP is a poor discriminator of health and disease. Substantial numbers of people with elevated IOP do not need treatment and will never develop

glaucoma, while conversely many patients with glaucoma have IOP within the range of that expected for the population (Kass et al 2002; Weinreb et al 2014). The key to glaucoma diagnosis is recognition of the morphological changes to the ONH and RNFL that result from RGC loss. However, it is functional losses that are of greater clinical importance, as loss of visual function is ultimately what matters most to the patient. The relationship between these structural and functional changes has been an important, and somewhat controversial, area of study (Medeiros et al 2016).

2.2. Measuring Structural and Functional Changes

2.2.1. Structural changes

2.2.1.1. Detecting glaucoma

Glaucomatous structural changes are typically detected using slit lamp fundoscopic examination or by observing for changes on stereophotographs, with typical features including narrowing of the neuroretinal rim, increased ONH excavation, increased CDR, and loss of the RNFL (Jonas et al 1999). However due to the wide variation in normal ONH appearance, diagnosis based on a single examination can be challenging. For example, the European Optic Disc Assessment Study showed that although ophthalmologists classify discs moderately well, with an average diagnostic accuracy of 80%, there is wide variation, with some ophthalmologists achieving an accuracy of only 60% (Reus et al 2010). Using the same set of disc photographs, similar findings were reported for UK optometrists, though optometrists had slightly higher sensitivity and lower specificity compared to ophthalmologists (Hadwin et al 2013).

The last 25 years has seen the introduction of ocular imaging devices such OCT (Figure 2-1), CSLO and SLP which enable clinicians to obtain objective quantitative measurement of ocular structure (Huang 1991; Wollstein et al 2000; Wollstein et al 1998; Zangwill et al 2001; Greaney et al 2002; Chang et al 2009; Mwanza et al 2012; Leung et al 2010; Medeiros et al 2008; Medeiros et al 2004; Strouthidis et al 2006). Imaging devices provide high-resolution topographic images of the ONH and RNFL and using sophisticated software can quantify these structures. The devices also contain normative databases so that observed

measurements can be compared to the normal range and eyes classified as normal, borderline or outside normal limits (Realini et al 2014).

Figure 2-1. Typical OCT summary showing RNFL thickness outside normal limits in the right eye and borderline in the left eye.

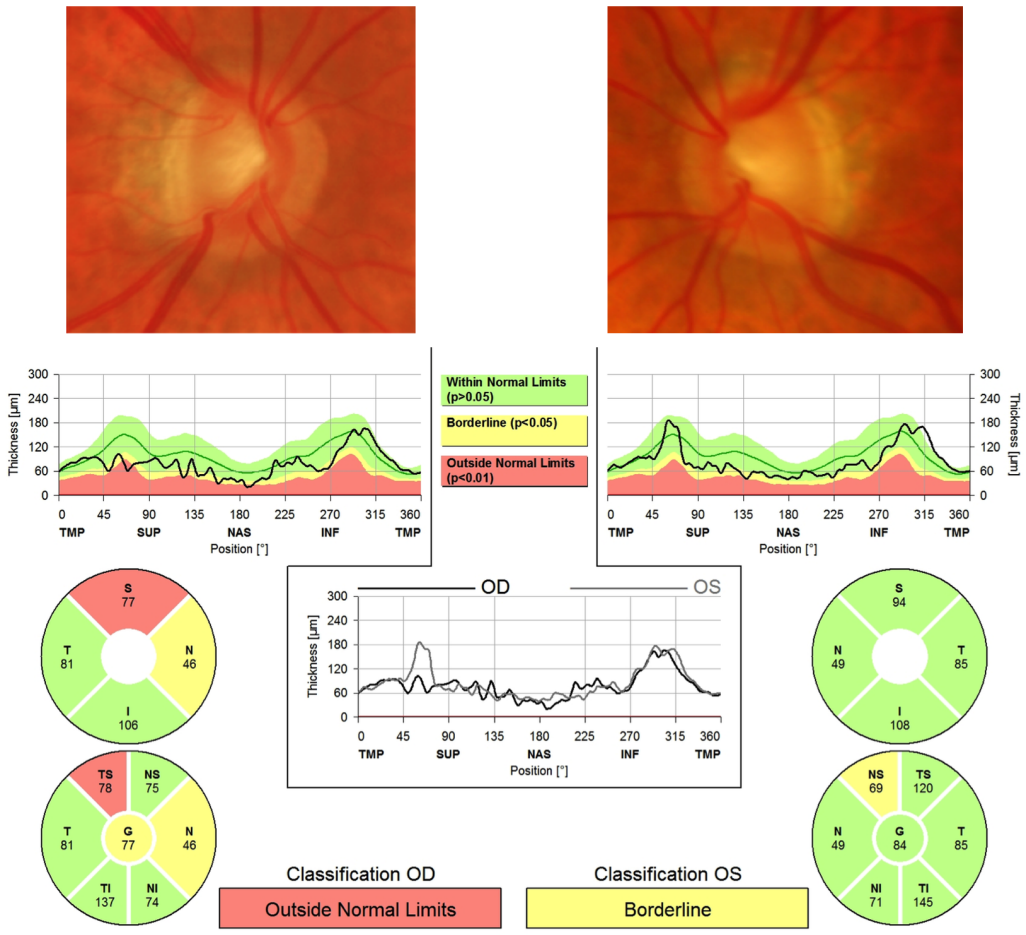

Imaging devices seem to have comparable or better ability to detect glaucoma compared to assessment of optic disc photographs (Reus et al 2010). In the European Optic Disc Assessment Trial, CSLO and GDx-VCC had better diagnostic accuracy than clinicians grading disc photographs, correctly classifying 93.2% and 89.8% of eyes respectively, compared to 80.5% for clinicians (Reus et

al 2010). However, of current imaging devices, OCT offers greatest versatility and it is OCT that has come to the fore in glaucoma imaging.

OCT was first used to image the eye in 1991 but has since evolved considerably (Figure 2-2) (Huang 1991). The original technology of TDOCT has been superseded by SDOCT, which offers enhanced image quality due to improved spatial resolution and averaging of multiple images within each scan, made possible by a faster scan speed. SSOCT, which uses a longer wavelength light source of 1050nm to allow deeper tissue penetration, is another recent development.

Figure 2-2. The first published OCT image of the human eye in 1991 (adapted from Huang, 1991) and a wide field SSOCT image from 2016 obtained using the Topcon DRI-OCT.

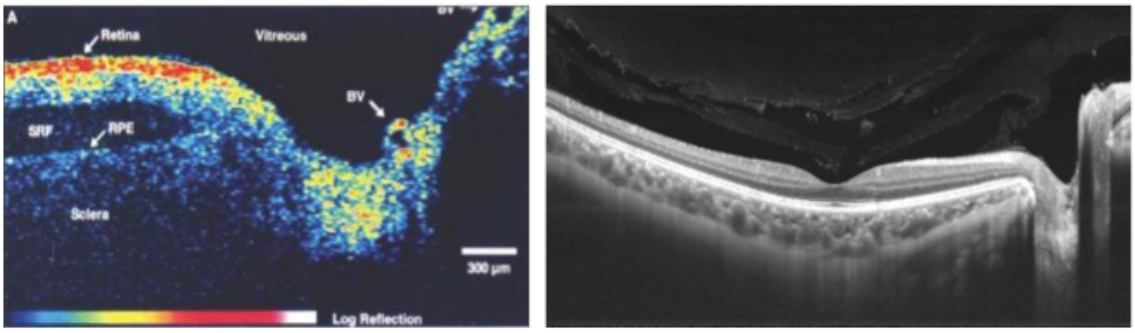

OCT can be used to obtain measurement of cpRNFL thickness, ONH parameters such as BMO-MRW, and macular thickness, with multiple studies demonstrating the ability of these parameters to differentiate glaucomatous and healthy eyes. Studies examining the ability of TDOCT to distinguish glaucomatous and healthy eyes have reported specificities of approximately 90%, with sensitivities of 70 to 80% (Budenz et al 2005; Bengtsson et al 2012; Deleón-

Ortega et al 2006). Using the Cirrus SDOCT (Carl Zeiss Meditec Inc.), Leung and colleagues found cpRNFL measurements to have a sensitivity of 91.6%, for a specificity of 87.6%, and an AUC of 0.962 (Leung et al 2009). Therefore, SDOCT achieves only slightly better sensitivity and specificity than TDOCT but has the advantage of lower measurement variability, which may allow it to better detect glaucoma progression than the older technology (Leung et al 2009; Leung et al 2011; Park et al 2009). Other studies examining the ability of SDOCT measurements to detect glaucoma are summarised in Table 2-1.

While these studies mainly report excellent AUCs, the results must be interpreted with some caution. Direct comparison of studies is somewhat problematic due to different reference standards employed and variable disease severities of included subjects. Many studies included subjects with significant visual field loss, in whom the use of OCT may add little to the diagnostic process. For example, the average MD of glaucomatous subjects in the 2009 study by Leung et al was -10.36 dB (Leung et al 2009). In an eye with a MD of -10.36 dB it is highly likely that the diagnosis of glaucoma could be made without recourse to OCT. A more clinically relevant question may be whether imaging is of value as a supplementary test in cases of diagnostic uncertainty, such as those with suspect glaucoma, or in other words, those with suspicious optic nerve appearance on fundoscopy but normal (or unreliable) visual field.

Table 2-1. Summary of selected studies examining the diagnostic ability of spectral domain optical coherence tomography (SDOCT) in glaucoma.

Study	Number of Eyes	SAP Mean deviation (dB)	SDOCT device	Parameter	AUC
Leung et al 2009	83 Glaucoma 97 Healthy	-10.36 -0.79	Cirrus	cpRNFL	0.962
Leung et al 2010	79 Glaucoma 76 Healthy	-10.36 -0.79	Spectralis	cpRNFL	0.978
Mwanza et al 2011	73 Glaucoma 146 Healthy	-10.4	Cirrus	Rim area cpRNFL	0.96 0.95
Mwanza et al 2012	58 Glaucoma 99 Healthy	-3.2 0.08	Cirrus	Rim area cpRNFL mGCIPL	0.91 0.94 0.94
Sung et al 2012	144 Early Glaucoma 109 Healthy	-2.54 -0.45	Cirrus	Rim area cpRNFL	0.831 0.943
Takayama et al 2012	38 Early Glaucoma 48 Healthy	-2.33 -0.07	Cirrus	cpRNFL mGCIPL Minimum mGCIPL	0.89 0.82 0.90
Lisboa et al 2012	48 Preperimetric Glaucoma 86 Healthy	-0.63 0.09	Spectralis	cpRNFL	0.86
Wu et al 2012	Early Glaucoma 85 Healthy	> -6 -1.25	Spectralis	cpRNFL	0.895
Lisboa et al 2013b	48 Preperimetric Glaucoma 94 Healthy	-0.81 0.02	RTVue	Rim area cpRNFL mGCC	0.72 0.89 0.79
Jeoung et al 2014	164 Early Glaucoma 119 Healthy	-2.68 -0.22	Cirrus	Rim area cpRNFL mGCIPL Minimum mGCIPL	0.86 0.90 0.82 0.90
Begum et al 2014	21 Preperimetric Glaucoma 53 Healthy	-1.9 -2.0	Cirrus	Rim area cpRNFL mGCIPL	0.85 0.79 0.59

Abbreviations: SAP = standard automated perimetry, AUC = area under the receiver operating characteristic curve, cpRNFL = circumpapillary retinal nerve fibre layer, mGCIPL = macular ganglion cell layer and inner plexiform layer thickness, mGCC = macular ganglion cell complex thickness (mGCIPL + mRNFL).

Lisboa and colleagues recently examined the ability of SDOCT and CSLO to different eyes with suspected glaucoma from those with preperimetric changes (Lisboa et al 2012). Preperimetric glaucoma was defined by the presence of progressive glaucomatous changes on optic disc stereophotographs with normal SAP. 134 eyes of 88 subjects suspected of having glaucoma due to optic disc appearance were enrolled at baseline. Over 5 years of follow-up 48 eyes developed preperimetric glaucoma. SDOCT could discriminate eyes with preperimetric glaucoma from those with suspected glaucoma with an AUC of 0.86 for global cpRNFL thickness. Subjects were also tested using CSLO, however the best performing CSLO parameter, global rim area, had an AUC of only 0.72, which was significantly less than the best performing SDOCT parameter of temporal superior cpRNFL thickness with an AUC of 0.88 ($P = 0.008$). Leite and colleagues also demonstrated the effect of disease severity on diagnostic performance of Cirrus SDOCT (Leite et al 2010). For a specificity of 85%, average cpRNFL thickness had an estimated sensitivity of 82% in eyes with early disease (defined using the independent reference of SAP VFI of 90%), compared to a sensitivity of 93% in those with advanced disease (SAP VFI of 70%).

Measurement of cpRNFL though has some limitations. The circumpapillary scan includes non-neural tissue such as blood vessels located within the RNFL and the scan may also pass through areas of parapapillary atrophy. To more accurately detect structural abnormalities, it is important to choose measures that use anatomically accurate landmarks as their reference point. In addition to measuring cpRNFL thickness, SDOCT provides a means to acquire 3D images of the ONH from which parameters such as rim area, cup to disc ratio and cup

volume can be measured; however, these parameters may not perform as well as cpRNFL thickness, especially in early disease (Sung et al 2012; Lisboa et al 2012; Lisboa et al 2013) For example, in a study including 144 eyes with early glaucoma and 109 healthy controls, Sung and colleagues found cpRNFL thickness to perform better than SDOCT ONH parameters (Sung et al 2012), which was similar to the findings of Lisboa and colleagues using CSLO and SDOCT (Lisboa et al 2012; Lisboa et al 2013).

Measurements of the macula may also be useful for detecting glaucoma, with the macula an attractive region for imaging due to its importance for central vision and its relative consistent structure between healthy individuals. Macula measurements may also be less affected by non-neural structures such as blood vessels than the cpRNFL and, therefore, less prone to OCT segmentation software failures. Several recent studies have shown that macular thickness measurements, which include mGCIPL and mGCC thickness have good ability to detect glaucoma (Garas et al 2011; Tan et al 2009; Mwanza et al 2012). mGCIPL includes the ganglion cell layer and inner plexiform layer and mGCC includes these layers plus the macular RNFL. Mwanza and colleagues recently reported mGCIPL measurements to have similar ability to detect glaucoma compared to cpRNFL (Mwanza et al 2012), however, others have found mGCIPL may perform less well than cpRNFL in early disease. Lisboa and colleagues reported AUCs of 0.79 and 0.89 for mGCC and cpRNFL respectively for differentiating eyes with preperimetric glaucoma from those suspected of having the disease (Lisboa et al 2013).

Following clinical observations and histological and SDOCT studies in non-human primates, Chauhan and colleagues recently proposed a novel structural measure for glaucoma, known as the BMO-MRW (Chauhan et al 2013). Traditionally the outer border of the neuroretinal rim is defined by the optic disc margin, however, this is not a sound landmark as measurements from disc margin to inner rim are affected by tissue orientation and the neuroretinal rim may extend inside the disc margin. Furthermore, clinicians differ in their assessment of the location of the optic disc margin and SDOCT cannot be used to aid identification, as the disc margin does not correspond to an anatomical structure visible on SDOCT. The BMO-MRW is a measure of minimum rim width from the true outer border of the rim, which is Bruch's membrane opening (BMO). The BMO is usually identifiable on SDOCT of the ONH and hence BMO-MRW measurements have a high level of reproducibility. In a study of 107 patients with early glaucoma (average MD of -3.92 dB) and 48 healthy controls, Chauhan and colleagues reported BMO-MRW to have a sensitivity of 81% for detecting glaucoma at 95% specificity, compared to a sensitivity of only 70% for cpRNFL thickness for similar specificity (Chauhan et al 2013). BMO-MRW is a promising parameter for glaucoma detection and monitoring for structural progression however further studies are needed.

As more parameters become available clinicians may decide to use multiple measures to detect disease or monitor for progression. This approach may lead to confusion when change occurs in one structural parameter but not another and increase the chance of falsely identify change when none has occurred. It should also be acknowledged that each of these parameters was evaluated in case-control series using strict inclusion criteria and so might not

reflect the ability of imaging devices to detect disease in real world practice. Recently Azuara-Blanco and colleagues, based in Belfast, examined the ability of SDOCT normative databases to distinguish glaucomatous and healthy eyes among patients referred from community optometrists to glaucoma clinics (Banister et al 2016). Using a reference standard for glaucoma as diagnosis of glaucoma by the ophthalmologist, without recourse to OCT, an OCT global classification of 'outside normal limits' achieved 77% sensitivity for 79% specificity. Therefore, OCT classification alone missed 20% of people who had glaucoma and resulted in a 20% false positive rate; a poor result, likely in part due to limitations of the normative database. OCT also missed 5% of cases of severe glaucoma indicating that imaging for structural changes should not be relied on alone to detect disease; visual fields remain essential.

2.2.1.2. Detecting progression

The assessment of structural changes is also important for attempting to detect change over time; with the gold standard masked grading of optic disc stereophotographs (Medeiros et al 2005). Glaucoma guidelines, such as those published by the UK National Institute of Clinical Excellence, also recommend obtaining baseline optic disc images for progression analysis (2009). However, even expert observers often fail to agree on the presence or absence of progression on optic disc photographs, limiting the reliability of monitoring for structural changes using this method (Azuara-Blanco et al 2003; Jampel et al 2009).

Imaging devices such as OCT can provide supplementary information and include progression analysis software to provide a quantitative measure of change by performing event and trend-based analyses. In event analysis, progression is deemed to occur when the difference between the baseline and subsequent measurements is greater than test-retest variability (Leung 2014). Trend analysis uses linear regression analysis over time to determine if there is a significant negative slope in measured parameters, representing a fast rate of change. The Guided Progression Algorithm (GPA) on Zeiss devices is one example of OCT progression software. The GPA performs both trend-analysis and an event-analysis that examines RNFL thicknesses at individual pixel locations and compares two baseline OCT images to a follow up scan.

OCT is more objective than disc photographs and has good short-term reproducibility, making it an attractive option for detecting progression. Mwanza and colleagues examined 55 patients with glaucoma using the Cirrus OCT and performed 3 scans during the same visit to examine intravisit reproducibility and then 4 scans on additional days to measure intervisit reproducibility (Mwanza et al 2010). cpRNFL measurements had excellent reproducibility leading to the conclusion that a decrease in cpRNFL thickness at least 4μm is likely to represent significant change (Mwanza et al 2010). However, it is important to note that this study did not examine long-term reproducibility, which may be less than short-term reproducibility; meaning larger changes in cpRNFL thickness may be needed to be confident change is genuine. Also, as cpRNFL thickness decreases with age at a rate of approximately 0.5 μm per year (Leung et al 2012), the change of 4μm suggested as significant by Mwanza and colleagues could occur in 8 years with normal ageing.

The first paper to evaluate OCT as a tool to detect glaucoma progression was published in 2005 (Wollstein et al 2005). Wollstein and colleagues used a prototype OCT device to measure cpRNFL thickness in 63 eyes with glaucoma or suspected glaucoma and followed them every 6 months over an average of almost 5 years. 22% of eyes progressed by OCT event analysis (defined as a reduction in cpRNFL thickness of at least 20 μm from baseline) compared to only 9% by visual field and 3% by both. However, as the study did not include an independent reference for progression it is difficult to determine if progression noted by OCT was true deterioration or due to false-positives.

Rates of change in eyes with glaucoma are highly variable (Leung 2014; Wollstein et al 2005; Medeiros et al 2009). In a study of 116 glaucomatous eyes of 64 patients followed for at least 3 years with Stratus TDOCT, Leung and colleagues reported a wide range of rates of change in cpRNFL thickness ranging from -1.2 to -15.4 μm per year (Leung et al 2010). However, such inter-individual variability is to be expected, especially given the known variability in rates of change in visual field sensitivity in patients with glaucoma (Section 2.2.2.2, page 41). Medeiros and colleagues also used Stratus TDOCT to examine 253 eyes with glaucoma or suspected glaucoma over an average follow up of 4 years (Medeiros et al 2009). Rates of cpRNFL loss were significantly faster in eyes progressing on SAP and optic disc stereophotographs compared to those not progressing using conventional measures, with average rates of cpRNFL loss of 0.72 μm per year and 0.04 μm per year respectively.

The finding that eyes progressing on SAP have faster rates of cpRNFL loss than non-progressing eyes provides some validity for the use of OCT

measurements of cpRNFL thickness as a surrogate for glaucoma progression. However, several studies have shown progression is rarely detected simultaneously in structural and functional domains, a subject discussed further in section 2.3, page 51). There are also limitations of using TDOCT that may decrease its ability to detect change. In particular, the measurements obtained using TDOCT are not registered and differences in scan alignment over time will considerably weaken performance (Leung 2014).

SDOCT uses strategies such as eye tracking and scan registration to attempt to obtain images from the same location at each visit to more accurately detect change. In the first study to examine glaucoma progression using SDOCT, Leung and colleagues compared the performance of TDOCT and SDOCT for detecting structural changes in glaucomatous eyes (Leung et al 2011). The agreement for detecting progression (using trend-analysis) between devices was poor (K = 0.188), with SDOCT identifying more eyes as progressing compared to TDOCT (19/81 (23.5%) versus 4/81 (4.9%) respectively). Rates of changes in cpRNFL thickness ranged between −1.52 μm per year and −5.03 μm per year using Cirrus SDOCT and between −2.22 μm per year and −7.60 μm per year using Stratus TDOCT (Leung et al 2011). The authors concluded that the discrepancy might be due to SDOCT detecting progression earlier, however it is difficult to be certain whether some eyes thought be progressing on SDOCT were false-positives, especially as in keeping with other studies, both TDOCT and SDOCT had poor agreement with progression on SAP VFI. Nevertheless, it is intuitive that SDOCT is likely to be better at detecting progression than TDOCT due to its improved reproducibility. OCT measurements of macular thickness may also be useful for detecting glaucoma progression; with one study suggesting

they may be particularly useful for monitoring advanced glaucoma when cpRNFL measurements are nearing their floor (Sung et al 2012).

Despite these improvements in imaging technology, there are several limitations of using OCT to measure progression. First, it is important to differentiate decreases in cpRNFL and macular thickness due to glaucoma from normal age-related changes (Leung et al 2013). Using the Cirrus OCT, Leung and colleagues reported an average age-related decrease in cpRNFL thickness of 0.52 μm per year (95% CI 0.17 to 0.86 μm per year) in 35 healthy subjects followed for an average of 30 months (Leung et al 2012), and others have found similar age-related changes (Celebi, & Mirza 2013). Leung and colleagues found 50% of eyes with glaucoma had statistically significant downward slopes in inner macular thickness over an average follow up of almost 4 years (Leung et al 2013). However, after accounting for age-related changes, this decreased to 20% of eyes. Age-related changes also should be considered when examining change in cpRNFL thickness, however cpRNFL measurements were less influenced by age than macular measurements.

A second limitation of using OCT to measure progression is the floor in measurements that occurs in advanced disease at approximately 50 μm due to limitations of the segmentation algorithms and residual non-neural tissue (Leung et al 2009). Moreover, even as the structural floor is approached patients still may have significant residual visual field. It is also important to be aware that faster rates of change in RNFL thickness occur in eyes with thicker RNFL at baseline (Leung et al 2013) and as the signal-to-noise ratio of OCT tends to decrease over

time due to media opacities, weaker signal strength may lead to the appearance of thinner RNFL.

Finally, although imaging devices such as OCT are now widely used to aid glaucoma detection and to measure progression, the clinical relevance of these changes depends on their relationship to visual function, and this relationship is incompletely understood. Current understanding of the relationship between structural and functional changes is critically appraised in section 2.3, page 51.

2.2.2. Functional Changes - SAP

It is easy to appreciate the relevance of functional changes to the patient and the assessment of visual function is an essential component of glaucoma diagnosis and detection of progression, with SAP the current gold standard for assessing the functional domain. SAP is a form of static threshold perimetry during which differential light sensitivity is measured at 54 test locations. The customary protocol is The Swedish interactive thresholding algorithm (SITA) - Standard 24-2 test, which evaluates visual field sensitivity in the central 24 degrees (Figure 2-3).

The SAP report includes a series of summary indices including; MD – a weighted average of the total deviation values, where zero equates to no deviation from normal and more negative values indicate more advanced loss; PSD – a summary index of localized visual field loss; and GHT – which categorizes eyes as within normal limits, borderline, or outside normal limits based on a comparison of pattern deviation scores in superior and inferior visual

field. The VFI is another global index, which assigns a number between 1% and 100% to the field, with 100% being the normal age-adjusted value (Bengtsson, & Heijl 2008). The VFI assigns greater weight to central test locations and the percentage of field remaining is calculated based on pattern or total deviations depending on the depth of loss.

Figure 2-3. Standard automated perimetry using the 24-2 SITA threshold strategy for the right eye of the same patient shown in Figure 2-1 showing a glaucoma hemifield test (GHT) within normal limits and a mean deviation (MD) of -1.02 dB.

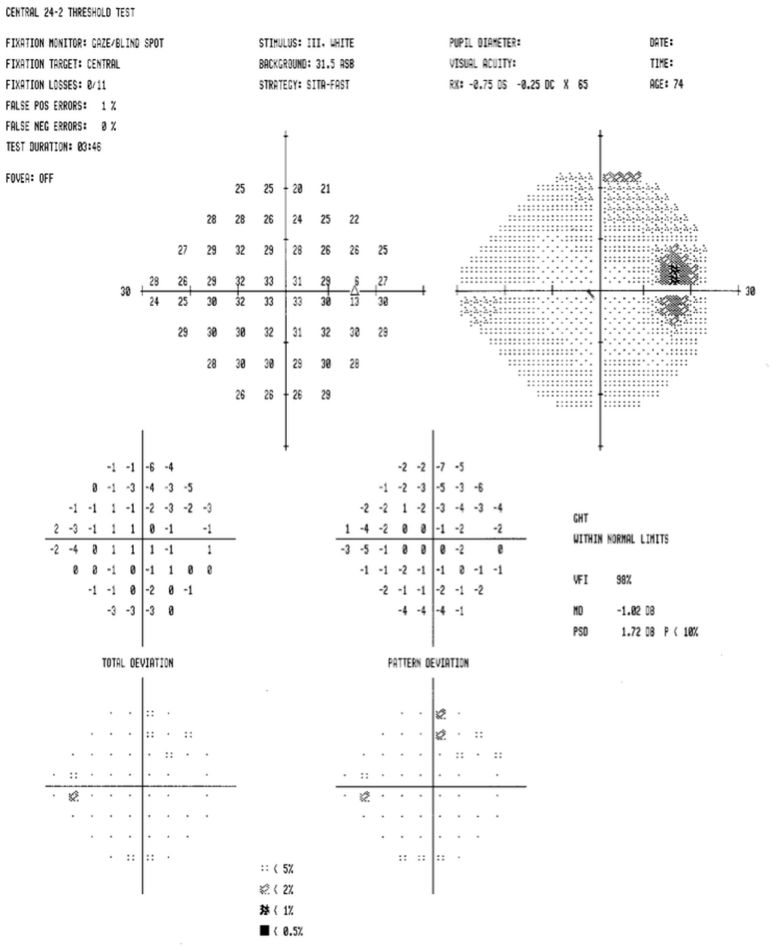

2.2.2.1. Detecting glaucoma

SAP has good ability to detect glaucoma and, in some patients, an abnormal SAP result may be the earliest manifest sign of the disease, however in others structural changes may be detectable first (Kass et al 2002). The relationship and timing of structural and functional changes is discussed more in section 2.3, page 51.

Overall SAP seems to have similar sensitivity and specificity for detecting glaucoma compared to imaging devices. Sample and colleagues evaluated the ability of SAP to differentiate healthy and glaucomatous eyes and found AUCs of 0.762 for SAP PSD and 0.731 for SAP MD (Sample et al 2006). SAP PSD had sensitivities of 48% and 52% for specificities of 90% and 80% respectively, compared to SAP MD sensitivities of 55% and 65%. Therefore, if SAP MD were used alone to detect glaucoma we would expect only 65% of glaucomatous subjects to be correctly identified and a relatively large number of false positives (20%). These results are slightly worse than those reported by Banister and colleagues for OCT, which achieved 77% sensitivity for 79% specificity (Banister et al 2016), however Sample and colleagues only evaluated SAP global indices, which are likely to perform worse than point-wise comparisons. Also, direct comparison of studies is problematic due to the different reference standards used and difference in disease severities of included patients.

There is also some debate regarding which SAP summary index might be best for detecting glaucoma. MD performed better than PSD in Sample and colleagues study (Sample et al 2006), however OHTS suggested PSD might be a better indicator of early glaucoma than MD (Gordon et al 2002). However, as

PSD is a summary index of localised visual field loss, PSD alone is unlikely to detect generalised reductions in visual field sensitivity that may be an early indicator of glaucoma in some patients (Henson et al 1999). For these reasons, when considering whether a patient has glaucoma or not, it is important to examine the whole visual field print out and not just the summary indices, and to interpret the visual field in the context of other findings from history and examination; a combination of information from structural and functional assessments is needed.

In common with most diagnostic tests including OCT, SAP is however less likely to be able to detect disease early compared to advanced disease (section 2.2.1.1, page 25). Simply put, it is more difficult to detect subtle differences between health and early disease compared to large differences between health and advanced disease. To illustrate this point, Medeiros and colleagues evaluated the effect of disease severity on glaucoma detection using SAP (Medeiros et al 2006). For 80% specificity, the SAP summary index PSD had a sensitivity of 85% in eyes with marked glaucomatous structural changes (70% loss of neuroretinal rim area), compared to a sensitivity of only 40% in eyes with early disease (10% loss of neuroretinal rim area).

2.2.2.2. Detecting progression

In addition to its role in glaucoma diagnosis, SAP is central to the detection and quantification of glaucoma progression. In fact, perimeters include sophisticated progression analysis software for this purpose, such as the Humphrey Perimeter's Guided Progression Analysis (GPA). GPA uses event

analysis to determine if there has been any statistical worsening of the visual field (based on significance limits for Pattern Deviation) and trend analysis to quantify the rate of change and aid the clinician in determining the patient's lifetime risk of visual loss. The GPA event analysis applies the progression criteria used in the Early Manifest Glaucoma Trial (EMGT) (Leske et al 1999). 'Possible Progression' is defined as 3 or more test points with statistically significant deterioration on two consecutive follow-up fields compared to two baseline examinations, and 'Likely Progression' is present when the same 3 or more deteriorated test points appear in at least 3 consecutive follow-up fields. Therefore at least 4 visual fields are required for the GPA event analysis to indicate 'Possible Progression' and 5 for 'Likely Progression'.

The GPA also uses a trend analysis to perform linear regression and examine the rate of change in VFI over time. The regression line derived from the VFI of previous tests can then be extrapolated to predict future visual field losses and lifetime risk of blindness. VFI is preferred to MD as it is less influenced by media opacities and has a weighting for central vision (Bengtsson, & Heijl 2008), however rates of progression measured using VFI may be non-linear and are likely to vary depending on disease severity (Pathak et al 2013; Rao et al 2011). In addition, relying on global indices such as VFI to detect progression may result in delayed recognition that a patient is worsening if changes are localised. As glaucoma often affects localised areas, a more sensitive approach, is to perform point-wise linear regression (PLR) analyses for each visual field test location and assess the significance and slope (Viswanathan et al 1997). Permutation analysis of point-wise linear regression (PoPLR) is a modification of PLR, reported to provide a better estimate of statistical significance of visual field

change (O'Leary et al 2012). PoPLR involves comparing change detected by PLR with change (or lack of change) in randomly reordered visual field tests from the same series. However, though PoPLR can help determine the probability change has occurred, it does not alter the rates of change calculated by PLR.

A further analytical tool for assessing rates of change in visual field, known as Analysis with Non-Stationary Weibull Error Regression and Spatial Enhancement ('ANSWERS') was recently described by Zhu and colleagues (Zhu et al 2014). 'ANSWERS' takes account of the two important factors not accounted for with other methods; the increasing variability that occurs as differential light sensitivity declines, and the correlation between spatially related regions (Garway-Heath et al 2000). Unlike PoPLR, 'ANSWERS' provides the rate of change for individual locations of the visual field, in addition to the probability of progression. Although 'ANSWERS' is a relatively new technique, there is evidence that it is a sensitive method of detecting visual field progression and that it may be better at predicting future visual field loss than other trend-based methods (Zhu et al 2015).

Several studies have examined rates of change in visual field in treated and untreated patients with glaucoma. The CNTGS and EMGT examined rates of field progression in untreated glaucoma (Anderson et al 2001; Heijl et al 2009). The average rate of change in MD in untreated NTG was 0.4 dB/year, compared to 1.08 dB/year in high-tension glaucoma and 3.13 dB/year in pseudoexfoliative glaucoma. Rates in treated patients are reassuringly less, but most treated patients still show some progression. Over a mean follow up time of 7.8 years, Heijl and colleagues found most patients with glaucoma progressed despite

treatment (Heijl et al 2013). The average rate of change was only -0.80 dB/year, however 5.6% of patients progressed very quickly with rates faster than -2.5 dB/ year.

Chauhan and colleagues' large Canadian cohort of 2,324 patients with glaucoma and suspected glaucoma had a much slower average rate of change of only 0.05 dB/year, perhaps due to fewer patients with PXF and having eyes with less severe disease at baseline (Chauhan et al 2014). However, 4.3% of patients progressed at a fast rate (<-1 to -2 dB/year) and 1.5% progressed at a catastrophic rate (<-2 dB/year). Saunders and colleagues examined rates of field loss in 3,790 UK patients with glaucoma and also found a small proportion of patients to be progressing quickly (Saunders et al 2014). 7.5% of eyes progressed at a rate faster than 1dB/year and only 3% of eyes progressed at rates faster than 1.5 dB/year. Interestingly, rates of visual field loss may be slowing down due to improvements in treatment, with Boodhna and colleagues recently showing slower rates of field loss in patients diagnosed after 2003, compared to those diagnosed in 1999 to 2003 (Boodhna et al 2015). However, the proportion of patients showing fast (worse than 1.5 dB/year) rates of progression did not change remaining at 6%.

Although SAP remains essential to the assessment of visual function in glaucoma, it has several limitations. It is patient's least preferred test (Glen et al 2014), it leads to greater patient anxiety than imaging (Chew et al 2016), it is influenced by media opacities such as cataract, and due to variability, multiple tests may be needed to be confident that change is genuine (Chauhan et al 2008). In fact, in areas of the field with advanced damage, test-retest variability

may span the entire dynamic range of the test (Malik et al 2012). There is also disagreement between experts examining visual field series as to whether there has been progression or not. Viswanathan and colleagues found a correlation kappa of only 0.32 for agreement between experts viewing series of reliable field tests (Viswanathan et al 2003).

2.2.3. Functional Changes – Other tests

Other psychophysical tests of visual function have been developed as possible alternatives to SAP, for example, frequency doubling technology (FDT), short-wavelength automated perimetry (SWAP) and flicker-defined form (FDF) perimetry (Johnson et al 1993; Landers et al 2003; Liu et al 2011; Sample et al 2006). These tests were developed with the aim of targeting subpopulations of RGCs by evaluating specific aspects of visual function, such as motion perception, contrast sensitivity or colour vision (Sample, & Weinreb 1990), however none have been shown to be superior to SAP (Burr et al 2007).

It has been hypothesised that in its early stages, glaucoma may predominately damage magnocellular RGCs projecting to the magnocellular layers of the lateral geniculate nucleus, i.e., the magnocellular (M) pathway (Johnson et al 1993; Shabana et al 2003). FDT perimetry was designed to selectively evaluate the M pathway by determining the contrast sensitivity for detecting a high temporal frequency counter-phase flicker stimulus, however there is now evidence that the response to motion perimetry is in fact generated by many RGC types and is cortically mediated (White et al 2002). In contrast, SWAP was designed to the parvocellular blue-yellow RGCs projecting to the

parvocellular layers of the lateral geniculate nucleus, i.e., the parvocellular (P) pathway, by using a narrow band blue-violet stimulus (440-nm wavelength) against a bright yellow background illumination. However, like FDT, the response to SWAP is likely to be mediated by a different pathway than originally thought. The blue-yellow cells are in fact small bistratified RGCs, which project their axons to the koniocellular layers of the lateral geniculate nucleus (Dacey, & Lee 1994; Sample et al 2006).

Whatever its exact mechanism, several studies have reported FDT to have good ability to detect glaucoma (Johnson, & Samuels 1997; Horn et al 2002; Quigley 1998; Cello et al 2000; Medeiros et al 2004), with at least one longitudinal study suggesting that, at least in some patients, abnormalities on FDT may precede SAP changes by several years (Landers et al 2003). However, most studies comparing functional tests were poorly designed, meaning their conclusions should be interpreted with caution. For example, Landers et al recruited patients with normal SAP at baseline, biasing the results in favour of FDT and poor choice of reference standard is a common problem. The ideal reference standard for comparison of functional tests is a structural marker of glaucoma, for example, progressive changes on optic disc photographs.

Several studies comparing the ability of SAP, SWAP and/or FDT to detect glaucoma have used a structural reference standard, however they have reached different conclusions (Medeiros et al 2006; Liu et al 2011; Sample et al 2006; Tafreshi et al 2009). Sample and colleagues found first generation FDT to have higher sensitivity than both SAP SITA and full threshold SWAP (Sample et al 2006). SWAP PSD and FDT PSD had AUCs of 0.775 and 0.875 respectively,

compared to 0.762 for SAP PSD for differentiating healthy eyes from those with progressive glaucomatous structural changes on stereophotographs. SWAP PSD achieved sensitivities of 45% and 48% for specificities of 90% and 80% respectively compared to sensitivities of 68% and 71% for FDT PSD for the same specificities. FDT was subsequently updated to Matrix FDT, which uses grating targets smaller than the original FDT to enable a 24-2 test strategy identical to SAP. Racette and colleagues reported Matrix FDT to be better than SAP for discriminating glaucomatous and healthy eyes (Racette et al 2008), however others have found no difference (Spry et al 2005). SWAP has also been modified over the years and now utilizes the SITA strategy to shorten the test duration. Despite these modifications, however, SWAP SITA generally does not have better diagnostic ability than SAP (Bengtsson & Heijl 2006).

Recently Liu and colleagues reported the results of a study in which they compared the ability of the latest versions of each test (Matrix FDT, SWAP SITA and SAP) to detect glaucoma, using cpRNFL thickness as the reference standard for glaucoma diagnosis (Liu et al 2011). There was no significant difference in performance between SAP and Matrix FDT but both were superior to SWAP SITA, with sensitivities of 82%, 84% and 57% for SAP, Matrix FDT and SWAP SITA MD respectively for 90% specificity. In a well-designed study, Tafreshi and colleagues also compared ability of SAP, Matrix FDT and SWAP SITA to distinguish glaucomatous and healthy eyes, but in contrast to Liu and colleagues found all 3 tests to be equally sensitive (Tafreshi et al 2009). The different results of these studies were probably due to differences in reference standard and subject selection. Liu and colleagues proposed that Matrix FDT might only outperform SAP in patients with early visual field loss; in which case inclusion of

patients with more advanced glaucoma is likely to diminish the ability to identify the optimum tests for detection of early disease (Liu et al 2011).

In a study including 196 healthy eyes and 174 eyes with glaucoma, Medeiros and colleagues used a regression model to examine the effect of disease severity on the diagnostic performance of Matrix FDT and SAP (Medeiros et al 2006). Glaucoma severity was determined from CSLO measurements of neuroretinal rim. For Matrix FDT PSD, areas under the ROC curves for 10%, 30%, 50%, and 70% loss of neuroretinal rim area were 0.766, 0.857, 0.922, and 0.962 respectively, compared to 0.638, 0.756, 0.852, and 0.920 respectively for SAP. Therefore, although Matrix FDT and SAP had similar ability to detect glaucoma in eyes with advanced structural losses, in the regression model, Matrix FDT was predicted to have significantly larger AUC than SAP for eyes with only 10% and 30% loss of neuroretinal rim, suggesting Matrix FDT may perform better than SAP in early disease. For a 10% loss of rim area, the AUC for SAP SITA was 0.638, with a sensitivity of only 21% for 95% specificity. Matrix FDT had an AUC of 0.766 for 10% loss of rim area, with a sensitivity of approximately 31% for 95% specificity, increasing to 58% for 80% specificity. Therefore, even though Matrix FDT performed better than SAP in early disease, it is still possible that many cases of early glaucoma could be missed if Matrix FDT were used alone to detect disease.

The FDF stimulus has recently been proposed as an alternative method for detecting glaucomatous visual loss (Lamparter et al 2012; Horn et al 2014). HEP uses the FDF stimulus, which is believed to stimulate the M-pathway (Mulak et al 2012). The stimulus consists of rapidly reversing black and white dots that

modulate in counter-phase at a temporal frequency of 15 Hz until the subject perceives an illusionary contour (edge) at the border of the random dot areas. The phase reversal frequency is varied to determine the minimum contrast needed for detection of the edge, which appears to the subject as a grey patch against the mean luminance background. Recent studies have examined the ability of FDF perimetry to detect glaucoma and compared it to Matrix FDT and SAP (Lamparter et al 2012; Horn et al 2014). Horn and colleagues tested 97 subjects with early glaucoma defined by optic disc appearance and found SAP MD to be abnormal in 42 (Horn et al 2014). Of the 55 subjects with normal SAP, 28 had abnormal FDF MD. 38 subjects had abnormalities on both SAP and FDF and 4 had abnormal SAP but normal FDF. This suggests that FDF may be able to detect glaucomatous functional changes at an earlier stage than SAP, though there is insufficient evidence at present to recommend this test.

Despite the interest in novel methods of perimetry, SAP remains the gold standard and so was selected as the primary test of visual function for my studies. Although FDT, SWAP and FDF perimetry attempt to minimize potential input from other pathways, it is unlikely any stimulus can be 100% specific for a single subset of RGCs. Moreover, glaucoma may affect different types of RGC, therefore were a test to target a specific pathway, it may miss some patients with early glaucoma with loss of other RGC subtypes and may also be less able to detect progression through all stages of disease. (Yücel et al 2003; Sample et al 2006). It is also important to be cautious when considering the introduction of a new clinical test as it may impact on the resources available to perform conventional SAP. Due to the variability inherent in psychophysical testing, when trying to detect glaucoma progression it is likely better to employ one method of

testing frequently than employ several different testing strategies infrequently. Figure 2-4 shows an example of SDOCT, SAP, FDT and FDF perimetry.

Figure 2-4. Optical coherence tomography (OCT), standard automated perimetry (SAP), Frequency doubling technology (FDT) perimetry and Heidelberg Edge Perimetry (HEP) for the right eye of a patient with glaucoma. Inferior retinal nerve fibre layer (RNFL) thinning (arrows) is visible on OCT maps as 'cooler' colours in the RNFL thickness map and red and yellow, indicating deviation from normal values, on the RNFL deviation map. SAP shows a small corresponding superonasal visual field defect which is more pronounced on FDT and HEP.

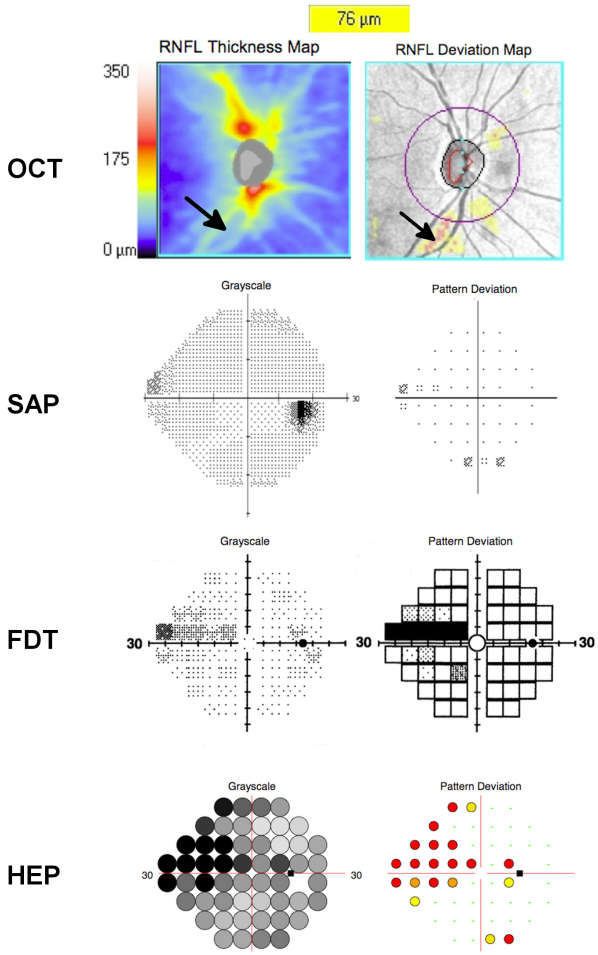

2.3. The relationship between structural and functional changes

The true relevance of structural changes in glaucoma depends on their relationship to visual function. Many previous studies have attempted to examine the relationship between structural and functional changes, however the relationship is complex (Malik et al 2012). In some eyes, structural changes are detected before functional changes, whilst in others functional changes are detected before structural changes, and in some structural and functional changes are detected concurrently (Kass et al 2002). Disagreement between tests can be confusing for the clinician; for example, when an eye shows progression in one domain but not the other it may be difficult to determine whether change is clinically significant. This has led to debate about which method is better to detect progression – structure or function – and whether or when clinicians should choose one method versus the other as they monitor patients with glaucoma or those suspected of having the disease (Medeiros et al 2016).

Histological studies are often quoted as proof that large numbers of RGCs may be lost before visual field abnormalities are noted (Quigley et al 1989; Harwerth et al 2004; Kerrigan-Baumrind et al 2000). For example, in a study of cadaver eyes, Kerrigan-Baumrind and colleagues concluded that at least 23 to 35% of RGCs would need to be lost for an abnormality on conventional perimetry, suggesting that in early disease, SAP may underestimate glaucomatous damage (Kerrigan-Baumrind et al 2000). However, the results

somewhat contradict this conclusion, indicating an eye with 100% of RGCs remaining would have an average loss of sensitivity of 5 dB. The study was also limited by inclusion of small numbers of eyes and at individual locations, the relationship between SAP sensitivity and RGC counts was highly variable. Moreover, as clinical studies have shown that the first manifest sign of glaucoma may be either a structural or functional loss it is essential to test both structural and functional domains (Kass et al 2002). In OHTS only 12 of 125 eyes (9.6%) that developed glaucoma during follow up had a visual field and structural endpoint detected concurrently, meaning there was often disagreement between tests (Kass et al 2002). 69 eyes (55.2%) had an optic disc endpoint first and 44 (35.2%) a visual field endpoint. Simultaneous detection of change in structure and function tests therefore seems to occur infrequently.

The differences in structural and functional measures can be partially explained by differences in measurement scale (Garway-Heath et al 2000). SAP is obtained and measured using a logarithmic decibel scale whilst structure is measured in linear units. The consequence is that in the early stages of disease SAP data is compressed, meaning a large reduction in the structural parameter is likely to be accompanied by only a small change in SAP sensitivity. Conversely, later in the disease a small reduction in the structural parameter is likely to be accompanied by a large reduction in SAP sensitivity measured using logarithmic units (Garway-Heath et al 2000; Medeiros et al 2012; Hood, & Kardon 2007; Swanson et al 2004). Figure 2-5 shows the non-linear relationship between SAP MD in decibels and cpRNFL thickness using cross-sectional data taken from eyes included in DIGS at UCSD.

Figure 2-5. Scatter and LOWESS plot showing cpRNFL thickness (in the linear unit of µm) compared to SAP MD (in the logarithmic unit of decibels) for eyes included in DIGS.

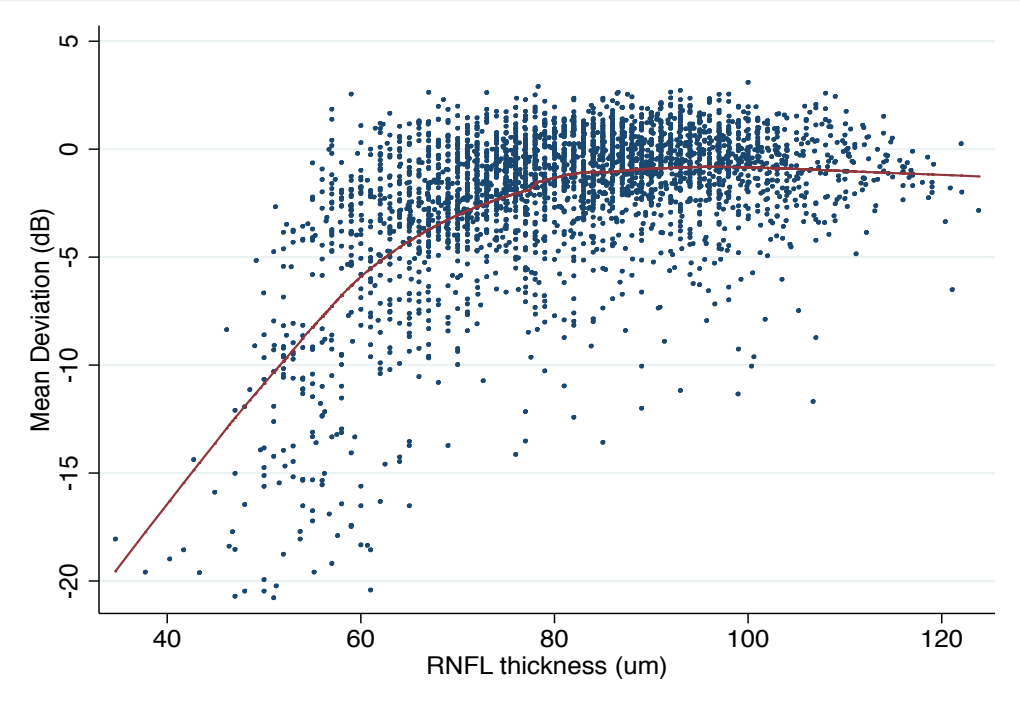

Figure 2-6 shows an example of how a large change in cpRNFL thickness in early glaucoma may be accompanied by only a small change in SAP sensitivity, whereas

Figure 2-7 shows an example of how in advanced disease, SAP sensitivity may continue to decline with no detectable change in cpRNFL thickness.

Figure 2-6. Example of patient with early glaucoma showing progressive glaucomatous changes to the optic nerve but no significant change in SAP. The right eye has increased excavation of the optic nerve head visible on optic disc photographs between 2004 and 2008. During this period, OCT measurements of average cpRNFL thickness decreased at a rate of 3.2 µm per year, however there was no significant change in SAP sensitivity.

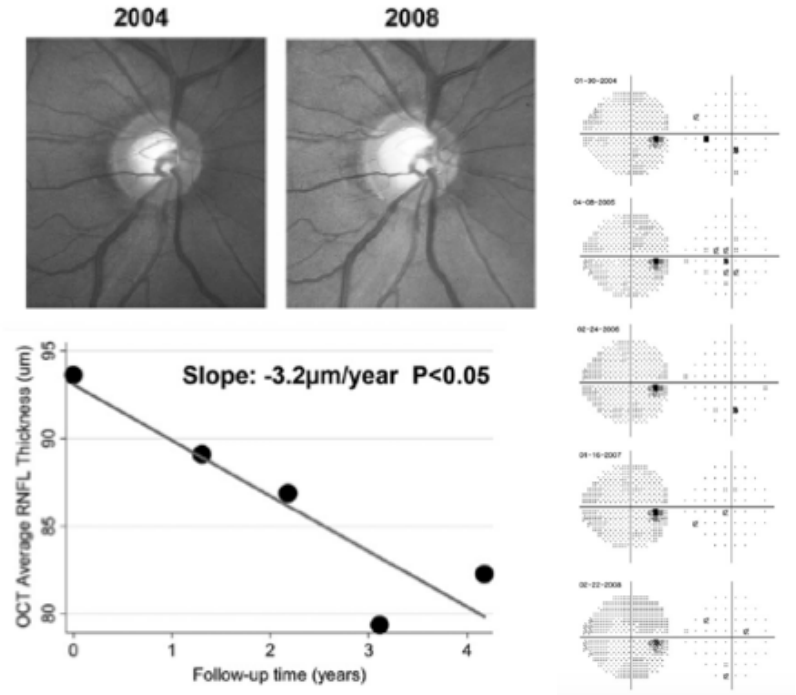

Figure 2-7. Example of a patient with advanced glaucoma showing progressive changes on visual field but no significant change in structural measurements. This patient has RNFL thickness approaching the floor in structural measures.

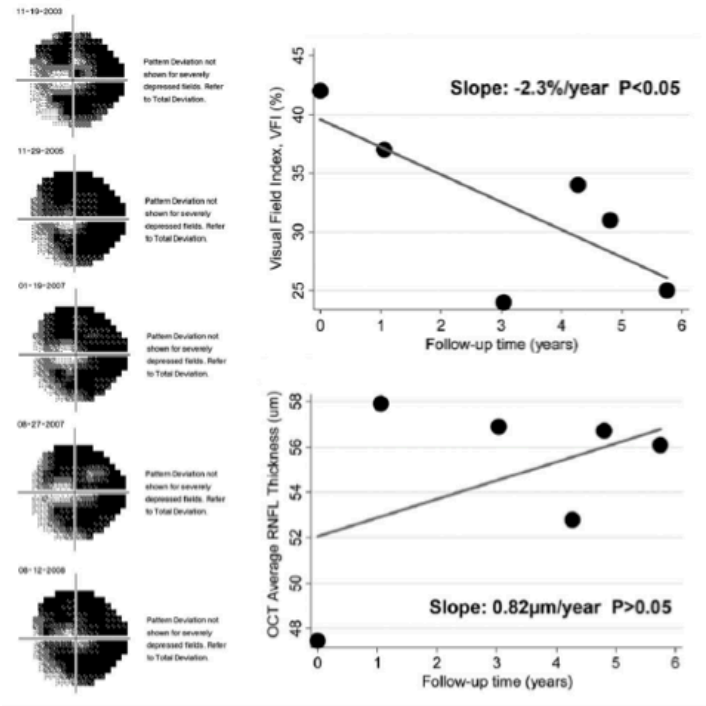

When SAP sensitivities are transformed to a linear scale, the relationship between structure and function becomes more linear, with a linear relationship also observed between structural measures and other tests of visual function, including multifocal visual evoked potential (mfVEP) (Hood et al 2002) and pattern electroretinogram (PERG) (Garway-Heath et al 2002). For example, Garway-Heath and colleagues showed a linear relationship between DLS (plotted on a 1/Lambert scale) and neuroretinal rim measured using CSLO (Garway-Heath et al 2002). However simple transformation of data does not overcome other reasons for disagreement between SAP and structural measures. As DLS is assessed using a logarithmic stepped algorithm, there are few steps at high

sensitivity and many steps at low sensitivity. This leads to loss of information and lower precision at high sensitivity that is not compensated for by transforming SAP sensitivity values to linear units. It has been suggested that a linear testing strategy might be useful in early disease, however this would be problematic in advanced disease as the logarithmic scale provides a large amount of information at low sensitivities (Malik et al 2006). It may be that different algorithms could be adopted at different stages, such as a linear increment at high sensitivity and a logarithmic increment at low sensitivities, or an algorithm used where the step size is a percentage of the previous luminance value (Malik et al 2006). Several investigators have attempted to model the relationship between structural and functional measures and these are discussed further in section 2.4, page 62.

Other reasons for disagreement between SAP and structural measures include sampling of different retinal areas, measurement variability inherent to SAP and OCT, overlap of RGC receptive fields, the contribution of non-neural components to RNFL thickness, and the effect of spatial summation (discussed further in section 2.4.10, page 76) (Malik et al 2012; Redmond et al 2013; Medeiros et al 2006; Garway-Heath et al 2000; Swanson et al 2004). The choice of statistical method also influences the apparent association between structure and function (Marín-Franch et al 2013). The relationship between structural and functional changes also differs at various stages of disease, with imaging devices appearing to be most useful in early disease, whereas perimetry seems to perform better when visual field losses are already present (Medeiros et al 2012). However, perhaps the most important reason for discrepancy between structure

and function is that RGCs may become dysfunctional before being lost completely.

One should expect disagreement between structural and functional measurements due to different properties of the tests used to assess these changes, such as their different scales, variability and dynamic range. It is also important not to dismiss structural measures purely due to an imperfect agreement with functional tests. Assessment of glaucomatous structural changes provides supplementary information to SAP and for some individuals offers an opportunity to detect disease and disease progression at an earlier stage. In addition, there is growing evidence that progressive structural changes are predictive of outcomes that are clinically relevant for patients.

Several studies have examined whether baseline structural measurements, including from disc photographs, CSLO and OCT are predictive of future development of the clinically relevant outcome of visual field loss (Medeiros et al 2009; Strouthidis et al 2010; Zangwill et al 2005; Lalezary et al 2006), however, overall there seems to be only weak association. An analysis of 639 eyes of 407 patients with suspected glaucoma from the DIGS at UCSD found baseline grading of disc photographs to be predictive of the development of abnormal visual fields over an average follow up of 8 years (Medeiros et al 2009). Eyes with an optic disc graded as glaucomatous at baseline had an almost 4 times increased risk of developing a visual field defect during follow up, with a 1.5-fold increase in risk for each 0.1 larger vertical cup disc ratio. The presence of progressive changes on optic disc photographs was a much better indicator of risk, associated with almost 26 times higher chance of developing a field defect

(Medeiros et al 2009). Therefore, although baseline disc photographs were predictive of future functional change, progressive changes on disc photographs performed much better.

Similar findings have been reported using CSLO and OCT. Strouthidis and colleagues found neither baseline MRA nor GPA classification alone were good at predicting future progression of visual field in patients with OHT (Strouthidis et al 2010), though abnormal CSLO at baseline was associated with increased risk of further structural changes. Although it is possible that baseline structural measures might have been better at predicting an alternative functional endpoint, they were also poorly predictive of future visual field loss in the CSLO ancillary study to the OHTS (Zangwill et al 2005). It seems likely that the poor performance of baseline structural measures is at least in part due to the wide variation in normal ONH appearance in healthy subjects, which frequently leads to difficulties in diagnosing glaucoma from a single disc examination, and therefore predicting risk of visual loss. Evidence of progressive structural damage seems to be a more robust indicator of glaucoma and more strongly predictive of progressive visual loss (Medeiros et al 2009).

In those suspected of having glaucoma, longitudinal changes in rim area measured using CSLO are strong predictors of future visual field loss (Medeiros et al 2013). Over an average follow up of 7 years, Medeiros and colleagues found that patients who developed visual field loss had a mean rate of change in rim area almost four times faster than those that did not. Each 0.01mm^2 / year faster rate of rim area loss was associated with an almost 3-fold higher risk of developing visual field loss. Progressive changes on CSLO are also predictive of

worsening visual field loss in patients with established glaucoma. Chauhan and colleagues examined 81 patients with glaucoma and found that progressive changes on CSLO topographic changes analysis during the first 3 years of follow up had earlier visual field progression defined using the EMGT criteria and worse rates of change in SAP MD (Chauhan et al 2009). It should be noted however that Chauhan's study included only patients with a baseline MD between -2 and -10 dB and the relationship between structural and functional changes is likely to be different at later stages of disease. A recent similar study examined rates of change in cpRNFL over time in patients with suspected glaucoma (Miki et al 2014). Rates of cpRNFL thinning were significantly faster in eyes that eventually developed a visual field defect compared to those that did not, with each 1 μm per year faster cpRNFL loss associated with a greater than 2 times higher risk of developing a future field defect.

Together these studies demonstrate that longitudinal glaucomatous structural changes are predictive of future visual loss, offering the opportunity to identify high-risk individuals and instigate treatment prior to worsening of functional impairment. It should be noted, however, that although abnormalities of RNFL thickness are often detected before changes on SAP, some patients develop visual field defects prior to the detection of structural changes. Assessments of both structure and function are needed; the difficulty lies in how best to integrate their results without increasing the chance of false-positives (discussed more in section 2.4.11, page 79). Also, whether progression is detected in the structural or functional domain first depends to a large degree on the choice of imaging and perimetric technology and the chosen endpoints. For example, in OHTS, more eyes might have reached a structural endpoint first if

OCT measurements, rather than disc photographs, had been the chosen method of detecting structural change (Kass et al 2002; Medeiros et al 2016). Conversely functional changes might be detected earlier with improved methods of perimetry.

Two recent studies from Claude Burgoyne and Brad Fortune in Portland, Oregon illustrate how choice of technology could influence the timing of disease detection. Using an experimental model of glaucoma, it was found that, although there was a strong linear relationship between cpRNFL thickness and histological optic nerve axon count, cpRNFL thickness did not begin to decrease until 10 to 15% of RGC axons were lost from the optic nerve (Cull et al 2012). This suggested that other structural changes might be detectable before RNFL thinning. As follow up to this work, Fortune and colleagues showed that loss of RNFL retardance measured using SLP could be detected in some eyes prior to cpRNFL thinning (Fortune et al 2013a). 41 rhesus macaques with experimental glaucoma had longitudinal SDOCT and SLP measurements. During follow up, 33 of 41 eyes reached a structural endpoint and of these 79% had evidence of reduced RNFL retardance before a reduction in RNFL thickness. This observation suggests that axonal cytoskeletal disruption may precede axonal loss, and therefore measures of RNFL birefringence might allow earlier detection of glaucomatous damage than measures of RNFL thickness. Whether an ability to detect structural changes prior to changes to cpRNFL will benefit patients is debatable however, as certainly the greatest unmet need is reducing the incidence of patients presenting with advanced disease. Also, the results of these animal studies may not be replicated in humans. A recent clinical study found progressive RNFL thinning occurred more frequently than changes in RNFL retardance (Xu et al 2013). It is also possible that other structural manifestations

of glaucoma such as changes in the ONH may be detected before RNFL loss (He et al 2014; Fortune et al 2013b). Nevertheless, this work provides insight into glaucoma pathogenesis and it's conceivable that in the future, detection of other structural changes such as loss of retardance might allow treatment to be instigated before RGC axons are lost irreversibly. However, although RNFL retardance was measured using SLP devices, SLP has largely been abandoned in clinical practice in favour of OCT. It is also important to emphasise that there is also strong evidence that in some patients, functional changes precede changes to the RNFL. For example, Banitt and colleagues reported that a reduction of amplitude on pattern electroretinography (PERG) occurred several years prior to changes on OCT in a cohort of patients with suspected glaucoma (Banitt et al 2013).

2.4. Comparing structure and function

Various approaches have been described to facilitate the comparison of measurements of structure and function including; the Harwerth model (Harwerth et al 2010), Garway-Heath model (Garway-Heath et al 2000), Hockey-Stick model (Swanson et al 2004), Hood-Kardon model (Hood, & Kardon 2007), Drasdo model (Drasdo et al 2008) and Zhu model (Zhu et al 2010). To allow comparison between domains, measurements from SAP can be converted to linear units, structural measures converted to logarithmic units, or both structural and functional measurements converted to a common unit, for example an estimate of RGC number. The next section of this thesis appraises each of the structure-function models (section 2.4.4, page 66), but before considering the models it is important to appreciate that the ideal model should account for 3 important factors; i) spatial summation, ii) stimulus modulation scale and iii) the contribution of non-neural components to structural measures (Malik et al 2012).

2.4.1. Spatial Summation

The relationship between glaucomatous structural changes, namely RGC loss, and functional changes, is influenced by visual processing mechanisms. Ricco's law states that if a sufficiently small stimulus is projected onto the retina, the total energy of the stimulus required for threshold detection remains constant (Redmond et al 2010). Therefore, for a small stimulus, the intensity of the threshold stimulus is inversely proportional to the stimulus area. The largest stimulus size for which Ricco's law applies is known as Ricco's area, or the

critical area. Stimuli smaller than or equal to the critical area meet the conditions for complete spatial summation, whereas when a stimulus is larger than the critical area, spatial summation is incomplete and the threshold is determined by probability summation. Detection of a stimulus by complete spatial summation depends on the summed response of detectors, whereas detection by probability summation depends on the non-linear pooling of responses (Mailk 2012}. Therefore, under conditions of complete summation, DLS is linearly related to the number of RGC receptive fields in the tested area (Garway-Heath et al 2000). Whereas under conditions of probability summation, the stimulus will be detected when recognized by at least one potential detector and the relationship between DLS and RGC count is determined by the relationship p=1-(1-p1)n, where p is the probability of detection, p1 is the probability of detection for each individual detector and n is the number of detectors (Pirenne 1943). The result of this exponential relationship is that with probability summation, reduction in DLS will be greater in regions of low RGC density than if the same number of RGCs were lost in a region of high RGC density.

Due to the varying distribution of photoreceptors and RGCs, the critical area is larger in the peripheral compared to central retina, ranging from approximately -2 log deg^2 to 0.75 log deg^2 in healthy individuals (Redmond et al 2010). The Goldmann III stimulus has an area of -0.83 log deg^2, therefore in healthy eyes, SAP thresholds are determined by complete spatial summation only in the mid to peripheral visual field, corresponding to an eccentricity of approximately greater than 15 degrees (Redmond et al 2010).

The physiological basis of Ricco's area is incompletely understood but it has been proposed that it increases with eccentricity to maintain a constant number of functioning underlying RGCs and that the critical number of RGCs is equal to the minimum number of RGCs needed to preserve detectability of a retinal signal against background cortical noise caused by spontaneous neural activity (Redmond et al 2010). Ricco's area does not seem to change with age but enlarges when there is a pathological reduction in RGCs, such as occurs with glaucoma (Redmond et al 2010). As RGCs are lost, the area of complete spatial summation enlarges, and may encroach on the central 15 degrees, an area normally characterized by probability summation. Therefore, the relationship between DLS and RGC counts will vary depending on disease severity, and once complete spatial summation occurs, one would expect a given loss of RGCs to result in a greater decline in DLS.

Improved understanding of spatial summation has the potential to lead to improved understanding of the structure-function relationship. It may also lead to improvements in perimetry, for example, if the perimetric stimulus size were scaled to account for changes in size of the critical area, the sensitivity of perimetry to detect small degrees of RGC loss could be improved, particularly in early disease and at locations close to fixation (Malik et al 2012). However, background luminance, stimulus duration, and wavelength also influence spatial summation (Swanson et al 2004).

2.4.2. Stimulus modulation scale

The relationship between measures of glaucomatous structural and functional change is influenced by the choice of scale used to acquire and present the data from each domain (Garway-Heath et al 2000). Therefore, models comparing structure and function must seek to overcome the difference between the logarithmic decibel scale used for SAP and linear structural measurements. Broadly, one of three approaches are used; either converting SAP data to 1/Lambert units, converting structural data to logarithmic units, or converting both to a third unit, for example, an estimate of RGC count. It should be noted however, that these approaches do not overcome logarithmic algorithm used to acquire DLS values with SAP, previously discussed in more detail in section 2.3, page 51, of this thesis.

2.4.3. Contribution of non-neural components

Models comparing SAP and structural measurements should also consider the non-neural components of the RNFL and ONH. For example, in addition to RGC axons, the RNFL consists of astrocytes and Muller cells, and the relative contribution of each component changes over time in healthy and glaucomatous subjects due to tissue remodelling (Harwerth et al 2010). Harwerth and colleagues reported that loss of RGCs is likely to be proportionally greater than loss of RNFL due to non-neural components of the RNFL (Harwerth et al 2010). However, previous studies, albeit in low numbers of patients, have suggested an age-related rate of RGC loss of approximately 0.6% per year (Kerrigan-Baumrind et al 2000; Harman et al 2000) compared to age-related cpRNFL losses of

between 0.17 μm to 0.86 μm per year (Leung et al 2013), which assuming a baseline RNFL thickness of 100 μm would approximate to RNFL loss of 0.17 to 0.86% per year (section 2.3, page 51).

Whatever the exact rate of loss, the relative proportion of non-neural components is likely to increase with worsening RNFL loss, with non-neural components contributing most the RNFL as the floor in structural measures is reached at near 50 μm (Leung et al 2009; Harwerth et al 2010). This will have a direct effect on the relationship between structural and functional changes.

2.4.4. Harwerth model

The pathology underlying both structural and functional glaucomatous changes is dysfunction and loss of RGCs; therefore, both structural and functional changes should correlate to the number of RGCs and were it possible to quantify RGCs, this would be an attractive method of gauging glaucoma severity and comparing structural and functional domains. The Harwerth model attempts to estimate the number of RGCs based on formulae derived from studies in nonhuman primates with experimental glaucoma (Harwerth et al 2010; Harwerth et al 2004; Harwerth et al 2007). These experiments showed that, accounting for retinal eccentricity, there was a linear relationship between histological RGC density, transformed to a logarithmic scale, and SAP sensitivity in decibels (Harwerth et al 2004). The structure-function relationship was steeper at locations in the peripheral retina meaning loss of a given number of RGCs would result in a greater reduction in SAP sensitivity in the peripheral compared to the central retina (Figure 2-8).

Figure 2-8. The structure-function relationship between SAP sensitivity and histological RGC density in monkeys with experimental glaucoma at 4 retinal eccentricities. Both SAP sensitivity and RGC density are shown in logarithmic units Adapted from Harwerth et al (Harwerth et al 2010).

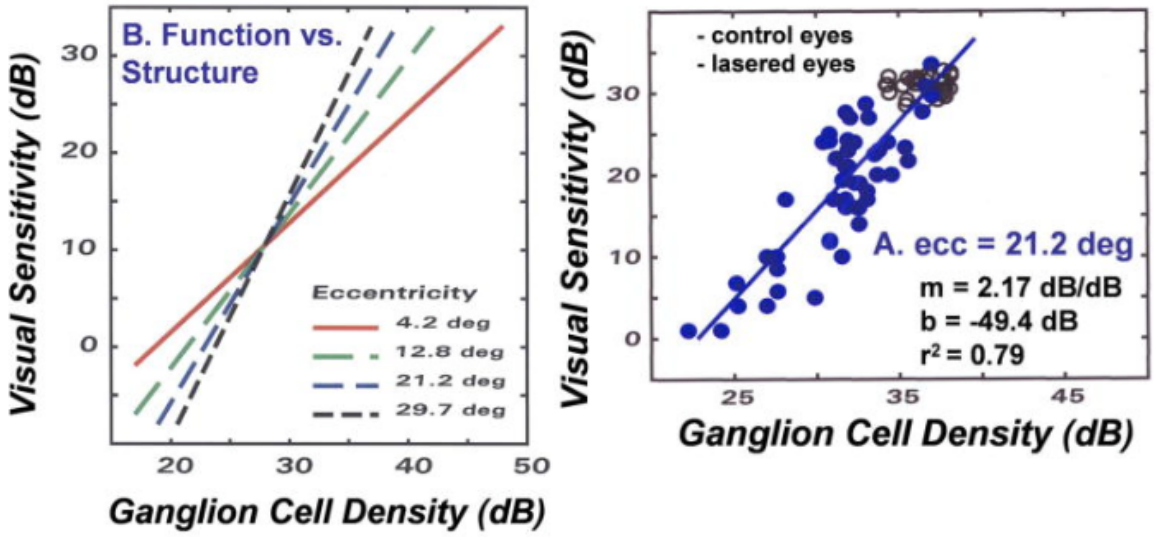

The following formulae were then proposed to estimate the number of RGC somas in an area of the retina corresponding to a SAP test location for given values of SAP sensitivity (Harwerth et al 2004). The eccentricity of the test point is denoted *ec*, *s* is SAP sensitivity in decibels, and *m* and *b* represent the slope and intercept of the linear function relating RGC quantity (gc) in dB to SAP sensitivity (s) in dB at a given eccentricity.

$$m = [0.054*(ec*1.32)] + 0.9$$

$$b = [-1.5*(ec*1.32)] -14.8$$

$$gc = \{[(s-1)-b]/m\} + 4.7$$

$$SAP_{rgc} = \Sigma\ 10\text{^}(gc*0.1)$$

The constant 1.32 is the ratio of human-monkey axial lengths to relate visual angles to retinal distance, -1 is a correction for the difference between full-threshold and SITA standard tests, and 4.7 converts RGC density to total RGCs in an area of the retina corresponding to a 6 x 6 degree area of visual space. By applying this formula to each SAP test location, an estimate of total number of RGCs (SAPrgc) may be obtained by summing the RGC estimates from all locations.

The structural component of the model was derived from subsequent experiments in 2007 showing a linear relationship between histological RGC counts and cpRNFL thickness measured using TDOCT (Harwerth et al 2007). To derive the total number of RGC axons from the global RNFL thickness measurement obtained by OCT (OCT*rgc*), the following formulae were applied:

$$d = (-0.007 * age) + 1.4$$

$$c = (-0.26 * MD) + 0.12$$

$$a = \text{average RNFL thickness} * 10870 * d$$

$$OCTrgc = 10^{[(\log(a) * 10 - c) * 0.1]}$$

where *d* corresponds to the axonal density (axons/μm^2) and *c* is a correction factor for the severity of disease to consider remodelling of the RNFL. The model considers the effect of ageing on axonal density and the effect of disease severity on the relationship between the neuronal and non-neuronal components of the RNFL thickness estimates obtained by OCT. It is important to note however that SAP MD is used as the measure of disease severity and therefore the OCT-

derived RGC estimate is not truly independent to the RGC estimate derived from SAP.

When these formulae were applied to a clinical population there was good agreement between SAP and OCT-derived RGC estimates, although agreement was poorer in more advanced disease as apparent in Figure 2-9 (Harwerth et al 2010).

Figure 2-9. Scatter plot showing the relationship between estimated numbers of RGC axons derived from OCT and estimated number of RGC soma derived from SAP for 488 patients with glaucoma. Adapted from Harwerth et al 2010 (Harwerth et al 2010).

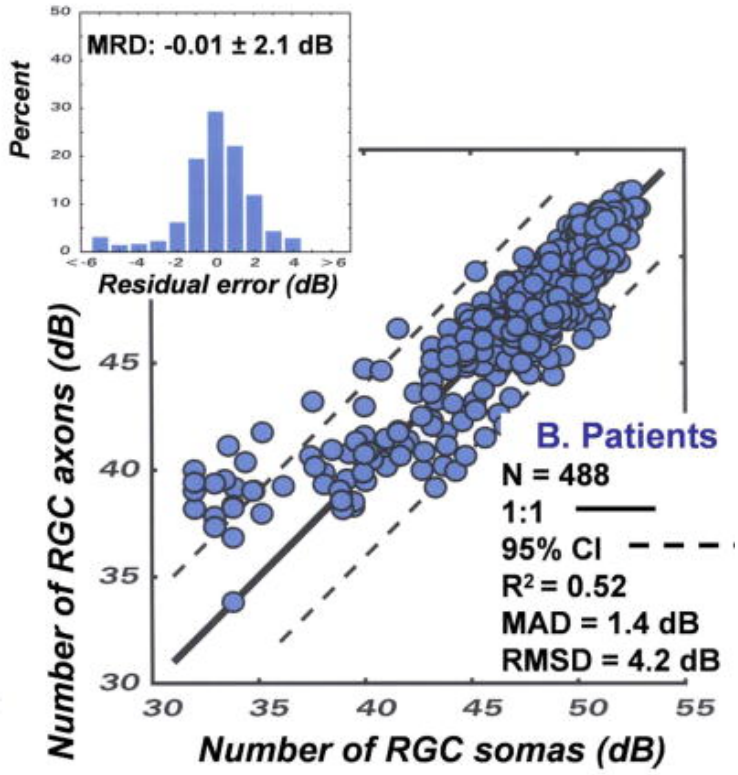

The ability to express the results of structure and function tests using unit of estimated number of RGCs is intuitive as it reflects glaucoma pathology and

raises the possibility of combining information from the two domains to increase the precision of the RGC estimates (section 2.4.11, page 79).

2.4.5. Garway-Heath model

Garway-Heath and colleagues examined the physiological relationship between RGC receptive field numbers and differential light sensitivity (DLS) measured using SAP (Garway-Heath et al 2000). RGC density values were derived from a previously published RGC density map of the healthy human retina, with a correction for lateral displacement of RGCs from the fovea, and these RGC densities were compared to corresponding normal DLS values from 30-2 white-on-white perimetry (Curcio, & Allen 1990; Heijl et al 1987) . The number of RGC receptive fields within a Goldman size III target was calculated based on the size of the target and receptive field density and spatial summation, derived from an analysis of 8 healthy subjects, was incorporated into the model.

The results of this study indicated that proportionally greater RGC loss is needed in the central compared to peripheral field for a similar change in DLS, and that the relationship between DLS and RGC density adjusted for local spatial summation is linear when sensitivity is converted from logarithmic to linear units. The coefficients from the linear regression of SAP sensitivity against RGC density could be used to estimate RGC density as follows:

$$\textbf{RGC density} = [(\textbf{DLS} + 392) / 208]^{1/k}$$

Where k = the location-specific spatial summation value, ranging from 0 near the fovea to 1 in the periphery, and DLS is the differential light sensitivity in

1/Lambert (dB = 10 × log10 (1/Lambert)). A major strength of this model is that is accounts for spatial summation, however the model only accounts for location-specific changes in spatial summation and not changes that occur due to glaucomatous RGC loss.

2.4.6. Hockey-Stick model

Swanson and colleagues used the same normative data (Curcio, & Allen 1990; Heijl et al 1987) as Garway-Heath to examine the relationship between SAP sensitivity and RGC density and developed a Hockey-Stick model, which is attractive as it acknowledges that the relationship between RGC number and sensitivity varies during the course of disease, and considers variation in spatial summation with eccentricity (Swanson et al 2004).

The relationship between SAP sensitivity and RGC receptive field density was modelled with a breakpoint occurring at 15-degree eccentricity to account for the change from probability summation to complete spatial summation in healthy subjects (section 2.4.1, page 62). The relationship between SAP sensitivity and RGC density was linear, with a slope of one at locations with greater than 15-degree eccentricity (region of complete spatial summation), and a shallower slope at locations with 15-degree eccentricity (region of probability summation) (Figure 2-10).

Figure 2-10. Scatter plot for normative data for the size III stimulus derived from Heijl et al (Heijl et al 1987) and Curcio et al (Curcio, & Allen 1990) and adapted from Swanson et al (Swanson et al 2004), fitted to the two-parameter spatial summation function. Points to the left of the of the figure represent locations at eccentricities of greater than 15 degrees, compared to points to the right of the curve at eccentricities of less than 15 degrees.

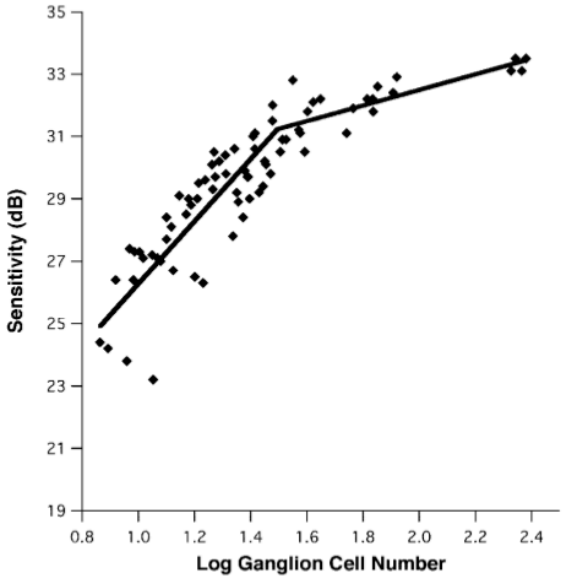

The change in slope can be explained by the size of the Goldmann size III stimulus in relation to the critical area of spatial summation (Ricco's area) (Redmond et al 2010). In healthy eyes the Goldmann size III stimulus is larger than the critical area at eccentricities of 15-degrees or less and smaller than the critical area at locations closer to the fovea. The breakpoint corresponds to a sensitivity of approximately 31.5 dB (Swanson et al 2004). In glaucoma, the size of the critical area enlarges with loss of RGCs, therefore more SAP test locations will fall to the left of the breakpoint (Figure 2-10).

2.4.7. Hood-Kardon model

The Hood-Kardon structure-function model is another model proposed as a method to relate OCT RNFL thickness to SAP measurements in decibels (Hood, & Kardon 2007). DLS values from each SAP test location are converted to linear units, which are then averaged and compared to global RNFL thickness. The model proposes that RNFL thickness is composed of 2 components, RGC axons and a residual thickness consisting of blood vessels and glial cells. The model also proposes decreases in DLS are accompanied by decrease in the RGC component but that the residual thickness does not change. This is contrary to the model of Harwerth and colleagues, which assumes that there is actually an increase in the residual thickness with loss of RNFL over time (Harwerth et al 2010). The Hood-Kardon model is summarised by the equation:

$$\textbf{RNFL thickness} = s0 \times 10^{0.1 \times D} + b \ (\text{if } D \geq 0)$$

$$\textbf{RNFL thickness} = s0 + b \ (\text{if } D \geq 0)$$

where s0 is the thickness of the RGC component, or signal, D is the loss of visual sensitivity on the decibel scale, and b is the residual thickness or base level. The authors estimated the base level from an analysis of eyes with severely depressed DLS due to anterior ischemic optic neuropathy. An interesting feature of this model is that it assumes that the relationship between RNFL thickness and SAP sensitivity is only significant in eyes with abnormal sensitivity (i.e., there is no relationship between RNFL thickness and SAP sensitivity in healthy eyes).

2.4.8. Drasdo model

The Drasdo model has been proposed as an alternative method of quantifying RGC loss from perimetric data (Drasdo et al 2008). The model considers increased RGC density in the central field, as well as the lateral displacement of RGC bodies from foveal cones (Drasdo et al 2007). RGC density corresponding to each of the 24-2 SAP test points was estimated. Similarly, to the other models, normative SAP data was obtained from the work of Heijl and colleagues, therefore for a healthy subject with a mean age of 34 years (Heijl et al 1987). RGC counts were assumed to decline by 0.59% per year, increasing to 0.79% at age 76 years, which translates to a loss of about 6,500 cells per year as described by Curcio and Drucker (Curcio, & Drucker 1993). Expected RGC density for any age above 34 years was then estimated using the formula:

RGC density at age 'a' = RGC density at age 34* {1-[(a – 34)/169]}

Age-expected SAP sensitivity was obtained using the method of point-wise age regression described by Heijl et al (Heijl et al 1987). Figure 2-11 shows an example of this analysis for a healthy 60-year-old subject.

Figure 2-11. Estimated RGC receptive field densities (D) and SAP sensitivities (S) for the right eye of a healthy 60-year-old subject. SAP sensitivity is displayed in bold as 1/Lambert units. Adapted from Drasdo et al 2008 (Drasdo et al 2008).

S_{60}			**316**	**372**	**302**	**288**		
D_{60}			64	66	68	78		
		501	**589**	**661**	**562**	**537**	**479**	
		87	111	118	119	123	128	
	468	**741**	**1148**	**1072**	**891**	**832**	**661**	**513**
	89	147	236	284	287	244	182	167
355	**617**	**1000**	**1318**	**1514**	**1479**	**1000**		**741**
67	108	219	481	1291	1327	505		188
331	**676**	**1175**	**1380**	**1660**	**1660**	**1148**		**832**
68	109	222	497	1533	1569	520		189
	575	**912**	**1413**	**1318**	**1175**	**1148**	**912**	**724**
	94	162	287	431	433	295	196	173
		661	**813**	**912**	**891**	**977**	**851**	
		107	151	190	190	164	148	
			562	**603**	**741**	**724**		
			96	105	107	109		

For eyes with glaucoma, Drasdo proposed a two-stage model, similar to the Hockey-Stick model (section 2.4.6, page 71), with a linear relationship between DLS and numbers of RGCs at locations with low DLS and a shallower relationship at locations with high DLS.

2.4.9. Zhu model

Recently Zhu and colleagues have recently described a novel method of predicting DLS from RNFL thickness using a type of neural network known as a Bayesian radial basis function (BRBF) (Zhu et al 2010). Classic linear regression analysis makes several incorrect assumptions about data, including an assumption that the relationship between RNFL thickness and DLS is linear or becomes linear after a transformation. In practice, the relationship between RNFL thickness and VF sensitivity is likely to change at difference stages of disease (or across the measurement range). Moreover, linear regression is

affected by outliers and assumes each RNFL value is independent of all other RNFL values, whereas in reality neighbouring RNFL values are topographically related. BRBF acts like a dynamic window that moves across the data spatially and at different disease stages, identifying groups of measurements that behave in a similar manner and improving predictions of DLS. The model provided a means to present structural information in the domain of the visual field and was found to predict DLS from RNFL thickness almost as well as another SAP test from the same patient.

2.4.10. Limitations of the models

Although each of the structure-function models provide insight into the relationship between glaucomatous structural changes (RNFL or RGC loss), and changes on SAP, they have limitations. For example, the Garway-Heath, Hockey-Stick and Drasdo models are all based on data obtained from histology of only 6 eyes from 5 young subjects, aged only 27 to 37 years (Curcio, & Allen 1990). The Harwerth model was derived from a much larger number of eyes, but from an animal model, with results extrapolated to humans (Harwerth et al 2010). Furthermore, close examination of previous studies shows that there is wide variation in SAP sensitivity for a given RGC density and many of the perimetric test locations with reduced sensitivity had normal RGC counts (Harwerth et al 2010; Kerrigan-Baumrind et al 2000; Malik et al 2012). Therefore, although, on average, estimates of RGC count from DLS may be accurate, estimates for individual patients may not. This is particularly true in healthy subjects, where variation in RGC counts and RNFL thickness is large.

A further limitation of the models is that although they attempt to relate changes in RNFL thickness to loss of SAP sensitivity, clinical studies have shown that the temporal relationship between structural and functional changes is imperfect (Kass et al 2002). RGCs may become dysfunctional without detectable changes to RNFL thickness, with the result that some patients may exhibit loss of SAP sensitivity without change on RNFL (Fortune et al 2013a), whereas others may have changes in RNFL prior to changes in SAP (section 2.3, page 51). Changes in RNFL thickness can also be caused by RGC shrinkage rather than frank loss of cells (Morgan 2002) and the RNFL may increase in thickness with surgical reduction of IOP (Aydin et al 2003). Agreement between structure and functional domains will also be affected by the choice of technology used; for example, SAP 24-2 has sparse sampling of the central field, which may reduce the strength of the structure-function correlation. Although some of the models consider non-neural components of the RNFL, one assumes this component does not change with disease progression (Hood-Kardon model) (Malik et al 2012).

Harwerth's model has some specific and serious limitations that should be emphasised. For example, although the model considers changes in RGC density at different eccentricities, it does not account for lateral displacement of foveal RGCs or changes in Ricco's area. Some of the effect of changes in Ricco's area is accounted for by correction for RGC density by eccentricity but the model does not account for changes in Ricco's area that occur with disease (section 2.4.1, page 62) (Redmond et al 2010). Due to the centre surround organization of receptive fields the influence of a RGC extends beyond its receptive field and with probability summation a single ganglion cell will contribute

little to the overall threshold response. Furthermore, Swanson and colleagues have recently highlighted that the OCT-derived RGC estimates assumes a mean RGC axon diameter of 0.9 μm, whereas the actual mean axon diameter is 0.5 to 0.7 μm (Swanson, & Horner 2015). This miscalculation results in OCT-derived estimates of RGC to be consistently lower than estimates derived from SAP and even this is a simplification as the diameter of RGC axons varies between axons and along the length of the same axon. RGCs have bulb shaped varicosities along their course, which are rich in mitochondria and in some instances these locations are 5 to 10 times larger than the diameter of the axon in the inter-bulb region (Wang et al 2003); a variation that may affect estimates of RGC count based on RNFL thickness measurements. In addition, there are 10 to 15 different types of RGC, each with different axonal and receptive field size (Dacey, & Lee 1994). Harwerth's model makes other unproven assumptions. For example, it is not clear from published data how the correction factor, *c*, was derived. Although it is proposed to correct for remodelling of the RNFL with advancing disease, remodelling of the RNFL is complex and has not been adequately quantified histologically. The correction factor for RGC estimates from RNFL may have been introduced to better fit RGC estimates from SAP and OCT, and later explained by remodelling.

It is also important to acknowledge that although structure function models strive to explain the relationship between glaucomatous structural changes and changes to visual function, there is unlikely to be a perfect relationship between structure and function. There is accumulating evidence, for example from Jonathan Crowston's group in Melbourne, that RGCs have the potential to recover some functional loss (Crowston et al 2017). Therefore, a sick RGC may

have impaired function but apparently normal structure on imaging, creating a disparity between structural and functional tests.

2.4.11. Integrating structural and functional measurements

The disparity between structural and functional tests means that we are likely to always need methods of assessing both domains. There has therefore been much interest in how to best integrate results from these tests in order to maximize the diagnostic and staging capabilities of available tests (Medeiros et al 2012; Russell et al 2012). At present, clinicians already integrate results as they intuitively combine information to decide if a patient is progressing. However, this approach is subjective and made difficult by the different measurement scales of devices.

Russell and colleagues have described how Bayesian mathematics can be used to incorporate information about rate of change in neuroretinal rim over time to improve estimates regarding rates of change in visual field and therefore better predict those at risk of visual loss (Russell et al 2012). A similar method could also be used to incorporate information about demographic and clinical risk factors as priors.

Another approach of combining information from structural and functional tests is the combined structure function index (CSFI) described by Medeiros at UCSD (Medeiros et al 2012). The CSFI is based on the formulae developed by Harwerth and colleagues described in section 2.4.4, page 66 and is an estimate of the percentage of RGCs lost compared to that expected for a healthy subject

of similar age. The CSFI combines the RGC estimates derived from OCT and SAP measurements, with a weighting that assigns greater emphasis to RGC estimates from OCT in early disease, and greater emphasis to estimates from SAP in advanced disease based on the evidence that accuracies of SAP and imaging tests are inversely related to disease severity. Medeiros proposed combining the estimates of RGC count from SAP (SAPrgc) and OCT (OCTrgc) using the formula:

Estimated RGC count = (1 + MD/30)*OCT*rgc* + (-MD/30)*SAP*rgc*

Where MD is the SAP MD. Medeiros estimated RGC counts in healthy eyes using the same formula and from this calculated an estimate of the percentage of RGCs an eye has lost compared to that expected for a healthy age-matched individual (Medeiros et al 2012). The CSFI was then calculated using the following formula:

CSFI = [(expected RGC count – estimated RGC count)/(expected RGC count)]*100

The CSFI has the advantage of providing an intuitive unit of measurement compared to Bayesian methods of integrating structure and function, and it has been shown to have good ability to distinguish healthy and glaucomatous eyes at all stages of disease, including in eyes with preperimetric glaucoma (Medeiros et al 2012). Moreover, by combining information from structural and functional tests it may reduce the effect of variability inherent in each test and obtain more accurate estimates of RGC number. The CSFI is however limited by the weakness inherent in Harwerth's formulae (section 2.4.10, page 76). Although the CSFI relies on primarily RNFL in early disease and SAP in advanced disease,

Swanson has recently shown that the Harwerth RNFL formula over-estimate neural loss compared to the Harwerth SAP formula at all stages of disease (Swanson, & Horner 2015). Therefore, it is likely that the CSFI underestimates RGC number in early disease compared to RGC estimates in late disease. However, despite these limitations the CSFI is currently the only index to provide an estimate of RGC loss compared to numbers expected for a healthy age-matched individual.

In summary, structure-function models broadly adopt one of two approaches; either they attempt to directly quantify the relationship between loss of RNFL and SAP sensitivity (Hood-Kardon model), or they relate these changes to estimated underlying loss of RGCs (Harwerth model, Swanson model, Drasdo model). The models provide evidence that structural and functional measurements are related, suggesting that structural changes are a clinically relevant surrogate for functional losses in glaucoma. However, the models are based on cross-sectional data and do not fully address the longitudinal relationship between structural changes and visual loss. In addition, large clinical studies have shown that disagreement between structure and function is common, something not addressed in structure-function models (section 2.3, page 51) (Kass et al 2002) Reasons for disagreement include differences in dynamic range and measurements scale, however, there is also growing evidence that RGCs may show some recovery with glaucoma treatment, indicating that RGCs may become dysfunctional prior to apoptosis and measurable permanent structural change. Disparity between structure and function should therefore be expected and for optimal detection of glaucoma and

glaucoma progression we need to continue to test both structural and functional domains. Combining information from structural and functional tests may also be useful for better understanding of how glaucoma affects important patient-relevant functional endpoints, such as the ability to perform vision-related tasks of daily living, however, there is a lack of research in this area. Also, while the implications of a detectable loss of visual field are obvious for the patient, that is not so much the case for structural changes such as thinning of the RNFL or neuroretinal rim (Medeiros et al 2016). Clinical studies have shown that progressive glaucomatous structural changes are associated with increased risk of visual loss but it is important to demonstrate that progressive structural changes are predictive of outcomes that are clinically relevant for patients. The aim of this body of work was to explore the structure-function relationship and to ascertain the point at which structural changes become associated with impaired ability to perform vision-dependent tasks. The following section of this thesis outlines the materials and methods of this research project.

3 SECTION III: MATERIALS AND METHODS

3.1. Hamilton Glaucoma Center

Most the work for this project was conducted at the HGC at UCSD working under the supervision of Dr Robert Weinreb, Dr Felipe Medeiros and Dr Linda Zangwill. Patients were recruited from two large on-going prospective longitudinal studies; the African Descent and Glaucoma Evaluation Study (ADAGES) and the Diagnostic Innovations in Glaucoma Study (DIGS) (Sample et al 2009). ADAGES is a 3-site collaboration including HGC at the Department of Ophthalmology, UCSD (data coordinating centre), the New York Eye and Ear Infirmary, and the Department of Ophthalmology, University of Alabama, Birmingham (UAB). The DIGS includes only patients recruited at UCSD and the protocol is identical to that of the ADAGES. Data are centrally processed and analysed at UCSD through established reading centres. The institutional review boards at all 3 sites approved the study methods for ADAGES and the institutional review board at UCSD approved the methods for DIGS and for the current body of work. Study methods adhered to the tenets of the Declaration of Helsinki and all participants gave written informed consent. Normal and patient participants were recruited from the glaucoma clinics and optometric practices at each of the 3 recruiting sites, by advertisement and community presentations, and by referral from other ophthalmologists.

3.2. Testing Protocol

At each visit, subjects underwent a comprehensive eye examination including relevant medical history, blood pressure measurement, best-corrected visual acuity, slit-lamp biomicroscopy, gonioscopy, Goldmann applanation

tonometry, central corneal thickness measurement, dilated fundoscopy, stereoscopic ophthalmoscopy of the optic disc with a 78-diopter lens, and simultaneous stereoscopic disc photography. Central corneal thickness (CCT) was calculated as the average of three measurements obtained during the same visit using an ultrasound pachymeter (Pachette GDH 500; DGH Technology, Inc, Philadelphia, PA, USA). Digital stereoscopic images were reviewed with a stereoscopic viewer (Screen-VU stereoscope, PS Mfg., Portland, Oregon, USA) by two or more experienced graders, with each grader masked to the subject's identity and to the other test results. SAP was obtained using the Humphrey Field Analyzer II (Carl Zeiss Meditec, Dublin, CA, USA) and the 24-2 Swedish Interactive Threshold Algorithm strategy. All subjects also had ONH and RNFL imaging using Cirrus SDOCT (software version 6.0; Carl Zeiss Meditec Inc, Dublin, CA), Spectralis SDOCT (Heidelberg Engineering, Dossenheim, Germany). Consecutive series of subjects participating in the DIGS and ADAGES had additional tests for the current body of work. This included testing with automated pupillometry (section 4.3, page 114) and performing a simulated driving task (section 4.4, page 137). These additional tests are described in detail in the relevant sections of this thesis.

3.2.1. Inclusion criteria

For inclusion in the study, all subjects were required to have open angles on gonioscopy, a best-corrected visual acuity of 20/40 or better, and refraction less than 5.0 dioptres sphere and 3.0 dioptres cylinder. All participants were older than 18 years. Diabetic participants with no evidence of retinal involvement were

included. Subjects were required to have at least one good quality stereophotograph and one reliable SAP result.

3.2.2. Exclusion criteria

Subjects were excluded if they presented with a best-corrected visual acuity of less than 20/40, spherical refraction outside ±5.0 dioptres and/or cylinder correction outside 3.0 dioptres, or any other ocular or systemic disease that could affect the optic nerve or the visual field. They were also excluded if they had a history of intraocular surgery (except for uncomplicated cataract or glaucoma surgery); secondary causes of glaucoma (e.g., iridocyclitis, trauma); other systemic or ocular diseases known to affect the visual field (e.g., pituitary lesions, demyelinating diseases); significant cognitive impairment; history of stroke, Alzheimer disease, or dementia or problems other than glaucoma affecting colour vision.

3.2.3. Optical coherence tomography

Measurements of cpRNFL were obtained using two SDOCT devices; Cirrus SDOCT (software version 6.0; Carl Zeiss Meditec, Inc, Dublin, CA) and Spectralis SDOCT (software version 5.4.7.0; Heidelberg Engineering, Dossenheim, Germany). The Spectralis OCT uses a dual-beam SDOCT and a CSLO that works by emitting a superluminescent diode light with a centre wavelength of 870 nm and another infrared scan to simultaneously provide images of ocular microstructures. A real-time eye tracking system is incorporated that couples CSLO and SDOCT scanners to adjust for eye movements and to ensure that the same location of the retina is scanned over time. 1536 A-scan points were acquired from a 3.45-mm circle centred on the optic disc. Spectralis

SDOCT images were reviewed by the UCSD Imaging Data Evaluation and Analysis Centre to ensure the scan was centred, that the signal strength was >15dB and that there were no artefacts. Scans that were inverted, clipped or those that had coexistent retinal pathological abnormalities were excluded. The RNFL segmentation algorithm was also checked for errors.

The Cirrus SDOCT uses a superluminescent diode scan with a centre wavelength of 840 nm and an acquisition rate of 27,000 A-scans per second. The optic disc cube 200 x 200 protocol was used to acquire RNFL thickness measurements. This protocol is based on a 3-dimensional scan of a 6 × 6 mm area centred on the optic disc in which information from a 1024 (depth) × 200 × 200 point parallelepiped is collected. The cpRNFL thickness measurements from Cirrus were calculated from a 3.46-mm diameter circular scan (10.87-mm length) automatically placed around the optic disc. The reported average RNFL thickness corresponded to the 360-degree measure automatically calculated by the OCT software. The Cirrus SDOCT images were also reviewed by the UCSD Imaging Data Evaluation and Analysis Centre and included if the signal strength was greater than 7, if movement artefacts were absent, and there was good centring on the optic disc.

3.2.4. Standard automated perimetry

SAP was performed using the Humphrey Field Analyzer II (Carl Zeiss Meditec, Dublin, CA, USA) and all fields were evaluated by the UCSD Visual Field Assessment Centre. Visual fields with more than 33% fixation losses or false-negative errors, or more than 15% false-positive errors, were excluded. The only exception was the inclusion of visual fields with false-negative errors of more

than 33% when the field showed advanced disease. Visual fields exhibiting a learning effect (i.e., initial tests showing consistent improvement on visual field indices) were also excluded. Visual fields were further reviewed for the eyelid and rim artefacts, fatigue effects, inappropriate fixation and evidence that the visual field results were caused by a disease other than glaucoma. An abnormal SAP test was defined as a visual field with a pattern standard deviation with $P < 0.05$ and/or a Glaucoma Hemifield Test outside normal limits.

3.3. Study Definitions

Participants were defined depending on the diagnosis in their worse eye as healthy or glaucomatous. Glaucoma was defined by the presence of three or more consecutive abnormal SAP tests or evidence of progressive glaucomatous optic disc changes based on masked assessment of stereophotographs. Glaucomatous optic disc damage was defined as evidence of excavation, neuroretinal rim narrowing or notching, localized or diffuse RNFL defect, or a between-eye asymmetry of the vertical cup-disc ratio more than 0.2. Suspect glaucoma was defined by the presence of suspicious neuroretinal rim narrowing or RNFL defects on masked stereophotograph assessment, without repeatable abnormal SAP defects. OHT was defined as eyes with IOP > 21 mmHg but with healthy-appearing optic discs and without repeatable abnormal SAP results. Healthy subjects were recruited from the general population through advertisements and from the staff and employees of UCSD. Healthy eyes were required to have IOP ≤ 21 mmHg with no history of increased IOP and normal SAP.

3.4. Statistical Methods

The statistical methods used for each part of my research are described in detail in the relevant sections, however in brief; normality assumption was assessed by inspection of histograms and using Shapiro-Wilk tests. Descriptive statistics included mean and standard deviation for normally distributed variables, and median, first-quartile and third-quartile values for non-normally distributed variables. Student *t*-tests were used for group comparison for normally distributed variables and Wilcoxon rank-sum test for continuous non-normal variables. For categorical variables, X^2 tests or Fisher exact tests were used. All statistical analyses were performed with commercially available software (STATA, version 12; StataCorp LP, College Station, TX, USA). The α level (type I error) was set at 0.05. The following section outlines the aims and plan of the research.

4 SECTION IV: EXPERIMENTS

4.1. Aims and Plan of Research

Structural parameters such as measurements of RNFL thickness from OCT are widely used to detect glaucoma and quantify rates of progression, however the true relevance of these measurements remains poorly understood. For example, it is not known at which point structural changes become associated with decreased ability to perform vision-dependent tasks of daily living. Furthermore, it is not known whether information from structural tests may provide additional information compared to conventional measures of visual function for predicting the impact of glaucoma on ability to perform such tasks. Improved understanding of the relationship between structural and functional changes could provide further validation for the use of structural measures as a clinically relevant parameter in glaucoma management. The aim of my MD(Res) was to explore the relationship between glaucomatous structural changes and measures of visual function. The body of work was divided into three parts.

1. In part 1 (section 4.2, page 94) I examine the relationship between structural and functional changes by examining estimated RGC losses in eyes with localised loss of the RNFL (Tatham et al 2013). Localised RNFL losses are often considered an early manifestation of glaucomatous structural damage, however I hypothesised that they might be associated with large underlying RGC losses. I identified eyes with localised RNFL defects on stereophotographs and estimated corresponding RGC losses in involved sectors using formulae proposed by Harwerth and colleagues (Harwerth et al 2010) and modified by Medeiros and colleagues (Medeiros et al 2012), described in detail in section 2.4.4, page 66 and section 2.4.11,

page 79. Although I found localised RNFL defects visible on photographs were associated with large estimated RGC loss, through this phase of my studies I discovered serious flaws in the assumptions of the model used to estimate RGC counts, which are discussed in this section.

2. Part 2 of my research (section 4.3, page 114) was to examine the relationship between glaucomatous structural loss and an objective measure of visual function related to RGC integrity – the pupillary light response (Tatham et al 2014b). Although previous investigators have examined the relationship between structural changes and DLS, little is known about the correlation between glaucomatous structural changes and pupil responses. The pupil response is a rapid, objective method of assessing the afferent visual pathway. Pupil responses were assessed using an automated pupillometer and the magnitude of pupil response asymmetry compared to inter-eye differences in RNFL thickness and SAP MD.

3. The final part of this body of work (section 4.4, page 137) examines the relationship between glaucomatous structural loss and the ability to perform a vision-related performance-based task related to activities of daily living (Tatham et al 2014a). Driving is an important activity of daily living for many patients with glaucoma and arguably a performance-based test, such as ability to drive, may be of more relevance to quality of life, than traditional tests of visual function such as SAP. It is therefore important to understand the relationship between glaucomatous structural changes and ability to perform tasks such as driving. This section also explores whether including

information from OCT might improve the ability to predict driving performance compared to perimetry alone.

4.2. The relationship between localised RNFL loss and estimated loss of RGCs

4.2.1. Background

A common structural manifestation of glaucoma visible on dilated fundus examination is the localised RNFL defect, often considered to occur early during disease (Quigley 1986). In fact, several tools used for glaucoma detection focus on detecting localised changes, typical of glaucoma, for example, the visual field indices GHT and PSD. For this section of my research I decided to examine the relationship between localized RNFL defects and estimated numbers of RGCs, to determine whether localised RNFL defects are indeed an early feature of glaucoma. As the number of RGCs is directly related to visual function and the prognosis for retaining useful vision, I also hoped this analysis would provide some insight into the relevance of localised RNFL loss for patients.

As RGC loss cannot be measured in vivo directly I decided to estimate RGC loss from observed structural and functional changes. After considering the methods of estimating RGC loss appraised in section 2.4, page 62 I opted to estimate RGC loss using the CSFI suggested by Medeiros from formulae developed by Harwerth and colleagues (Harwerth et al 2010; Medeiros et al 2012). Although the CSFI has limitations, discussed in detail in sections 2.4.10, page 76, and 2.4.11, page 79, were the formulae accurate it would provide an attractive method of estimating the percentage of RGCs lost compared to that expected for a healthy eye from a similar aged individual and it is currently the only model designed for this purpose.

The CSFI was developed as a global index, however, as eyes with localised RNFL defects may have relative preserved RNFL in sectors outside the visible defect, a global index may fail to reflect the depth of localised loss. This is often apparent on OCT cpRNFL analysis, when compared to the normative database, the global average cpRNFL thickness may be classified as normal despite one sector being abnormal. To estimate RGC losses in the region of a visible localised RNFL defect I needed to modify the global CSFI to obtain a sector CSFI. As the estimate of RGC numbers is obtained from information from OCT and SAP it was important not to use information from these instruments when identifying patients and the location of structural losses. I decided to identify patients by reviewing the library of stereophotograph images from patients involved in the DIGS at UCSD. All patients with a localised RNFL defect visible on stereophotographs were identified and further examined as outlined in the methods (4.2.3).

In healthy eyes the RNFL has a bright, striated appearance, and is most readily identifiable close to the superior and inferior poles of the optic disc where the RNFL is thickest (Quigley 1986). RNFL striations are due to bundles of RGC axons separated by Muller cell processes, with the bright component the highly reflective parallel RGC axon bundles and the dark component the thick non-reflective dividing Muller cell glial septa (Radius, & Anderson 1979). RGC axonal loss leads to a reduction in the reflectivity of RGC axon bundles. Diffuse loss leads to a darkened appearance to the inner retina and increased visibility of blood vessels, whereas localised RNFL defects tend to be wedge-shaped with sharply demarcated borders narrowing towards the disc margin as the RNFL bundles converge. Localised RNFL defects may be associated with non-

glaucomatous conditions, including other optic neuropathies or optic disc drusen, however, they have high specificity for glaucoma and are not found in healthy eyes (Jonas, & Schiro 1994b; Jonas, & Schiro 1994a).

Although localised RNFL defects are traditionally viewed as an early sign of glaucomatous damage (Sommer et al 1991; Quigley 1986), a previous primate study found that a localized RNFL defect was only apparent on fundus photographs if more than 50% of the thickness of the RNFL had been lost (Quigley, & Addicks 1982). A second study, including human eyes also found large neural losses with localized loss of 28 to 45% of RNFL thickness in areas corresponding to visible RNFL defects (Quigley 1986).

4.2.2. Purpose

The purpose of this phase of my research was to estimate the percentage of RGC loss in eyes with localised RNFL defects visible on stereophotographs. I modified the CSFI to obtain a sectorial estimate of RGC loss, which could be related to regions of RNFL loss visible on stereophotographs. Estimates of RGC loss in sectors with a visible RNFL defect were compared to estimates of RGC numbers in areas without a visible RNFL defect and to estimates in healthy eyes.

4.2.3. Methods

This phase of my research included 264 eyes of 193 individuals recruited from the DIGS at UCSD. There were 66 eyes of 55 subjects with glaucoma and localised RNFL defects visible on fundus stereophotographs and 198 eyes of 138 healthy subjects. All subjects underwent testing as described in section 3.2, page 84. Localised RNFL defects, identified by at least 2 graders, were defined as

defects wider than twice the width of an arteriole, extending from close to the disc margin into the parapapillary area, widening en route (i.e., wedge-shaped) (Quigley 1986). Slit defects narrower than the diameter of adjacent vessels were not included as they are frequently found in normal eyes (Jonas, & Schiro 1994b).

Estimating sectorial RGC loss

The CSFI involves estimating RGC loss from RNFL and SAP measurements, and combining the estimates, with a weighting to account for disease severity (Sector 2.4.11) (Medeiros et al 2012). To estimate localised RGC loss, it was necessary to use a structure-function map to relate RNFL thickness to corresponding SAP sensitivities. Several structure function maps have been described (Wirtschafter et al 1982; Weber et al 1990; Yamagishi et al 1997; Anton et al 1998; Garway-Heath et al 2000; Garway-Heath et al 2002; Harwerth et al 2010), the foremost of which is the Garway-Heath map (Garway-Heath et al 2000). The Garway-Heath map was derived from examination of 69 eyes with well-defined localised RNFL defects or prominent RNFL bundles. A scaled Humphrey 24-2 visual field and ONH reference circle was superimposed onto fundus photographs for these eyes and the visual field test points related to regions of the ONH (Figure 4-1). The map divides the ONH into 6 sectors, with 3 regions of the visual field corresponding to the nasal half of the ONH falling largely outside the region of the 24-2 field. The central region of the visual field is associated with the temporal sector of the ONH from 311 to 40 degrees, the superior arcuate region of the field is associated with the inferior temporal ONH from 271 to 310 degrees, and the inferior arcuate region of the field is associated

with the superior temporal sector from 41 to 80 degrees. The map has subsequently been shown to be a good predictor of correlation between DLS and quantitative measurements of RNFL thickness obtained using OCT (Ferreras et al 2008) and a slightly modified version of the map was published in 2002 with the ONH divided into sectors to match the divisions on CSLO (Garway-Heath et al 2002).

Figure 4-1. Garway-Heath et al structure-function map showing division of the visual field and optic nerve head (A) with the regions of the RNFL profile that correspond to the superior (blue) and inferior (red) temporal arcuate fibres. Adapted from (Garway-Heath et al 2000) and (Hood, & Kardon 2007).

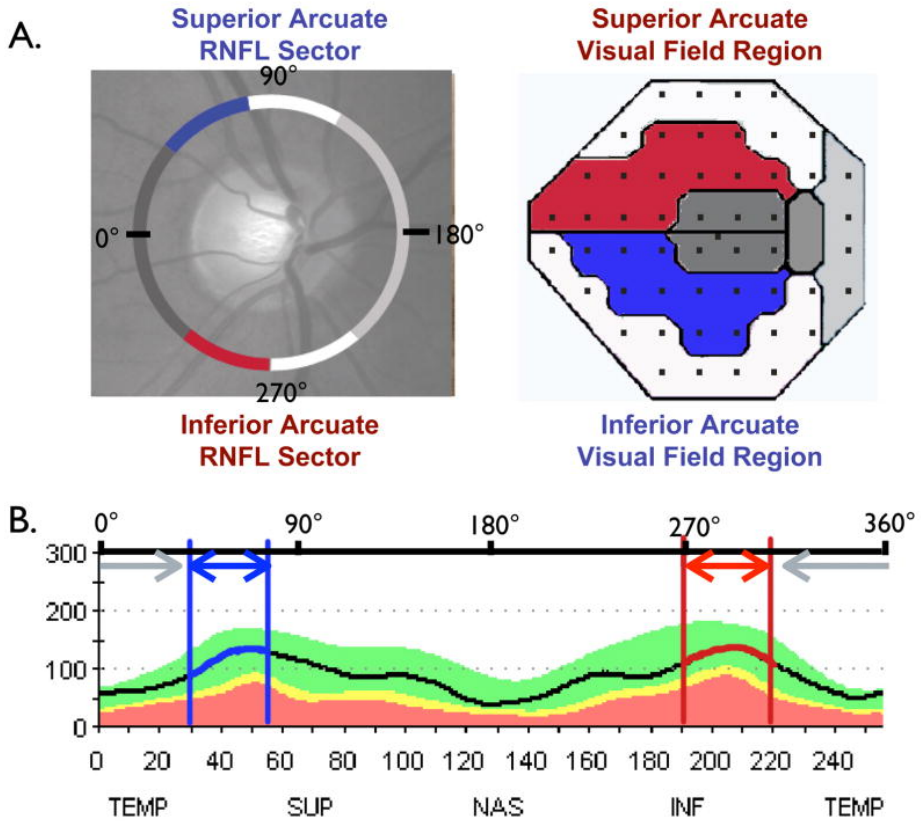

The Harwerth map was developed following studies in nonhuman primates described in section 2.4.4, page 66 (Harwerth et al 2007). The map was

designed to maximise correlation between estimates of RGC number derived from SAP sensitivities and measurements of RNFL thickness on OCT. The final map involved dividing the ONH into 10 equal 36-degree sectors (Figure 4-2) (Harwerth et al 2007). The number of SAP locations assigned to each ONH sector varied from one SAP location near the fovea (entering the ONH at sector 1 or 10) to 13 SAP locations for the arcuate regions (entering the ONH at sectors 4 or 7).

Figure 4-2. Harwerth structure function map showing 10 sectors of the visual field and 10 corresponding ONH sectors (Harwerth et al 2007).

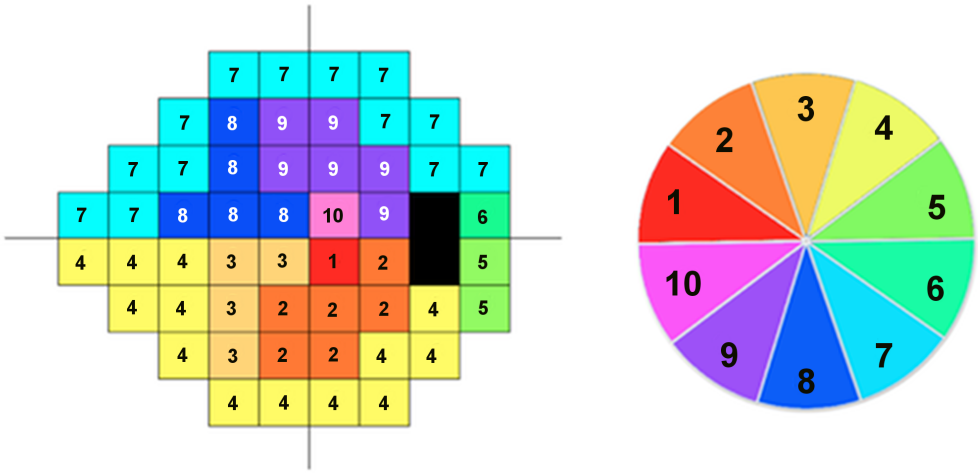

Using the Harwerth map, I planned to estimate the number of RGCs in each of the 10 sectors and then relate these estimates to the location of the visible RNFL defects. All subjects had cpRNFL thickness measured using Spectralis OCT, which provides 1,536 A-scan points from a 3.45mm circle scan. The average cpRNFL thickness in each of the sectors was calculated by taking the average of 154 adjacent A-scans for each of sectors 1 to 6, and the average of 153 adjacent A-scans for sectors 7 to 10. The number of RGC axons in each

sector was estimated using the following formula adapted from Harwerth and colleagues' original formula (Harwerth et al 2010) (section 2.4.4, page 66).

$$d = (-0.007 * age) + 1.4$$

$$c = (-0.26 * sMD) + 0.12$$

$$\text{sector } OCTrgc = 10^{(\{[\log10(\text{sector RNFL} * 10870 * d)] * 10 - c\} * 0.1)}$$

Where d is the axonal density (axons/μm^2), c is a correction factor for the severity of disease to consider remodelling of RNFL axonal and non-axonal composition, *sMD* is the sector mean deviation and sector OCTrgc is the estimated number of RGC axons in the sector. *sMD* was calculated by measuring the deviation of the SAP sensitivity from the expected sensitivity of SAP test locations in each sector. Expected values were derived from the SITA normative database using the method described by Harwerth and colleagues (Table 4-1) (Harwerth et al 2010). *sMD* was calculated as the geometric mean by converting logarithmic values from each visual test location to linear values prior to averaging.

Table 4-1. Predicted mean visual field sensitivities for healthy eyes in each of the 10 sectors of Harwerth and colleagues structure function map (Harwerth et al 2010).

Sector Number	1	2	3	4	5	6	7	8	9	10
Slope (dB/year)	-0.057	-0.061	-0.060	-0.062	-0.057	-0.057	-0.061	-0.057	-0.062	-0.060
Intercept (dB)	34.68	33.60	33.32	31.68	31.68	31.68	31.19	33.46	33.01	34.45

The numbers of RGCs was also estimated from SAP sensitivities at the test locations corresponding to each sector using the formulae previously described in section 2.4.4, page 66, to obtain sector SAPrgc estimates. A combined structure-function estimate of RGC numbers (weighted RGC count, wrgc) was then calculated by averaging OCTrgc and SAPrgc using the weighting described by Medeiros (Medeiros et al 2012) (section 2.4.11, page 79), assigning relatively greater value to OCT in early disease and to SAP in more advanced disease.

sector *wrgc* = (1 + *sMD*/30)*sector OCT*rgc* + (-*sMD* /30)*sector SAP*rgc*

I then calculated an estimate of percentage of RGC loss in each sector compared to that expected for a healthy eye of similar age – the sector CSFI, like the global CSFI previously described by Medeiros and colleagues (Medeiros et al 2012).

To estimate sector RGC counts in healthy eyes I used a development sample of 169 healthy eyes recruited from the general population, involved in the DIGS. The inclusion criteria for healthy subjects has been detailed elsewhere in this thesis (section 3.3, page 88). Numbers of RGCs were estimated for each sector of the structure-function map and 10 regression models developed (one for each sector) to relate estimated numbers of RGCs to age and optic disc area, which have been shown to influence RGC numbers (Harwerth et al 2010). To avoid model over fitting none of the eyes in the development sample were included in the subsequent analysis. The sector CSFI was then calculated as an estimate of the percentage of RGCs lost in each sector using the formula:

Sector CSFI = [(expected number of RGCs in sector - sector *wrgc*) /

(expected number of RGCs in sector)]*100

The location of the RNFL defect was determined from optic disc stereophotographs by superimposing a 10-segment (36-degree) circle, corresponding to the 10 zones of the structure function map (Figure 4-3). The circumference of the 10-segment circle was manually adjusted for best possible fit to the margin of the optic disc using image processing software (GNU Image Manipulation Program, 2.8.18, https://www.gimp.org). The ONH sectors of the structure-function map corresponding to the visible RNFL defect were noted with the defect deemed to affect all sectors that it straddled. Left eyes were transposed horizontally to a right eye position so that the 9 o'clock sector represented the inferior-temporal ONH in all eyes.

Figure 4-3. Example of an eye included in the study with a localised RNFL defect (arrows). The location of the RNFL defect was determined by superimposing a 10-segment circle on the ONH image, corresponding to the 10 zones of Harwerth's structure function map. In this example, the visible RNFL defect is in sector 8.

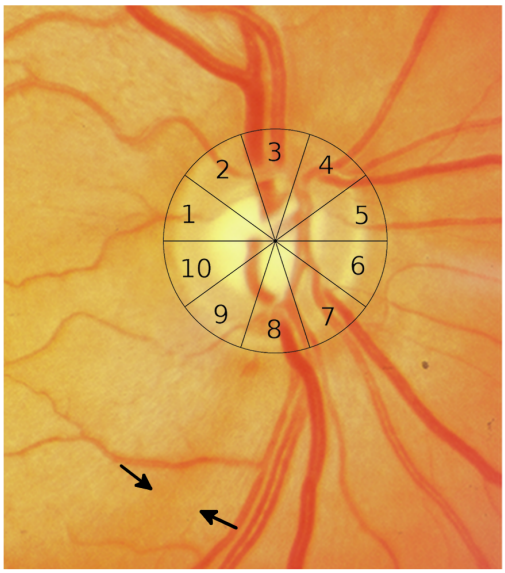

Statistical Analysis

Descriptive statistics were performed according to the methods described in section 3.4, page 89. The sector CSFI in sectors with localised RNFL defects was compared to the sector CSFI in sectors without defects in patients with glaucoma and healthy controls.

4.2.4. Results

The demographic and clinical characteristics of patients included in this phase of the research are summarised in Table 4-2. Fifty-six eyes had a single RNFL defect and 10 had RNFL defects at two discontiguous locations, resulting in a total of 76 RNFL defects. Twenty-six contiguous RNFL defects (34.2%) involved 1 sector, 40 (52.6%) involved 2 sectors, and 10 (13.2%) involved 3 sectors for a total of 136 sectors with and 524 sectors without localised RNFL defects in eyes with glaucoma. Sector 9 (inferior-temporal sector) had most RNFL defects (52 eyes, 78.8%), followed by sector 8 (46 eyes, 69.7%), sector 2 (12 eyes, 18.2%), sector 3 (10 eyes, 15.2%), sector 10 (7 eyes, 10.6%) and sector 7 (6 eyes, 9.1%). There was only one RNFL defect in sector 1 and one in sector 5 and none involved sectors 4 or 6 (nasal sectors).

Table 4-2. Demographic and clinical characteristics of glaucomatous patients with visible localised RNFL defects compared to similarly aged healthy subjects.

	Healthy Eyes = 198 Subjects = 138	**Visible localised RNFL defect** Eyes = 66 Subjects = 55	**P Value**
Age (years)[a]	62.5 (55.7 to 69.5)	63.4 (56.1 to 71.6)	0.248[c]
Race			0.001[d]
European Ancestry	126	27	
African Ancestry	72	39	
Mean Deviation (dB) [a]	-0.1 (-1.0 to 1.0)	-3.3 (-5.9 to -1.4)	<0.001[c]
Mean RNFL thickness (um)	96.3 ± 10.2	76.0 ± 12.9	<0.001[b]
Estimated number of RGCs	968,883 ± 170,230	657,172 ± 163,599	<0.001[b]
Global CSFI (%)	1 ± 13	39 ± 15	<0.001[b]
CSFI1 (%)	4 ± 19	10 ± 27	0.027[b]
CSFI2 (%)	1 ± 21	13 ± 31	0.007[b]
CSFI3 (%)	-2 ± 22	30 ± 22	<0.001[b]
CSFI4 (%)	-1 ± 20	19 ± 23	<0.001[b]
CSFI5 (%)	2 ± 28	16 ± 30	0.012[b]
CSFI6 (%)	3 ± 27	4 ± 34	0.985[b]
CSFI7 (%)	2 ± 23	26 ± 28	<0.001[b]
CSFI8 (%)	-1 ± 18	52 ± 24	<0.001[b]
CSFI9 (%)	2 ± 21	52 ± 26	<0.001[b]
CSFI10 (%)	3 ± 16	19 ± 42	0.004[b]

[a]Median (interquartile range), [b]t-test, [c]Wilcoxon-Rank sum test, [d]Chi-square test

Sectors with visible RNFL defects had significantly worse CSFI, indicating greater estimated percentage loss of RGCs, compared to sectors of glaucomatous eyes without localised RNFL defects (59 ± 21% versus 15 ± 29% respectively, P<0.001) (Table 4-2). The distribution of CSFI in sectors with a localised RNFL defect visible defects is shown in Figure 4-4.

Figure 4-4. Histogram showing the distribution of CSFI in sectors of glaucomatous eyes with visible localised RNFL defects.

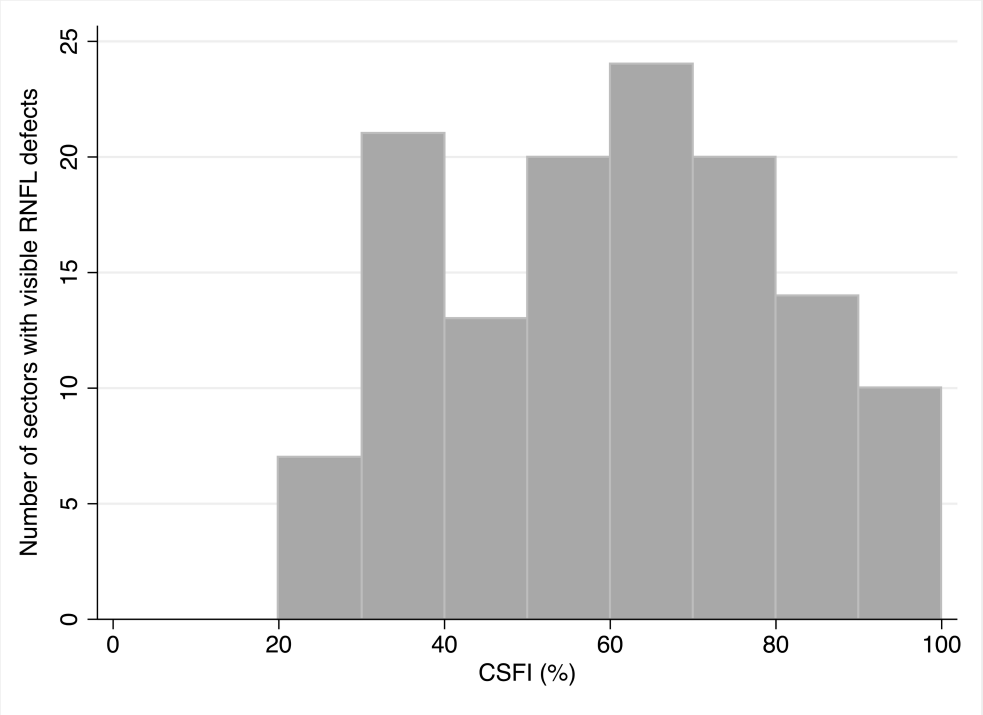

Glaucomatous eyes had on average lost 59% of RGCs in sectors with visible RNFL defects and 15% in sectors without visible RNFL defects. The sector CSFI was worse in glaucomatous compared to healthy eyes in all sectors, except sector 6.

Figure 4-5. Box plot showing distribution of sector CSFI in healthy eyes compared to sectors of glaucomatous eyes with and without visible localised RNFL defects.

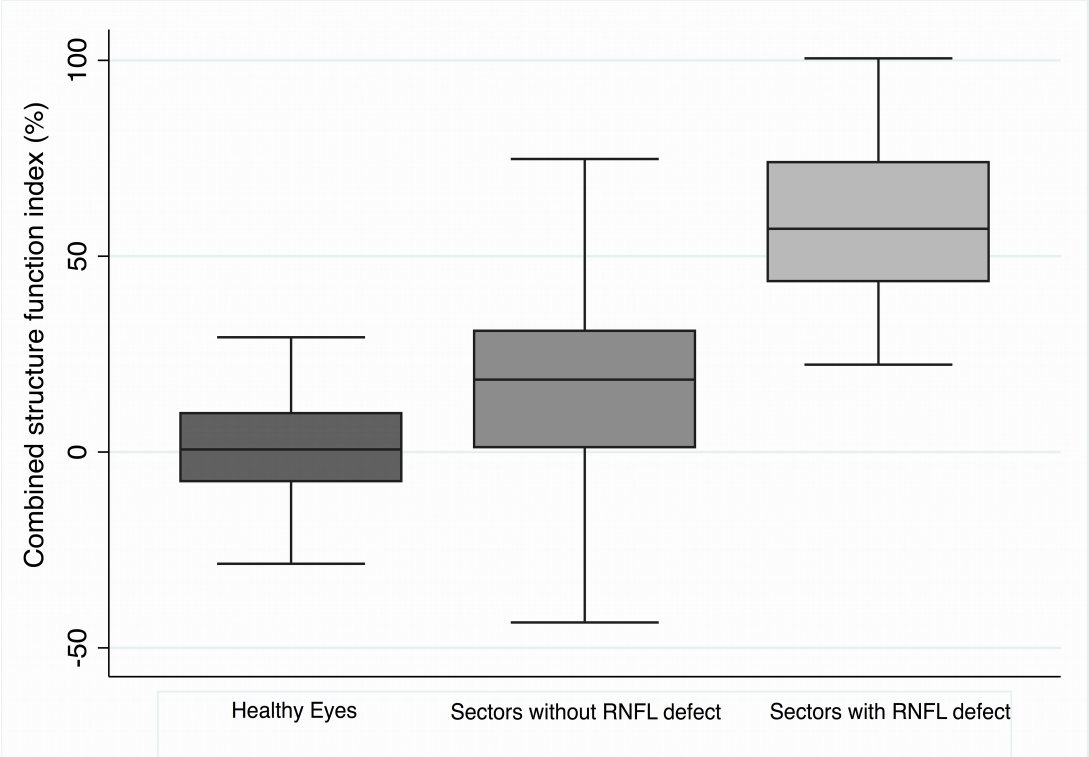

Sectors with an RNFL defect had significantly higher CSFI than the immediately adjacent sectors (P <0.001), with an average CSFI of 22 ± 24% in sectors immediately clockwise and anti-clockwise to RNFL defects. The sector with the maximum estimated RGC loss was in the same sector as a localised RNFL defect in 50 eyes (75.8%) and in the same or adjacent sector as a localised RNFL defect in 59 eyes (89.4%). Examples of eyes included in this phase of the research are shown in Figure 4-6 and Figure 4-7.

Table 4-3. Sector CSFI for sectors of glaucomatous eyes with and without visible localised RNFL defects (n = 660 sectors).

	Number of RNFL defects	CSFI for sectors of glaucomatous eyes without RNFL defects	CSFI for sectors of glaucomatous eyes with RNFL defects	P-value[a]
Sector 1	2	9 ± 27	43	
Sector 2	12	5 ± 27	50 ± 17	<0.001
Sector 3	10	25 ± 18	61 ± 14	<0.001
Sector 4	0	19 ± 23	No eyes with defect in sector 4	
Sector 5	1	16 ± 30	65	
Sector 6	0	4 ± 34	No eyes with defect in sector 6	
Sector 7	6	23 ± 27	62 ± 18	<0.001
Sector 8	46	39 ± 22	58 ± 22	0.002
Sector 9	52	23 ± 22	60 ± 20	<0.001
Sector 10	7	12 ± 38	75 ± 32	<0.001
All sectors	136	15 ± 29	59 ± 21	<0.001

[a]t test.

Figure 4-6. Optic disc photographs, SDOCT and SAP for 3 eyes of patients included in the study. Patient one (left column) has an inferior-temporal RNFL defect visible on photographs. The CSFI in the sectors corresponding to the defect was 57 to 68%. Patient two (central column) has an RNFL defect associated with a CSFI of 81 to 85%, indicating an estimated 81 to 85% loss of RGC axons in this region. Patient three (right column) has an RNFL defect with a CSFI 21 to 35% in corresponding sectors.

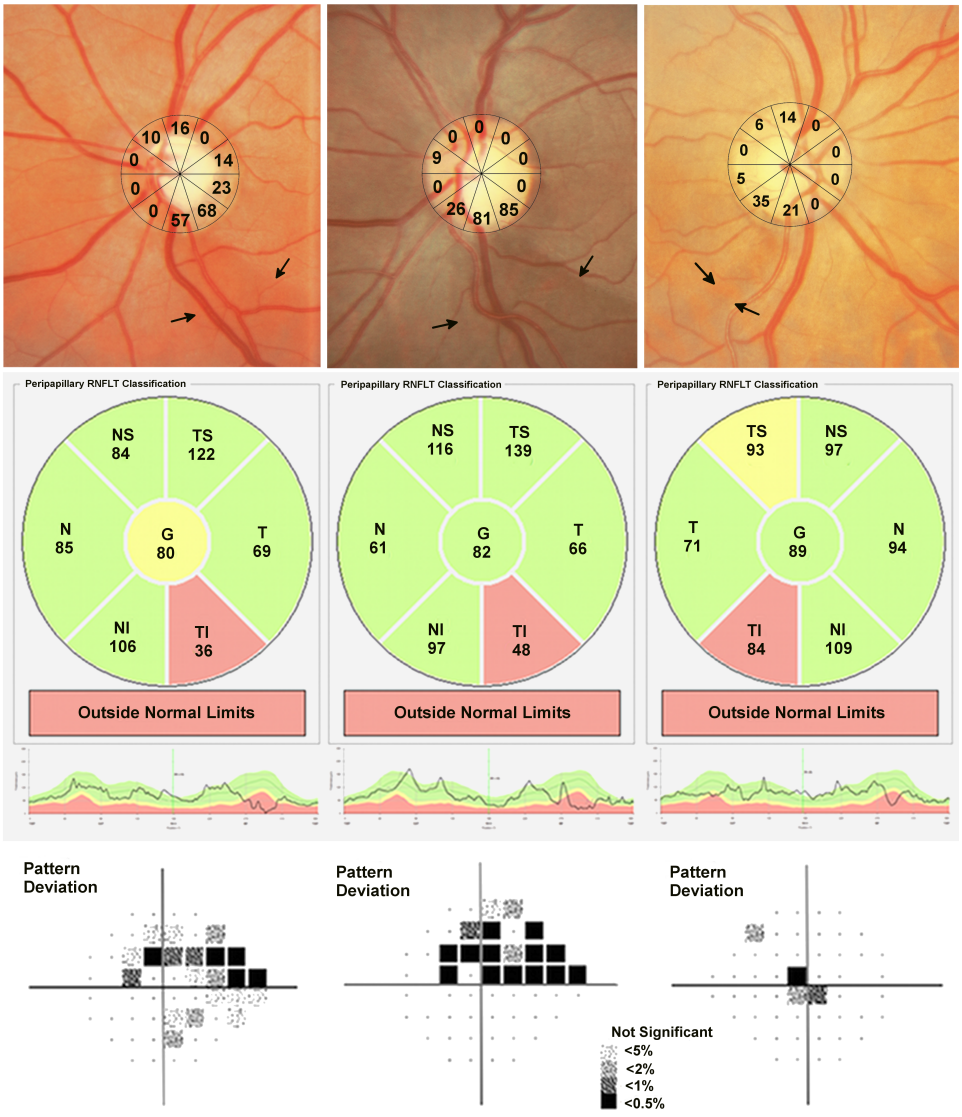

Figure 4-7. Patient four had a localised RNFL defect visible on photographs (arrows) with a CSFI in these sectors of 42 to 48% and a CSFI in other sectors of 0 to 26%. SDOCT showed localised thinning of the RNFL in the inferior-temporal region. Despite high estimated RGC losses, SAP global indices were within statistically normal limits.

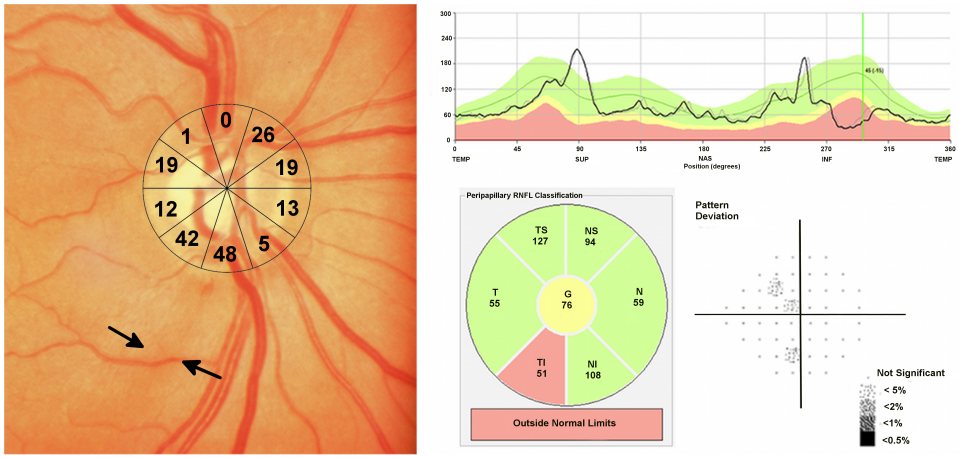

4.2.5. Discussion

This phase of my research explored the relationship between a common structural manifestation of glaucoma, often regarded as an early sign of the disease, and estimated losses of RGCs. The results suggest that if a localised RNFL defect is visible on fundoscopy or photographs, it may be associated with large localised RGC loss. Eyes with localised RNFL defects had on average 39% fewer RGCs than that expected for a healthy similar age subject, this weas despite an average MD of only -3.3 dB. Individual sectors with a visible RNFL defect had lost an estimated 59% (range of 20 to 100%) of RGCs compared to that expected for a healthy eye, which was significantly greater than estimated RGC losses in sectors without RNFL defects and in healthy eyes. This estimate

was close to the results of histological studies showing loss of 28 to 50% of RNFL thickness in regions of a visible RNFL defect (Quigley, & Addicks 1982; Quigley 1986). The results therefore suggest that rather than being an early sign of glaucoma, as traditionally taught, localised RNFL defects visible on photography are likely to be associated with large underlying neural losses.

Most eyes with localised RNFL defects also had repeatable defects on perimetry (Figure 4-6), however, 17 of 66 eyes with localised RNFL defects (25.8%) had normal SAP. Figure 4-7 shows an eye included in the study with a localised RNFL defect visible on photography but without a repeatable SAP defect, despite an estimated RGC loss of almost 50% in the sectors corresponding to the RNFL defect. Although most sectors with localised RNFL defects had large estimated RGC losses, 11 of 136 sectors with an RNFL defect (8.1%) had estimated losses of less than 30%, including a single sector with an estimated loss of only 20%.

Localised RNFL defects are defined as areas of abnormality within areas of relatively preserved RNFL, therefore detection of a localised defect depends on RNFL thickness in neighbouring regions (Quigley, & Sommer 1987). An example of this is shown in Figure 4-6, which shows an eye with an RNFL defect and relatively low estimated RGC losses (right column). Sectors corresponding to the RNFL defect had estimated RGC losses of only 21 to 35%, but the RNFL defect may have been visible due relative preservation of the surrounding RNFL, with estimated losses of only 0 and 5% in neighbouring sectors. The natural history of localised RNFL defects is for them to enlarge to become diffuse defects and therefore localised defects are less likely in eyes with more advanced

glaucoma (Sommer et al 1977). They are also more difficult to detect in older patients due to poorer visibility of the neighbouring RNFL (Quigley, & Sommer 1987; Sommer et al 1977; Jonas et al 1989).

This phase of my research had several major limitations, which mean the results should be interpreted with caution. First, although eyes with localised RNFL defects were found to have large estimated RGC losses, this was a cross-sectional study and it is possible that the RNFL defects were visible earlier when RGC losses were less. Second, although efforts were taken to minimise rotation errors and ensure correct alignment during image acquisition, and fovea-to-disc (FoDi) alignment technology was used to automatically track and align circle scans, there may have been variation in head or eye position between stereophotographs and OCT scans. This may have led to discordance between sectorial estimates of RGC count and the sectors with visible RNFL defects. Ensuring scans were aligned along the BMO-fovea axis may have produced more anatomically sound results; however, the BMO-fovea axis is not visible on photographs (Chauhan et al 2013). A further limitation was the choice of structure-function map. Although there is inter-individual variation in the point of entry of a particular axon into the ONH (Garway-Heath et al 2000), closer examination of the Harwerth map shows some conspicuous areas of disagreement between the map and known RGC axon distribution. For example, whilst sectors 7 and 9 are adjacent to one another in the Harwerth visual field map, they are non-contiguous in the ONH map. This is anatomically implausible and does not explain what happens at the point of transition between zones 7 and 9 and how RGC axons from adjacent zones could come to enter the ONH at non-adjacent locations. The Garway-Heath map, which was developed from

observation of fundus photographs, would likely have been a better choice of map, however, I selected the Harwerth map to be consistent with the method of RGC estimation, which was developed using the Harweth map using the same *sMD* estimates.

The most serious limitation though was that during the course of the work, I realised there are major flaws in the assumptions of Harwerth's formulae (also discussed in section 2.4.10, page 76). Foremost, the estimates of RGCs derived from SAP and OCT are not independent as the correction for disease severity in the OCT-derived estimates defines severity based on SAP MD. The origin for the correction factor is also not clear and it has even been suggested by Swanson and colleagues that this may have been introduced to allow better correlation between SAP and OCT derived estimates and then later explained as a correction for disease severity (Swanson, & Horner 2015). A further flaw is that OCT-derived estimates of numbers of RGC are consistently lower than estimates derived from SAP, which is likely due to Harwerth's formula assuming the mean RGC axon diameter to be larger than that reported in previous studies (Swanson, & Horner 2015). Also, the formulae were developed from studies in a limited number of animal eyes, in which there was wide variation in histological RGC counts and SAP sensitivity at individual locations (Harwerth et al 2010). It is therefore possible that the observation that estimates of RGC loss in regions of localised RNFL defects were similar to histological studies was a chance finding, rather than due to the accuracy of the RGC estimates.

Although the possibility of being able to estimate RGC loss in glaucoma is intriguing, current methods are based on histological data from a very limited

number of eyes. Moreover, combining RGC estimates from OCT and SAP may not be appropriate given that estimates from SAP will include dysfunctional RGCs (some with potential for recovery), whereas estimates from OCT will likely only account for RGCs that have shown shrinkage or have undergone apoptosis. Due to the limitations of the Harwerth formulae, which are not possible to address satisfactorily without further histological studies, the estimates should be interpreted with extreme caution.

My conclusions from this phase of research were that the results suggest that localised defects of the RNFL, a common manifestation of glaucomatous structural change, may be associated with large underlying RGC losses. Therefore, rather than being an early feature of disease, localised RNFL defects may be associated with significant neural loss. However, the conclusions regarding estimates of RGC loss should be interpreted with extreme caution given the limitations of the formulae used. In next phase of my research, I aimed to evaluate the relationship between structural changes to the ONH and an objective measure of function; the pupillary light response.

4.3. The relationship between structural changes and pupil response

4.3.1. Background

Although glaucoma is typically a bilateral disease, asymmetry is common, particularly in the early stages. For example, the Blue Mountains Eye Study, a large population study, which examined 3,654 people aged over 49 years in Australia, found that of those with glaucomatous visual field loss, 50.5% had unilateral defects and 49.5% bilateral defects (Lee et al 2003). Intereye differences in IOP (Williams et al 2013; Levine et al 2006), optic disc characteristics (Ong et al 1999; Armaly 1969), OCT measurements of cpRNFL and macular thickness (Sullivan-Mee et al 2013), and visual field sensitivity (Levine et al 2006; Greenfield et al 2007) are all features that raise suspicion of glaucoma. In fact, an intereye difference in cup-disc ratio of more than 0.2 has long been quoted as a diagnostic criterion for glaucoma (Armaly 1969).

The detection of intereye asymmetry in optic nerve or macula parameters has some possible diagnostic advantages over using isolated measures from one eye. For example, OCT normative databases are often used to classify cpRNFL thickness as normal, borderline or outside normal limits, however, normative databases consist of relatively few subjects, and these subjects have homogenous ocular and systemic characteristics (Realini et al 2014). Parameters such as cpRNFL thickness exhibit wide overlap between healthy subjects and those with early glaucoma and are influenced by patient-specific factors including age, gender and ethnicity, increasing the chances of patients with different

characteristics to those included in the normative database being misclassified. As many of these factors are intrinsic to the individual and will not influence intereye asymmetry, using the fellow eye of the same individual for comparison may overcome some of these limitations (Sullivan-Mee et al 2013). Eye-specific factors such as axial length, which also exhibit wide inter-individual variation, and influence structural measurements, are also likely to be similar between eyes and so have less influence on intereye asymmetry. A patient's fellow eye could therefore serve as a useful comparative reference for the index eye. Several investigators have examined whether assessment of macular or optic nerve asymmetry is useful for discriminating between glaucomatous and healthy eyes and asymmetry analysis is now incorporated in commercial OCT software for glaucoma detection (Figure 4-8).

Figure 4-8. Spectralis SDOCT posterior pole asymmetry analysis for a patient with glaucoma. Most cells in the left-right eye (OS-OD) asymmetry plot are shaded greyscale indicating thinner retinal thickness in the left compared to right eye. In contrast, few of the cells in the left eye are thinner than the right (right-left (OD-OS) asymmetry plot). The hemisphere analysis indicates that the inferior retina in both eyes is thinner than the superior retina.

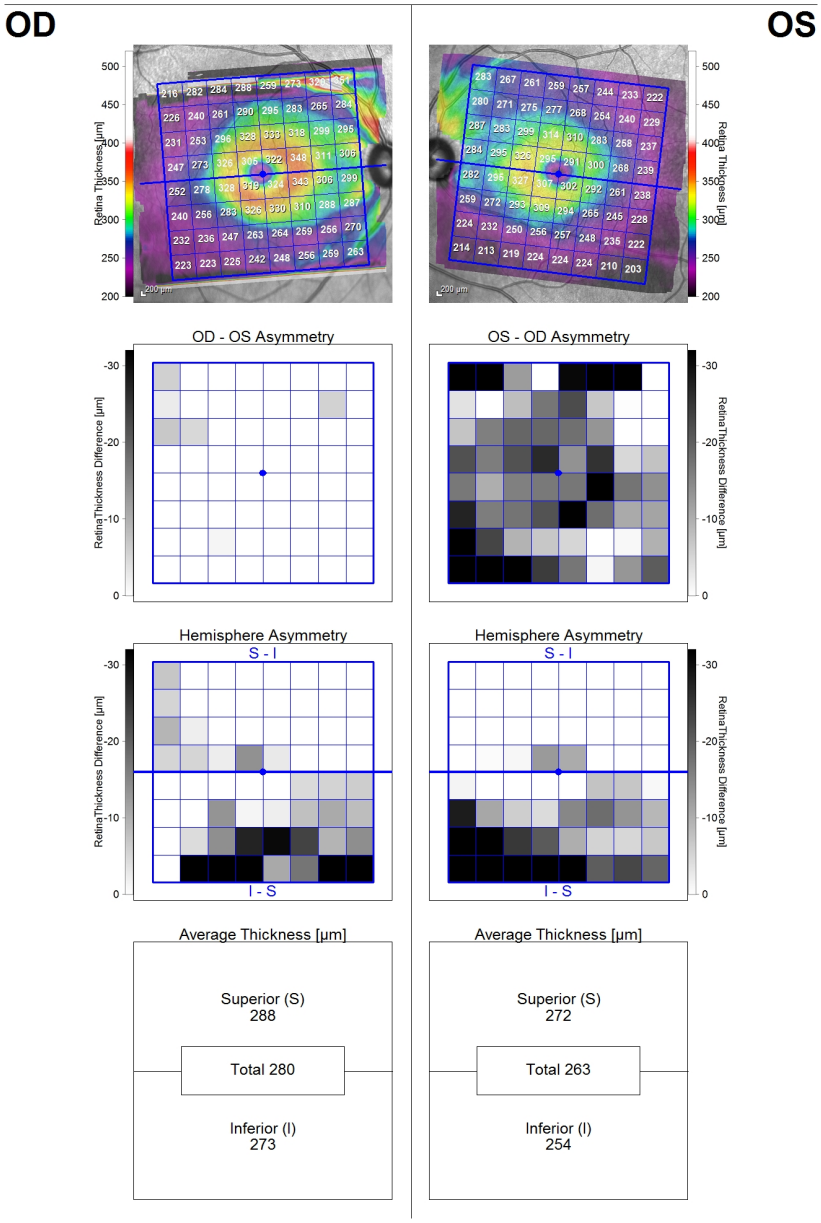

A commonly used rapid method of detecting asymmetric damage to the afferent visual pathway is the assessment of pupil responses for a relative

afferent pupillary defect (RAPD). A RAPD is defined as a difference in average pupillary constriction when each eye is stimulated monocularly (Levatin 1959; Wilhelm, & Wilhelm 2003; Lankaranian et al 2005).

The aim of this phase of my research was to evaluate the relationship between glaucomatous structural changes and a quantitative measure of pupil response. The pupil response serves as a useful objective measure of functional impairment; however, asymmetry of pupil response will only be present if there is asymmetric impairment to the afferent pathway. Therefore, I planned to determine the magnitude of inter-eye asymmetry in glaucomatous damage required for a patient with glaucoma to have a manifest RAPD. I quantified 'glaucomatous damage' in terms of asymmetry in cpRNFL thickness from OCT and DLS from SAP. Although aware of the limitations of the Harwerth formula I also decided to explore the intereye asymmetry in estimated numbers of RGCs using the formulae described in section 2.4.4, page 66. Although a RAPD is not specific for glaucoma, previous studies have reported a RAPD in one to two thirds of patients with glaucomatous optic neuropathy (Charalel et al 2014; Skorkovská et al 2011) leading some to suggest that detection of a RAPD might be a useful screening tool (Chang et al 2013b).

RAPDs are typically detected using the swinging flashlight test, which involves illuminating each eye alternately and comparing the velocity and amplitude of the pupil response between eyes (Levatin 1959). A RAPD is present when there is asymmetry of the light reflex. RAPDs can be quantified by placing neutral density filters in front of the normal eye and repeating the swinging flashlight test until the pupil responses become symmetric (Thompson et al 1981). However, the

swinging flashlight test is somewhat subjective and may be difficult in eyes with anisocoria, or dark irides (Wilhelm, & Wilhelm 2003). Automated pupillometry allows quantification of individual elements of the pupil response and can detect RAPDs with greater sensitivity than the swinging flashlight test (Lankaranian et al 2005; Jonas et al 1990). For example, Lankaranian and colleagues found a RAPD in 39 of 70 patients (56%) with glaucoma using pupillometry compared to only 20 (29%) of the same patients with the swinging flashlight test (Lankaranian et al 2005).

Although the magnitude of a RAPD is correlated to the difference in visual field loss between eyes (Thompson et al 1982; Johnson et al 1988) and to inter-eye RNFL differences (Chew et al 2010), there are few studies examining the asymmetry of neural loss required for a pupillary abnormality (Kerrison et al 2001). Kerrison and colleagues found unilateral loss of 25 to 50% of RGCs was required for a RAPD of 0.6 log units in non-human primates, however, this study used a macula diode laser to induce RGC loss and assessed pupil reactions using the swinging flashlight test, rather than automated pupillometry.

4.3.2. Purpose

The aim of this phase of my research was to evaluate the relationship between structural changes in glaucoma and pupil responses. Specifically, I aimed to examine the asymmetry of cpRNFL, DLS and estimated RGC counts required for a clinically detectable RAPD.

4.3.3. Methods

For this phase of research 103 participants from DIGS were recruited for

pupillometry, in addition to the routine testing previously described (Section 3.2, page 84). cpRNFL thickness values were obtained using Cirrus SD-OCT (Section 3.2.3, page 86).

Pupillometry

Pupil responses were tested using a binocular infrared computerised pupillometer (RAPDx, Konan Medical USA Inc., Irvine, CA) that measures bilateral pupil responses to monocular stimuli (**Figure 4-9**) (Tatham et al 2014b). Stimuli were presented on an LCD screen with a central barrier creating optical channels for each eye. The subject viewed the screen at infinity through 50mm objective lenses providing an approximate 25-degree field of view in each eye. Each half of the screen was selectively activated to stimulate each eye separately. Eyes were also illuminated by a pair of infrared emitting diodes, with peak emission at 880 nm, mounted at a 35-degree angle.

Figure 4-9. Binocular infrared computerised pupillometer used to obtain quantitative RAPD measurements (image copyright Konan Medical USA Inc., Irvine, CA.).

The pupil diameter was measured in pixels and converted to millimetres. During testing participants were instructed to look at a fixation target displayed on the LCD screen. Dark pupil diameter was measured; following which one eye was stimulated with a full field white flash stimulus. The stimulus was presented for 200ms followed by a period of darkness resulting in a 2.1s duty cycle. The stimulus was presented 9 times for each eye for a total test time of 37.8s. The right eye was stimulated first, followed by the left, then the right, with further stimuli presented to alternate eyes. The stimulus had a luminance of 384 cd/m^2 and there was a nominal background luminance of 0.01 cd/m^2. Testing was conducted under dark room conditions with an illuminance of <0.5 lux.

Pupil diameter was continuously monitored during testing to generate a pupil diameter waveform. Pupil parameters measured included pre-stimulus pupil diameter, minimum pupil diameter following the stimulus, response latency (time between stimulus onset and when pupil velocity reached 50% of the peak velocity of constriction), time to peak constriction and response amplitude (maximal contraction of the pupil as a percentage of the pre-stimulation size). Repetitions were averaged (median) before analysis to minimise noise. The RAPDx automatically calculates the direction and magnitude of pupil response asymmetry as a RAPD score. The RAPD score is calculated as the difference in the amplitude of pupil constriction between stimulation of the two eyes using the following formula (Sarezky et al 2014):

RAPD score = $10*\text{Log}_{10}$ (mean response amplitude in both eyes in response to right eye stimulation / mean response amplitude in both eyes in response to left eye stimulation)

A positive RAPD score therefore indicates a relative abnormality of the left afferent system and a negative value an abnormality of the right afferent system. As pupil responses may be influenced by medications affecting the autonomic nervous system, patients using systemic or topical cholinergic or anticholinergic medications were not included in the study. Patients who had previous ocular trauma, or intraocular surgery, except for uncomplicated phacoemulsification cataract surgery were also excluded.

Statistical Analysis

Descriptive statistics were performed using the methods outlined in section 3.4, page 89. The relationship between magnitude of RAPD and inter-eye (right minus left eye) differences in MD, RNFL thickness, and estimated RGC losses (CSFI) were examined using scatter plots and linear regression. To investigate the effect of disease severity on asymmetry needed for a RAPD, absolute RAPD score was calculated and average MD or RNFL thickness included in the regression analysis, with the effect of age also examined as a covariate.

4.3.4. Results

Seventy-seven patients with glaucoma and 26 healthy controls were recruited to this phase of the project (Table 4-4). 52 patients had glaucoma in both eyes and 23 had glaucoma in one eye and suspected glaucoma in the other. Table 4-4 shows patients with glaucoma had significantly higher absolute RAPD scores

than controls (P = 0.002) with a mean absolute RAPD score of 0.26 in glaucoma compared to 0.10 in controls (Figure 4-10).

Figure 4-10. Boxplot showing the median, interquartile range, and outside values of the absolute RAPD scores in glaucoma and controls.

Table 4-4. Characteristics of healthy and glaucomatous subjects.

	Controls N = 26	Subjects with glaucoma in at least one eye N = 77	P-value
Age (years)*	50.0 ± 15.2	68.9 ± 12.3	<0.001
Gender	14 (54%) Female	41 (53%) Female	0.958
Response amplitude (%)†			
Worse eye stimulated	29.4 (30.4) 27.8 to 32.6	26.9 (27.7) 23.5 to 30.8	<0.001
Better eye stimulated	29.5 (31.7) 27.6 to 32.9	27.5 (27.2) 24.2 to 30.3	0.002
Inter-eye difference	0.6 (0.6) 0.4 to 0.9	1.6 (1.0) 0.5 to 1.9	<0.001
Response latency (ms)†			
Inter-eye difference	4.9 (4.2) 2.2 to 5.3	6.3 (4.6) 1.4 to 9.2	0.652
Peak constriction (ms)†			
Inter-eye difference	7.6 (5.5) 3.1 to 7.9	11.1 (10.2) 3.6 to 16.6	0.007
Absolute RAPD score†	0.10 (0.09) 0.05 to 0.14	0.26 (0.16) 0.08 to 0.30	0.002
SAP MD (dB)*			
Worse Eye	-0.4 ± 1.1	-5.0 ± 5.7	<0.001
Better Eye	0.3 ± 0.9	-2.1 ± 4.1	0.004
Inter-eye difference	0.6 ± 0.5	3.0 ± 3.1	<0.001
RNFL thickness (µm)*			
Worse Eye	94.5 ± 10.3	74.6 ± 15.4	<0.001
Better Eye	94.5 ± 10.5	80.9 ± 12.8	<0.001
Inter-eye difference	4.0 ± 3.6	10.0 ± 7.9	<0.001
Estimated RGC count (1000's cells)*			
Worse Eye	1032 ± 191	599 ± 211	<0.001
Better Eye	1071 ± 211	724 ± 205	<0.001
Inter-eye difference	61 ± 49	148 ± 123	<0.001
CSFI (%)*			
Worse Eye	3 ± 11	33 ± 22	<0.001
Better Eye	0 ± 11	18 ± 21	<0.001
Inter-eye difference	5 ± 4	17 ± 14	<0.001

Abbreviations: Response amplitude = maximal contraction of the pupils as a percentage of the pre-stimulation pupil size; Response latency = time between stimulus

onset and pupil velocity reaching 50% of peak velocity of constriction; Peak constriction = time between beginning of stimulus and peak constriction; Relative afferent pupillary defect (RAPD) score = $10*Log_{10}$ (mean response amplitude of both eyes (in response to right eye stimulation) / mean response amplitude of both eyes (in response to left eye stimulation)). SAP MD = standard automated perimetry mean deviation, RNFL = retinal nerve fibre layer, RGC = retinal ganglion cell, CSFI = combined structure and function index. *Mean ± standard deviation, t-test. †Mean, (median), interquartile range, Wilcoxon-rank sum test.

Thirty-two subjects with glaucoma (42%) had an absolute RAPD score ≥ 0.2 and 19 (25%) had a score ≥ 0.3. In contrast, large absolute RAPD scores were not observed in controls, with only 2 having a score ≥ 0.2 and none a score ≥ 0.3. There was no significant association between age and absolute RAPD score in healthy subjects ($R^2 = 0.02$, $P = 0.315$) or those with glaucoma ($R^2 = 0.002$, $P = 0.563$). Patients with glaucoma had greater inter-eye asymmetry in MD, RNFL thickness and CSFI (Table 4-4). The average number of RGCs estimated in those with glaucoma was 598,645 ± 211,062 cells in the worse eye and 723,532 ± 205,344 cells in the better eye compared to 1,031,521 ± 190,906 cells in the worse eye of healthy participants and those with glaucoma had an average estimated difference of 100,795 cells between eyes compared to 50,456 cells in controls. There was reasonable association between the RAPD score and inter-eye differences in MD ($R^2 = 0.55$, $P < 0.001$), RNFL thickness ($R^2 = 0.36$, $P < 0.001$), estimated RGC counts ($R^2 = 0.49$, $P < 0.001$) and CSFI ($R^2 = 0.48$, $P < 0.001$) (Table 4-5, Figure 4-11).

Table 4-5. Regression analysis of RAPD score compared to inter-eye difference (Δ, right minus left eye) in MD, RNFL thickness, estimated RGC count and CSFI.

Inter-eye difference (Δ)	Constant	Coefficient	R^2	P value
MD-Δ (dB)	-0.21	8.23	0.55	<0.001
RNFL thickness-Δ (μm)	1.61	19.99	0.36	<0.001
RGC estimate-Δ (cells)	21,896	353,272	0.49	<0.001
CSFI-Δ (%)	-1.97	-40.0	0.48	<0.001

As RAPD score is the log of a ratio, and the difference in MD between eyes is essentially also a log of a ratio, as it derived from subtracting two logarithmic values, I also examined the association between the inter-eye difference in RNFL thickness (Figure 4-12) and estimated numbers of RGCs transformed to their logarithmic values (

Figure 4-13). This showed a similarly strong association between higher (or lower) RAPD score and greater difference in log RNFL thickness and log estimated number of RGCs, with R^2 values of 0.32 (coefficient = 0.26, P<0.001) and 0.53 (coefficient = 0.64, P<0.001) respectively.

Figure 4-11. Scatter plot showing the relationship between RAPD score and inter-eye differences in MD (A), RNFL thickness (B), estimated RGC count (C) and CSFI (D).

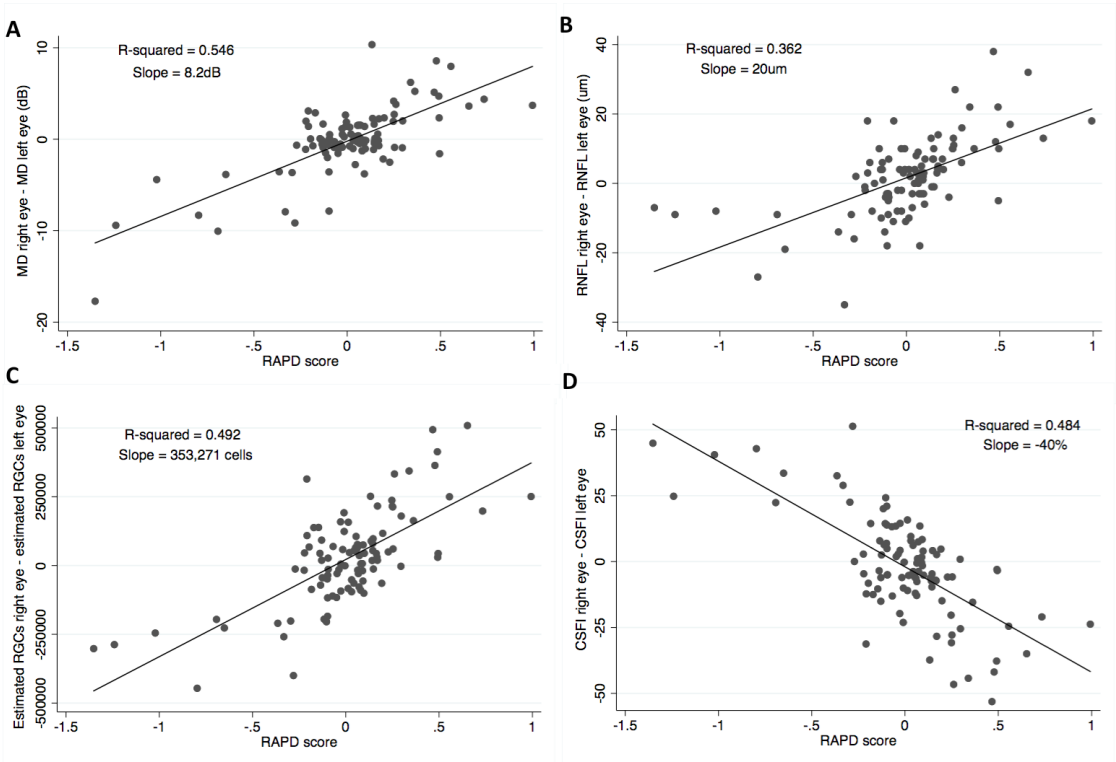

Figure 4-12. Scatter plot showing the relationship between RAPD score and inter-eye difference in log RNFL thickness.

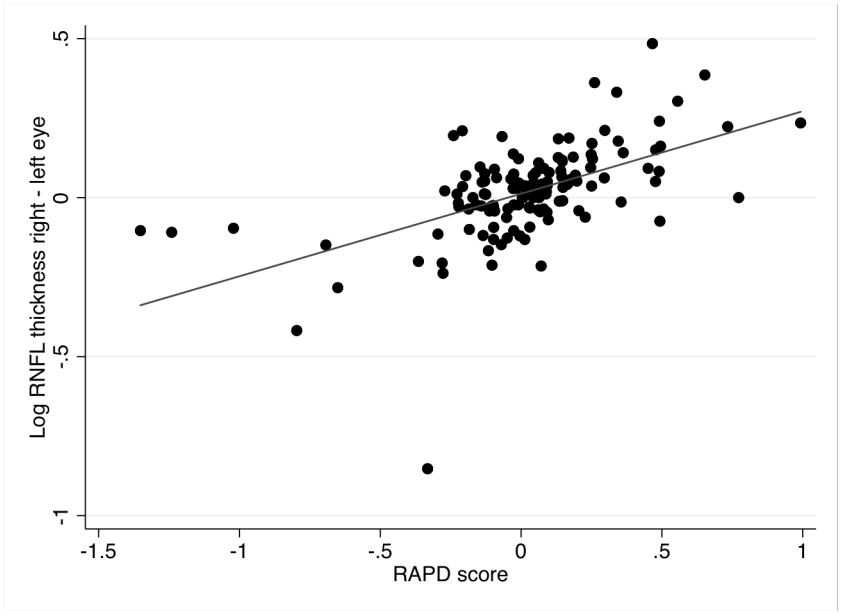

Figure 4-13. Scatter plot showing the relationship between RAPD score and inter-eye difference in log estimated number of RGCs.

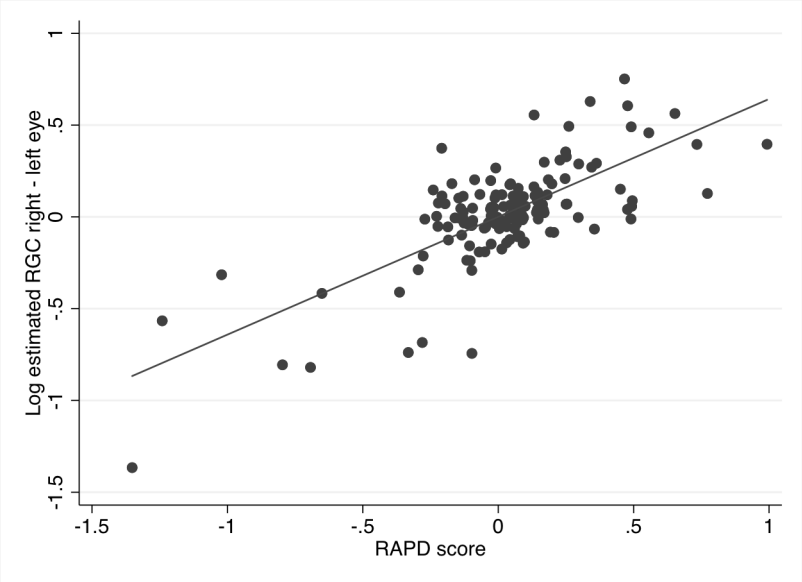

Multivariate analysis showed, subjects with worse average MD tended to need a greater inter-eye difference in MD for the same magnitude RAPD score as subjects with better average MD (Table 4-6). Table 4-6 shows average MD significantly affected the relationship between inter-eye difference in MD and magnitude of RAPD. Similarly, subjects with thinner average RNFL thickness tended to need greater inter-eye differences in MD for the same magnitude RAPD score as subjects with thicker average RNFL (Table 4-7). Subjects with thinner average RNFL thickness also needed greater inter-eye differences in RNFL thickness for similar magnitude RAPD scores compared to those with thicker average RNFL thickness (Table 4-8). Age had no significant effect on the relationship between absolute RAPD score and inter-eye differences in structural or functional measures.

Table 4-6. Multivariate regression analysis of absolute RAPD score and absolute inter-eye difference (Δ) in MD including the covariate of average MD (R^2 = 0.62, P < 0.001).

	Coefficient	95% CI	P value
Absolute RAPD score	6.47	5.41 to 7.53	<0.001
Average MD	-0.25	-0.31 to -0.19	<0.001
Constant	0.27	-0.07 to 0.61	0.003

Table 4-7. Multivariate regression analysis of absolute RAPD score and absolute inter-eye difference (Δ) in MD including the covariate of average RNFL thickness (R^2 = 0.51, P < 0.001).

	Coefficient	95% CI	P value
Absolute RAPD score	6.59	5.64 to 7.54	<0.001
Average RNFL	-0.05	-0.07 to -0.04	<0.001
Constant	4.99	3.53 to 6.45	<0.001

Table 4-8. Multivariate regression analysis of absolute RAPD score and absolute inter-eye difference (Δ) in RNFL including the covariate of average RNFL (R^2 = 0.19, P < 0.001).

	Coefficient	95% CI	P value
Absolute RAPD score	10.23	6.95 to 13.51	<0.001
Average RNFL	-0.10	-0.16 to -0.04	<0.001
Constant	13.75	8.70 to 18.79	<0.001

I also examined the ability of the RAPD to differentiate healthy and glaucomatous subjects. The RAPD score had a sensitivity of only 50% for a specificity of 80% (AUC = 0.68, 95% CI 0.58 to 0.78). Expected inter-eye differences for a range of RAPD scores are shown in Table 4-9.

Table 4-9. Average expected inter-eye differences (Δ) MD, RNFL thickness, estimated RGC counts and CSFI for given values of RAPD score.

Absolute RAPD score	MD-Δ (dB) if average MD = -5dB	MD-Δ (dB) if average MD = -15dB	RNFL thickness-Δ (μm)	Estimated RGC number-Δ (cells)	CSFI-Δ (%)
0.3	3.5	6.0	6.0	105,982	12
0.5	4.8	7.3	10.0	176,636	20
0.7	6.0	8.5	14.0	247,290	28
0.9	7.3	9.8	18.0	317,945	36
1.1	8.6	11.1	22.0	388,599	44

Figure 4-14 and Figure 4-15 show examples of two patients included in this phase of the study.

Figure 4-14. 56-year-old patient with early glaucoma in the left eye. The blue pupillometer trace shows the average of right and left pupil diameters on right eye stimulation and the red trace the average pupil diameters on left eye stimulation. MD was 0.73 dB and -0.39 dB in right and left eyes with estimated RGC counts of 1,005,524 and 864,756 respectively. The average response amplitude (A) on right eye stimulation was 0.30 compared to 0.27 on left eye stimulation, giving a RAPD score of $10*Log_{10}(0.30/0.27) = 0.46$ and indicating a relative abnormality of the left afferent pathway.

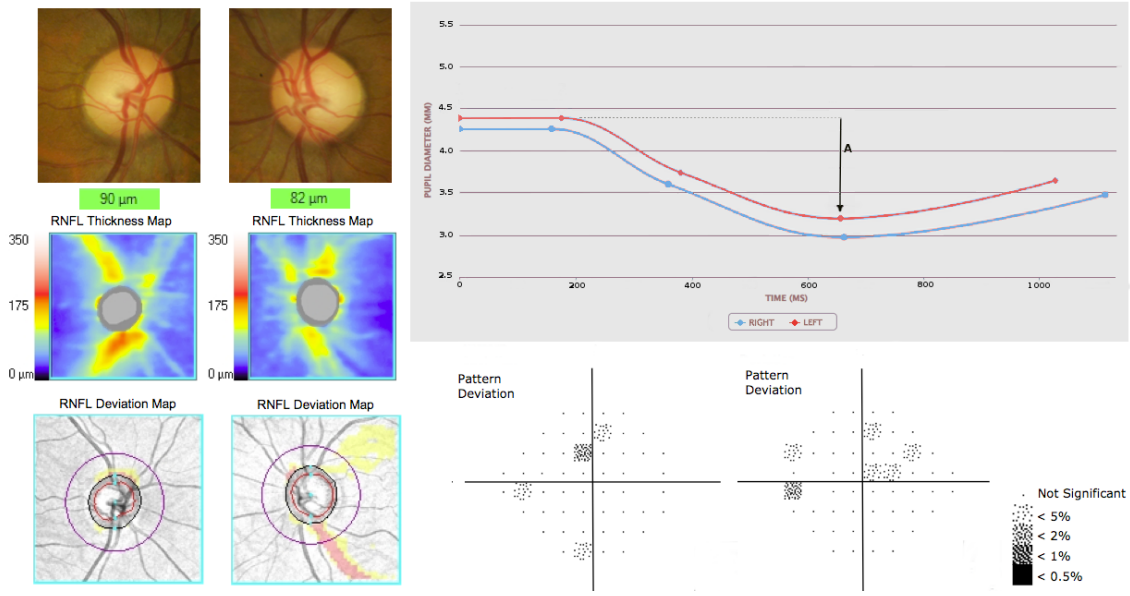

Figure 4-15. 70-year-old patient with advanced glaucoma in both eyes. MDs were -23.56 dB and -15.79 dB in right and left eyes with estimated RGC counts of 111,000 and 237,996 respectively. The RAPD score was -0.10, indicating a small relative abnormality of the right afferent pathway.

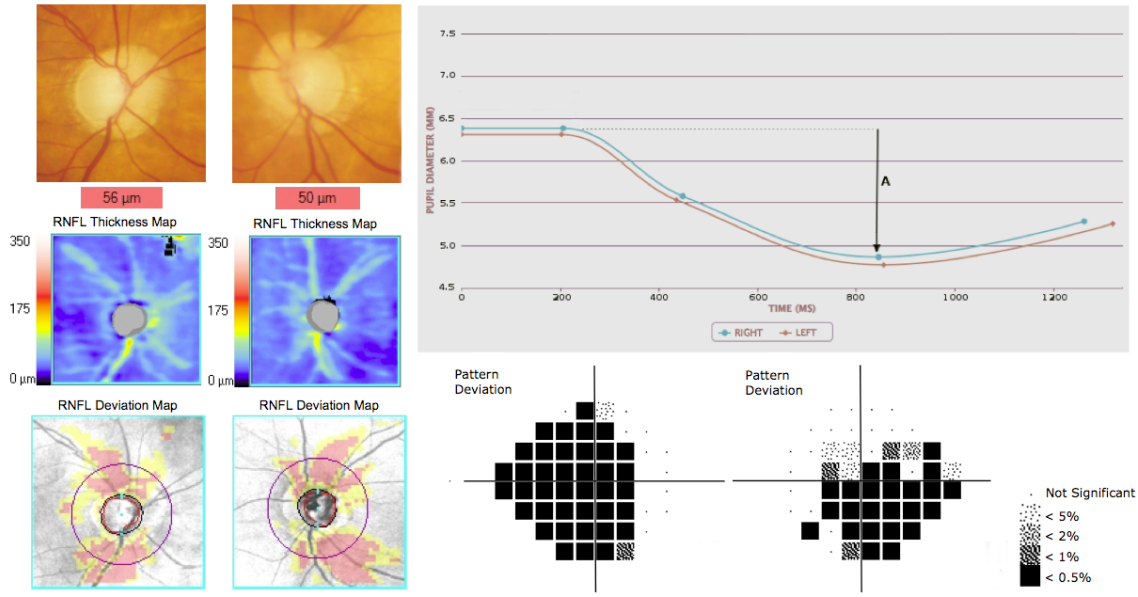

4.3.5. Discussion

This component of my research examined the relationship between glaucomatous structural and functional changes and magnitude and direction of RAPD and found a strong relationship between these measures (Figure 4-11). Individuals with larger RAPDs had greater inter-eye differences in RNFL thickness, MD and estimated RGC losses. Table 4-5 shows that each 0.1 increase in RAPD score was likely to correspond to an increase in RNFL asymmetry of 2 µm. Therefore, a RAPD score of 0.5 (or -0.5) is likely to represent an inter-eye difference in RNFL thickness of 10 µm and a RAPD score of 1.1, an inter-eye difference in RNFL thickness of 22 µm. A RAPD score of 0.5

corresponded to an inter-eye estimated RGC difference of approximately 177,000 cells compared to an inter-eye difference of 389,000 cells for a RAPD score of 1.1.

Although pupil response asymmetry was quantified using a pupillometer rather than by using neutral density filters, the results suggest that a RAPD score of 0.6 would correspond to an inter-eye CSFI difference of approximately 24%, which is like the results of a previous histological study showing unilateral loss of at least 25% of RGCs was required for a 0.6 log unit RAPD measured using neutral density filters (Kerrison et al 2001). The estimates were also similar to a previous study in human subjects with a variety of neurological diseases in which RGC numbers were estimated by overlying templates of known RGC density on visual fields (Lagrèze, & Kardon 1998). A 1.0 log unit RAPD was associated with asymmetric RGC losses of 30-40%, compared to an estimated loss of 40% of RGCs for a similar magnitude RAPD in our study. An important difference is that Lagrèze and colleagues used visual field sensitivity alone to estimate RGC counts, whereas in my analysis RGC numbers estimated from a combination of SAP and OCT information.

Previous studies have examined inter-eye differences in RNFL thickness and MD associated with asymmetric pupil responses to a flashlight (Chew et al 2010; Tatsumi et al 2007) or pupillometer (Chang et al 2013a). Using the swinging flashlight test, an inter-eye difference in RNFL thickness of 17 to 27%, or an inter-eye difference in SAP MD of 9.5 dB to 12 dB was needed for a RAPD of at least 0.3 to 0.6 log units (Chew et al 2010; Tatsumi et al 2007). Automated pupillometry is likely to be able to detect smaller RAPDs and the results of my

analysis show a RAPD score of 0.3 was associated with an inter-eye difference in MD of only 6.0 dB if the average MD in both eyes was -15dB and only 3.5 dB if the average MD was -5 dB. Using a similar pupillometer to that used in this phase of my research, Chang and colleagues found a RAPD score of 0.3 to be associated with an inter-eye difference in MD of 2.6 dB and RNFL thickness of 3.2 μm, which was similar to my results (Chang et al 2013a). However, Chang and colleagues did not examine the influence of disease severity on this relationship. Results from my work at UCSD showed that patients with worse average MD required a greater inter-eye difference in MD for a similar size RAPD as patients with earlier disease. For example, when average MD is -5 dB, an inter-eye difference in MD of approximately 4.8 dB is likely to be required for an absolute RAPD score of 0.5, compared to an inter-eye difference in MD of 7.3 dB for a similar magnitude RAPD in patients with an average MD of -15dB.

Average MD is likely to influence the relationship between inter-eye difference in MD and magnitude of RAPD as the inter-eye difference in numbers of functioning RGCs is likely to decrease with worsening disease severity in patients that may have initially had symmetrical disease. Further, SAP thresholds are acquired and presented using a logarithmic scale. As discussed in section 2.3, page 51, due to the logarithmic scale of SAP, in early disease one would expect large RGC losses to occur for a relatively small change in MD. Therefore, in early disease a small difference in MD between eyes may represent a relatively large difference in numbers of RGCs between eyes. Later in disease a small difference in MD between eyes may represent a relatively small inter-eye difference in functioning RGCs. It should however, also be emphasised that the RAPD score is also a logarithmic scale, which is useful for measuring small degrees of pupil

response asymmetry, but may lead to loss of information. To evaluate this, I also examined the relationship between inter-eye differences in structural and functional measures and pupil response asymmetry measured as the difference in response amplitude between eyes. Similar results were obtained compared to using the RAPD score.

Of course, it is important to emphasise that as glaucoma is usually a bilateral disease, assessment of RAPD is unlikely to be a useful tool for screening, as has been suggested by some (Chang et al 2013b). Furthermore, the presence of a clinically detectable RAPD in a patient with suspected glaucomatous optic neuropathy and good vision should in fact alert the clinician to the possible presence of a non-glaucomatous optic neuropathy. Few patients included in this phase of the research had grossly asymmetric disease, with only 13 subjects with glaucoma (17%) having an inter-eye mean deviation difference ≥5 dB. Using the data from this phase of my research, the RAPD score had a sensitivity of only 50% for a specificity of 80% for distinguishing those with glaucoma from healthy subjects (AUC = 0.68, 95% CI 0.58 to 0.78). It is also important to recognise that healthy subjects often have small RAPDs by pupillometry that are not seen on clinical examination, with one study reporting RAPDs between 0.08 and 0.22 log units in 42% of healthy subjects (Wilhelm et al 2007).

An aim of this phase of my research was to determine the inter-eye asymmetry in structural parameters needed for a clinically detectable RAPD in glaucoma. Although I did not use the swinging flashlight test in this study, the swinging flashlight test can detect a RAPD of approximately 0.3 log units, which

equated to an inter-eye difference in RNFL thickness of 6 μm in the present study (or a difference in estimated RGC losses of 12%) (Wilhelm et al 2007).

This phase of my research had several limitations, in addition to the limitations of the method of estimating RGC counts previously discussed (section 2.4.10, page 76). First the healthy subjects were significantly younger than those with glaucoma. Although RGC loss occurs with normal ageing, this is likely to be symmetrical and not affect the symmetry of pupil responses. Further, age had no effect on the relationship between inter-eye measures of glaucoma severity and magnitude of RAPD score. Also, specific RGC subtypes (e.g., the intrinsically photosensitive melanopsin containing RGCs or ipRGCs (Kawasaki, & Kardon 2007; Kankipati et al 2011)) are involved in the pupillary light response and loss of these cells may disproportionately affect the pupil response. Although the pupillometer did not specifically target individual RGC subtypes this may not have been important as previous investigations have shown ipRGCs have a uniform distribution and therefore loss is likely to be proportional to total RGC loss (Kawasaki, & Kardon 2007; Kankipati et al 2011). The symmetry of pupil responses may also be affected by differences in decussation of fibres at the optic chiasm and midbrain, which was not evaluated. In addition, some subjects with asymmetric glaucoma whom one might expect to have a large RAPD did not. Figure 4-15 shows a patient with bilateral advanced glaucoma and a large 8 dB difference in MD between eyes but a RAPD score of only 0.1. This patient had an estimated RGC difference of 126,996 cells between eyes, however the model suggested a RAPD of 0.1 would be associated with an inter-eye difference in estimated RGC count of only 35,327 cells. The large difference in estimates for this patient is because the model only explains 50% of the variability in RAPD

score. Furthermore, I only evaluated a full-field stimulus and it is possible that, depending on the location of visual field loss, by stimulating smaller sections of the retina, a larger proportion of patients with glaucoma may be found to have a RAPD. However, this strategy may also increase the number of false positives as small RAPDs detectable by pupillometry are not that infrequent in healthy subjects.

Despite these limitations, this component of my research has provided several new insights into the relationship between glaucomatous structural losses and functional change. Overall there was good correlation between magnitude of a RAPD and the inter-eye difference in RNFL thickness, MD and estimated number of RGCs. A large RAPD is therefore likely to indicate significant asymmetry of each of these parameters. It is though important to emphasise that patients with severe bilateral disease may have symmetric pupil reactions. The final phase of this body of work was to examine the relationship between glaucomatous structural changes and a more complex task related to visual function, and of direct relevance to quality of life: the ability to drive.

4.4. The relationship between structural changes and ability to perform vision-related tasks

4.4.1. Background

Although structural measurements, such as RNFL thickness, are widely used for diagnosing glaucoma and measuring progression, the real clinical relevance of these measurements remains unclear (McKean-Cowdin et al 2007; Medeiros et al 2012). For example, it is not known at which point structural changes become associated with decrease in the ability to perform vision-related tasks important for daily living. It is important to understand this relationship as structural measurements are increasingly used to inform management decisions regarding follow up intervals and treatment, whereas the impact of disease on daily living is of paramount importance to patients. Until recently there has been insufficient research into how glaucoma affects quality of life and activities of daily living, and most previous studies have relied solely on questionnaires (Glen et al 2011). Responses to questionnaires can be affected by patient's personality and attitudes, which vary, limiting the usefulness of cross-sectional data.

Although SAP is used to assess visual function in glaucoma, when it comes to assessing the impact of visual impairment on real-world tasks, SAP has limitations (Richman et al 2010). SAP has relatively few test points in the central field and does not evaluate important components of vision such as motion perception. In addition, SAP is performed under artificial conditions with minimal visual distractions whereas daily activities often require the ability to divide attention or multi-task (Broman et al 2004; Owsley, & McGwin 2010). Divided

attention is defined as the ability to process and/or respond to information from one task while simultaneously conducting another (Ball, & Owsley 1993). Therefore, rather than investigate the relationship between structural measurements and SAP, as has been done by previous investigators, the aim of the next phase of my research was to investigate the relationship between structural measurements and ability to perform a task of direct relevance to daily living, in this case driving. A secondary aim was to determine whether structural information might provide additional value compared to SAP alone in predicting the ability to perform vision-related tasks.

Previous studies have shown that ability to drive is intimately related to health-related quality of life, with driving cessation associated with increased risk of depression, social isolation and entry into residential care (Marottoli et al 1997; Fonda et al 2001; Ragland et al 2005). On the other hand, driving is a highly visual task, and continued driving in the presence of significant visual impairment is likely to be associated with increased risk of collisions, with potentially serious implications for the individual and society (Wood et al 2016). Previous studies have shown that drivers with glaucoma are at increased risk of collisions (Haymes et al 2007; Tanabe et al 2011; McGwin et al 2005). Haymes and colleagues reported drivers with glaucoma to be over 6 times more likely to have been involved in a collision compared to similarly aged controls (Haymes et al 2007). However, perhaps as driving is a complex task, and due to the limitations of SAP discussed above, previous studies have shown only a weak association between motor vehicle collisions and SAP (Richman et al 2010; Owsley, & McGwin 2010).

The ability to divide attention is intrinsically related to driving, as a driver is required to continuously monitor information from the roadway while simultaneously maintaining awareness of potential hazards surrounding the vehicle (Owsley, & McGwin 2010; Owsley et al 1998). For this reason, failures of divided attention are a leading cause of collisions, accounting for as many as 22 to 50% of incidences (Brouwer et al 1991; Klauer et al 2006; Rubin et al 2007). Problems with divided attention have also been associated with difficulties performing other activities of daily living such as walking (Broman et al 2004). The Visual Performance Laboratory at UCSD, led by Professor Felipe Medeiros, has recently developed a driving simulator that provides a means to assess ability to divide attention under simulated driving conditions. The aim of the Visual Performance Laboratory is to explore the effect of eye disease on visual function and ability to perform activities of daily living. I was fortunate to be able to use this apparatus for this component of my research secondment at UCSD.

4.4.2. Purpose

The purpose of this phase of my research was to improve understanding of the 'structure-function relationship' by determining the relationship between an objective measure of glaucomatous structural damage and ability to perform a vision-related task of direct relevance to an activity of daily living.

4.4.3. Methods

Drivers with glaucoma attending HGC were recruited for involvement in this cross-sectional observational study. Written informed consent was obtained from all participants. All subjects underwent a comprehensive ophthalmologic examination, SDOCT (Spectralis, Heidelberg Engineering, Dossenheim,

Germany) and SAP in accordance with the methods outlined in Section 3.2, page 84. Patients were categorised has having glaucoma using the criteria defined in Section 3.3, page 88 Categorisation was based on diagnosis in the worse eye.

Driving Simulator

The driving simulator consisted of a driving seat, a steering wheel, brake and accelerator pedals, and a flat screen monitor as shown in Figure 4-16. The position of the seat, wheel and pedals could be adjusted but the distance between the subject's head and the centre of the screen was set at 43-inches. The screen width was 35-inches resulting in a driving scene with a 45-degree horizontal field of view.

Erwin Boer, Professor in the Department of Mechanical Engineering at Delft University of Technology, Netherlands, and Visiting Professor at the Institute for Transport Studies, University of Leeds, UK, developed the software for the driving simulator. The aim was that the simulator should assess a wide range of patient response parameters to simulated driving scenarios and, given the importance of failures of divided attention in motor vehicle collisions, a divided attention task was included in the programme. The simulator used two basic driving tasks involving car following and curve negotiation. For the car following task the driver was instructed to follow a lead vehicle that varies its speed at a short distance, controlling the accelerator and brake (Figure 4-17).

Figure 4-16. Photograph of the driving simulator apparatus.

Figure 4-17. Screenshot of the driving simulator car following task.

For the curve negotiation task, the driver was required to stay in the centre lane of a three lane, winding road Figure 4-18). The velocity of the vehicle was constant such that the driver only had to operate the steering wheel. The vehicle

speed was set at 15 m/s (54 km/h) for the first half of the test, increasing to 25 m/s (90 km/h) for the second half of the test (Marsden et al 2001).

Figure 4-18. Screenshot of the driving simulator curve negotiation task.

While performing the central tasks (car following or curve negotiation), simultaneous peripheral (divided attention) stimuli were periodically shown at about 20-degrees of visual angle in the upper right and upper left of the driving simulator screen and at three different contrasts (low, medium and high with Michelson contrasts of 0.04, 0.14 and 0.27) (Figure 4-17 and Figure 4-18). The background was a constant cloudy sky. The driver was required to press a button on the steering wheel to register that the stimulus had been perceived.

There was an average of 5 stimuli presented at each contrast for each central driving task (a total of about 15 per 3 minutes or about one every 12 seconds) and stimuli stayed on the screen for a maximum of 3 and 6 seconds (uniform distribution) or until the driver responded. The next stimuli appeared between 3 and 6 seconds (again uniform distribution) after the driver responded or when the

maximum display time had elapsed. To minimize the effect of unreliable tests and learning effect, all subjects underwent driving simulator training prior to test commencement. Training consisted of 2 minutes of practice acceleration and deceleration, followed by 1 minute of each of the car following and curve negotiation tasks.

Driving Simulator Outcome Variables

The main outcome variable of interest was *reaction time* to the divided attention peripheral stimulus, which was defined as the time interval between appearance of the peripheral stimulus and the subject pressing the button, with a longer reaction time indicating worse performance. The mean reaction time for each central task and contrast was calculated to give a total of 6 sets of reaction times for each subject (high, medium and low contrasts for car following and curve negotiation tasks). We also calculated the *false positive percentage,* defined as the number of button presses occurring when no stimulus had been presented divided by the total number of stimuli presented. Reaction time was chosen as the outcome variable as difficulties with divided attention tasks seem to be related, at least in part, to a slowing of visual processing speed. Visual processing speed, which is the time needed to make a correct judgment about a visual stimulus, is commonly studied in behavioural research by measuring reaction times.

As a subject might neglect the central driving task to concentrate on the peripheral stimuli, and thereby achieve falsely fast reaction times, it was important to also measure central task performance and ensure the patient was truly dividing attention. Central task performance was assessed using *curve*

coherence and *speed coherence*. Curve coherence, which is a measure of correlation between road curvature and the vehicle path curvature, was calculated using the following equation, where n is the number of samples of the two signals and SD is the standard deviation of the signals.

$$Curve\ Coherence = \frac{1}{n}\sum_{t,Delay}\frac{(ownCurvature(t) - Mean_{ownCurvature})(roadCurvature(t, delay) - Mean_{roadCurvature})}{SD_{ownCurvature}SD_{roadCurvature}}$$

A coherence of 1 indicated exact agreement between the road and vehicle path curvature or good performance on the central driving task. Speed coherence is like curve coherence but measures how well the driver can match the speed changes of the lead vehicle. Speed coherence was calculated using the following equation, where CCF is the cross-correlation function, n is the number of samples of the two signals and SD is the standard deviation of the signals (Brookhuis et al 1994).

$$Speed\ CCF = \frac{1}{n}\sum_{t,delay}\frac{(ownSpeed(t) - Mean_{ownSpeed})(leadSpeed(t, delay) - Mean_{leadSpeed})}{SD_{ownSpeed}SD_{leadSpeed}}$$

A potential problem of using reaction times as a measure of visual processing is that registering the reaction time includes a motor response, likely to be influenced by age, among other factors (Hultsch et al 2002). As one would expect the motor response for a subject to be constant regardless of stimulus contrast, we attempted to minimise the contribution of the motor response by calculating the difference in reaction times to the low and high contrast stimuli. Reaction times and driving ability are also dependent on cognitive ability so all subjects

completed a Montreal Cognitive Assessment, a 30-point, ten-minute cognitive screening tool (**Figure 4-19**) (Nasreddine et al 2005). As driving experience might also affect performance on the driving simulator, driving habits questionnaires were completed to assess the average number of miles driven over the past 3 years.

Statistical Analysis

Descriptive statistics were performed using the methods outlined in section 3.4, page 89. The relationship between the reaction times and RNFL thickness in each subject's better and worse eyes were examined using scatter plots and locally weighted scatterplot smoothing (LOWESS) curves. As reaction times were positively skewed, base-10 logarithms were calculated for further analysis. Other variables examined as potentially confounding factors included age, Montreal Cognitive Assessment score, SAP MD and distance driven per week. The relationship between reaction times and stimulus contrast was also examined using a mixed effects linear regression model.

Figure 4-19. Montreal Cognitive Assessment.

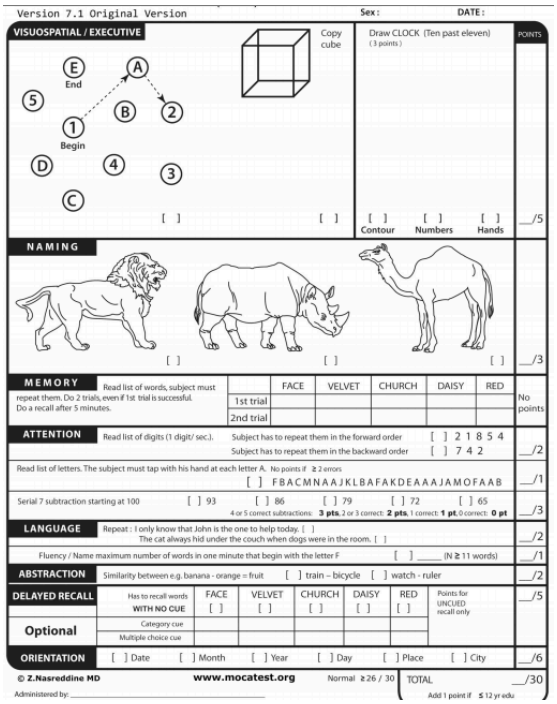

4.4.4. Results

The study included 82 subjects with glaucoma and 76 similarly aged controls, including 30 healthy subjects and 46 with suspect glaucoma and OHT but normal visual fields. There were no significant differences in age, gender, ancestry, cognitive ability or average distance driven per week between controls and those with glaucoma (Table 4-10).

Table 4-10. Demographic and clinical characteristics (mean (median, interquartile range)) of patients with glaucoma compared to controls.

	Controls (76 subjects)	Glaucoma (82 subjects)	P-value
Age (years)	61.2 ± 9.2	64.2 ± 12.2	0.093[a]
Sex, female (%)	34 (44.7%)	35 (42.7%)	0.873[c]
Ethnicity Caucasian African-American	 53 (69.7%) 17 (22.4%)	 51 (62.2%) 19 (23.2%)	0.783[c]
MD worse eye (dB)	-0.2 (0.1, -0.8 to 0.7)	-6.4 (-3.9, -8.7 to -1.6)	<0.001[b]
MD better eye (dB)	0.5 (0.7, -0.2 to 1.3)	-2.3 (-1.2, -3.4 to 0.1)	<0.001[b]
RNFL thickness worse eye (µm)	90 (91, 83 to 98)	71 (70, 60 to 80)	<0.001[b]
RNFL thickness better eye (µm)	94 (94, 87 to 100)	79 (78, 67 to 90)	<0.001[b]
Pseudophakic in at least one eye (number of patients (%))	10 (13.2%)	17 (20.7%)	0.290[c]
Montreal Cognitive Assessment score	28 (29, 27 to 30)	28 (28, 26 to 30)	0.350[b]
Average distance driven per week (miles)	143 ± 18	125 ± 18	0.065[a]
Curve Negotiation Metrics			
Curve coherence	0.93 (0.95, 0.90 to 0.97)	0.91 (0.95, 0.89 to 0.98)	0.978[b]
False positives (%)	9.2 (3.1, 2.0 to 6.7)	9.2 (2.4, 0 to 9.1)	0.599[b]
Divided Attention Reaction Time – Low contrast (s)	0.64 (0.59, 0.52 to 0.70)	1.05 (0.70, 0.61 to 1.02)	<0.001[b]
Divided Attention Reaction Time – Medium contrast (s)	0.55 (0.52, 0.48 to 0.63)	0.59 (0.57, 0.49 to 0.64)	0.142[b]
Divided Attention Reaction Time – High contrast (s)	0.55 (0.53, 0.46 to 0.60)	0.58 (0.55, 0.49 to 0.66)	0.167[b]
Low contrast minus high contrast reaction time (s)	0.09 (0.07, 0.03 to 0.10)	0.47 (0.13, 0.07 to 0.40)	<0.001[b]
Car Following Metrics			
Speed coherence	0.93 (0.95, 0.90 to 0.97)	0.91 (0.95, 0.89 to 0.98)	0.978[b]
False positives (%)	6.5 (2.7, 0 to 5.5)	6.3 (2.7, 0 to 5.6)	1.000[b]
Divided Attention Reaction Time – Low contrast (s)	0.77 (0.62, 0.54 to 0.85)	1.19 (0.69, 0.58 to 1.22)	0.025[b]
Divided Attention Reaction Time – Medium contrast (s)	0.62 (0.54, 0.50 to 0.64)	0.62 (0.56, 0.50 to 0.66)	0.956[b]
Divided Attention Reaction Time – High contrast (s)	0.57 (0.54, 0.50 to 0.61)	0.65 (0.55, 0.50 to 0.64)	0.412[b]
Low contrast minus high contrast reaction time (s)	0.20 (0.08, 0.03 to 0.30)	0.48 (0.11, 0.03 to 0.60)	0.199[b]

[a]t-test, [b]Wilcoxon rank sum test. [c]Fishers exact test.

Subjects with glaucoma had slower reaction times to the low contrast divided attention stimuli compared to controls (

Figure **4-20** and Table 4-10) with median reaction times of 1.05 and 1.19s for the curve negotiation and car following tasks in those with glaucoma compared to 0.64 and 0.77s respectively in controls ($P < 0.001$ for both comparisons). There was no significant difference between groups for the less demanding medium and high contrast stimuli, and false positive rates were similar between groups (Table 4-10).

Figure 4-20. Box-plots showing reaction times to the curve negotiation and car following driving simulator divided attention tasks for drivers with glaucoma and controls.

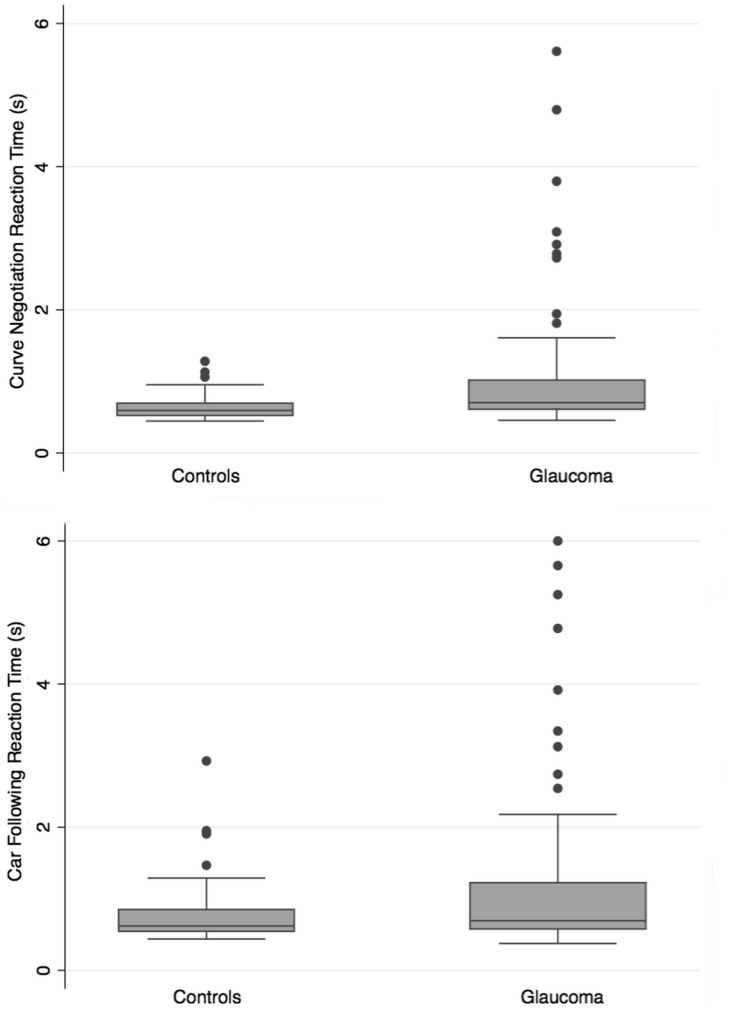

There was a significant non-linear relationship between RNFL thickness in the better and worse eyes and $\log_{10}$ reaction times to the driving simulator divided attention tasks at low contrast ($\rho = -0.480$; $P < 0.001$ and $\rho = -0.481$; $P < 0.001$ for the better and worse eyes respectively for the curve negotiation task and $\rho = -0.280$; $P < 0.001$ and $\rho = -0.281$; $P < 0.001$ for better and worse eyes using the car following task (Figure 4-21). There was a similar exponential relationship between RNFL thinning and reaction times before the logarithmic transform.

Although there was a similar relationship between RNFL thickness and reaction times to the medium and high contrast stimuli, the strongest relationship was with the more demanding low contrast stimulus, which was used for all further analyses. There was also a significant relationship between SAP MD in the better and worse eyes and $\log_{10}$ reaction times to the driving simulator divided attention tasks at low contrast ($\rho = -0.480$; $P < 0.001$ and $\rho = 0.509$; $P<0.001$ for better and worse eyes respectively for the curve negotiation task and $\rho = -0.315$; $P < 0.001$ and $\rho = -0.324$; $P < 0.001$ for the better and worse eyes for the car following task) (Figure 4-22 and Figure 4-23). There was a significant increase in divided attention reaction times with increasing age ($\rho = 0.434$; $P<0.001$ for the curve negotiation task and $\rho =0.324$; $P<0.001$ for the car following task) (Figure 4-24).

Figure 4-21. Scatter and LOWESS plots showing the relationship between RNFL thickness in the better eye and reaction times to low contrast divided attention stimuli during the curve negotiation and car following simulated driving tasks.

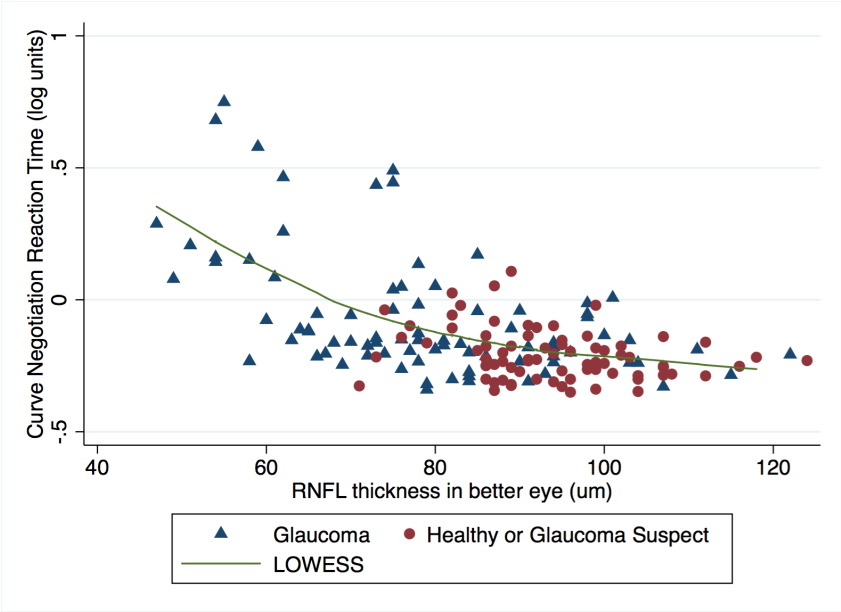

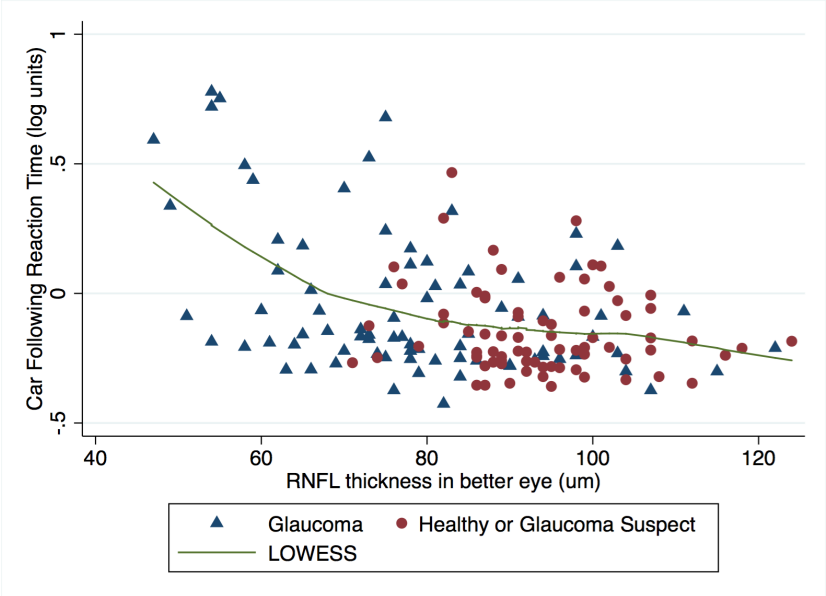

Figure 4-22. Scatter and LOWESS plots showing the relationship between MD in the better eye and reaction times to low contrast divided attention stimuli during the curve negotiation and car following simulated driving tasks.

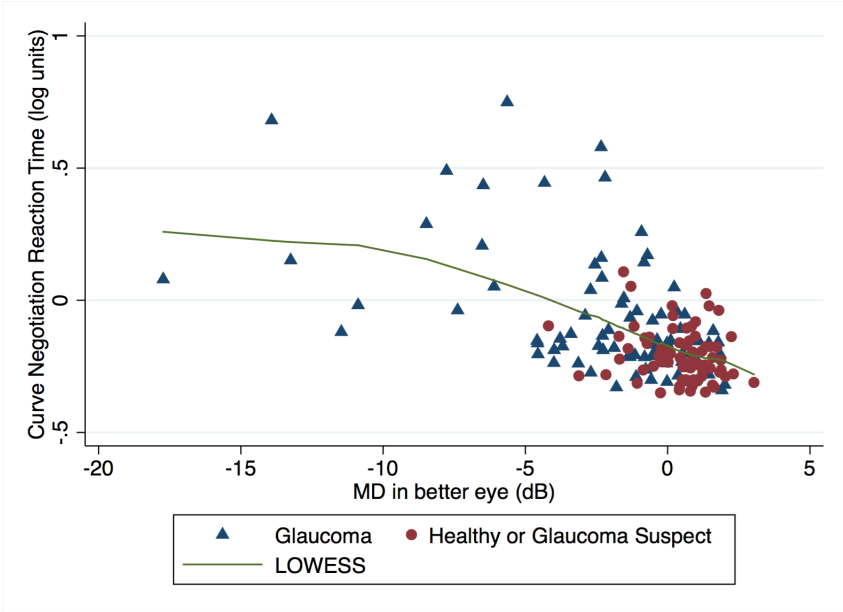

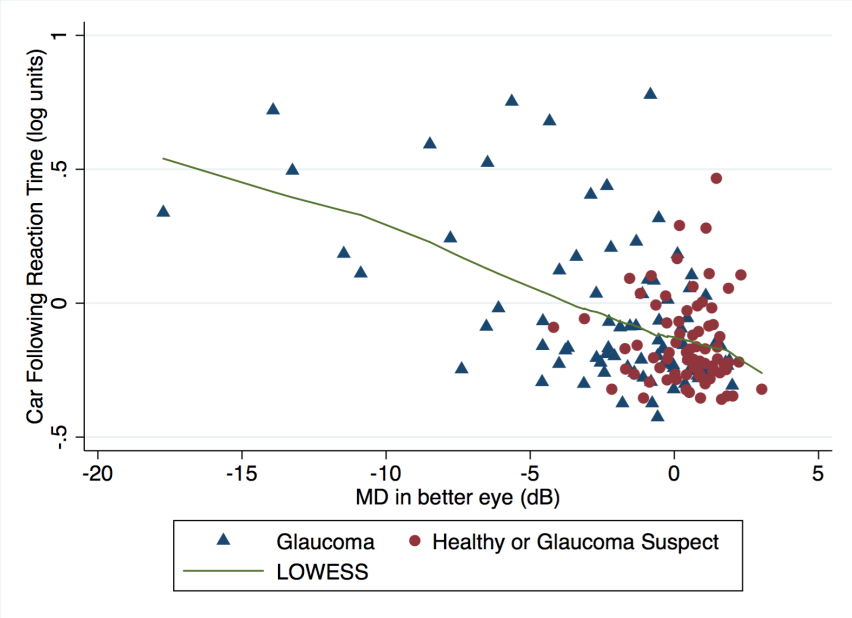

Figure 4-23. Scatter and LOWESS plots showing the relationship between MD in the worse eye and reaction times to low contrast divided attention stimuli during the curve negotiation and car following simulated driving tasks.

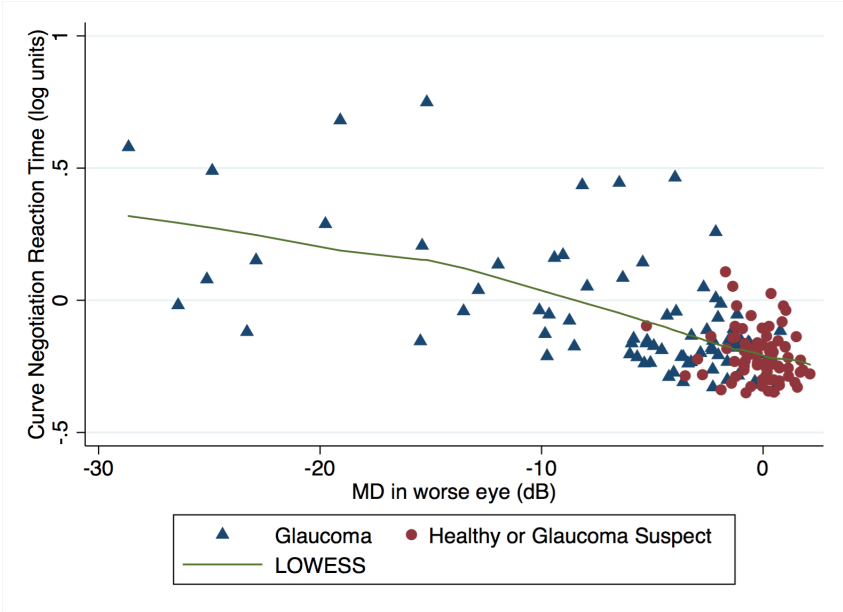

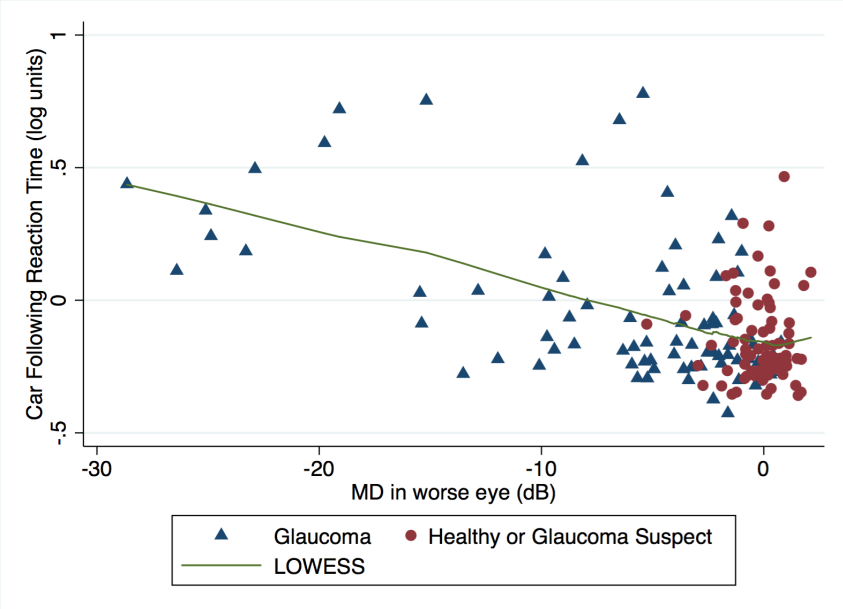

Figure 4-24. Scatter and LOWESS plots showing the relationship between age and reaction times to low contrast divided attention stimuli during the curve negotiation and car following simulated driving tasks.

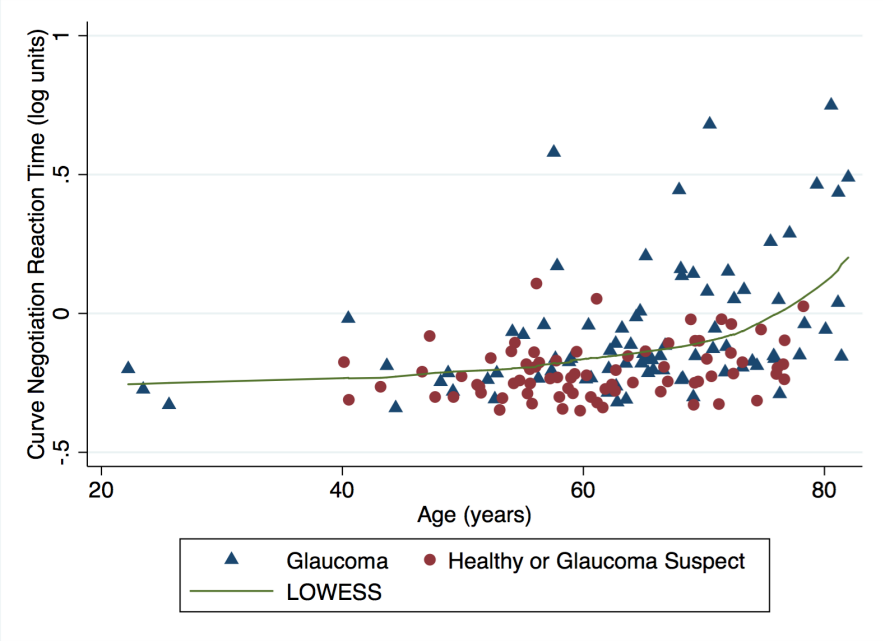

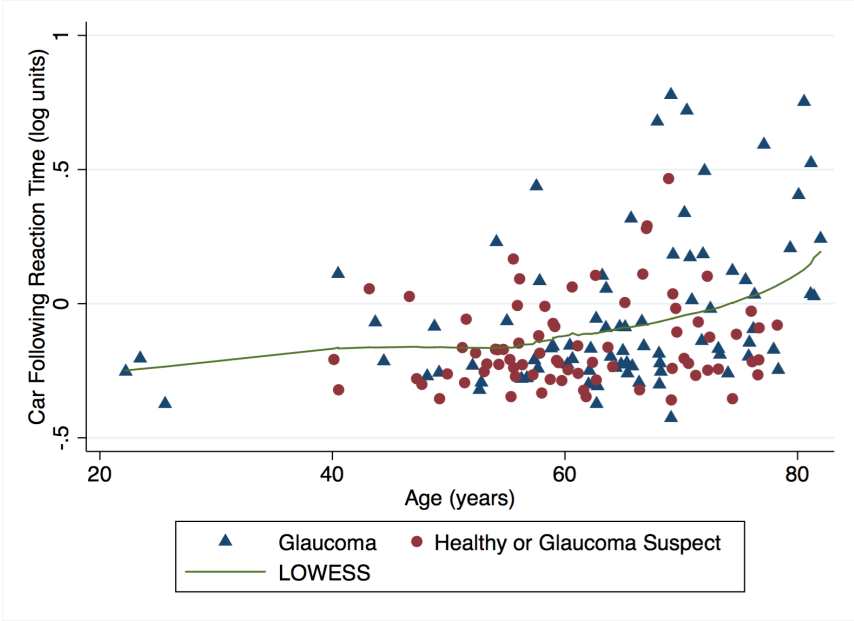

A multivariable model was developed to characterise the relationship between RNFL thickness and reaction times to the driving simulator divided attention tasks. The model included a quadratic term to account for nonlinearity. RNFL thickness in the better eye remained significantly predictive of reaction times, even after accounting for age, MD in the better eye, performance on the central driving task, and the cognitive assessment score (P = 0.001 (joint Wald test) for curve negotiation task and P = 0.019 for car following task) (Table 4-11). Worse MD in the better eye and worse performance on the central driving tasks were also associated with slower reaction times to the divided attention tasks, as was older age for the curve negotiation task (Table 4-11). The modelled relationship between RNFL thickness in the better eye and reaction times to the divided attention tasks are shown in Figure 4-25.

Table 4-11. Results of multivariable regression analyses examining the relationship between RNFL thickness in the better eye and driving simulator divided attention reaction times at low contrast (in logarithmic units).

Curve Negotiation Task **Divided attention reaction time at low contrast, adjusted R^2 = *0.469***			
	Coefficient	**95% CI**	**P-Value**
RNFL thickness in better eye (per 10μm)	-0.24	-0.40 to -0.10	0.001
RNFL thickness in better eye squared (per 100μm^2)	0.01	0.00 to 0.02	0.004
Age (per 10 years)	0.03	0.02 to 0.05	0.035
MD in better eye (dB)	-0.02	-0.03 to -0.01	<0.001
Curve coherence	-0.63	-1.10 to -0.15	0.010
Montreal Cognitive Assessment score	-0.01	-0.02 to 0.01	0.337
Constant	1.59	0.74 to 2.44	<0.001

Car Following Task **Divided attention reaction time at low contrast, adjusted R^2 = 0.316**			
	Coefficient	**95% CI**	**P-Value**
RNFL thickness in better eye (per 10μm)	-0.22	-0.41 to -0.04	0.019
RNFL thickness in better eye squared (per 100μm^2)	0.01	0.00 to 0.02	0.004
Age (per 10 years)	0.03	0.00 to 0.06	0.057
MD in better eye (dB)	-0.02	-0.03 to -0.01	0.001
Speed coherence	-0.34	-0.65 to -0.04	0.029
Montreal Cognitive Assessment score	0.00	-0.01 to 0.02	0.712
Constant	0.99	-0.05 to 2.02	0.062

Figure 4-25. Predicted reaction times to the low contrast divided attention stimuli for the curve negotiation and car following simulated driving tasks.

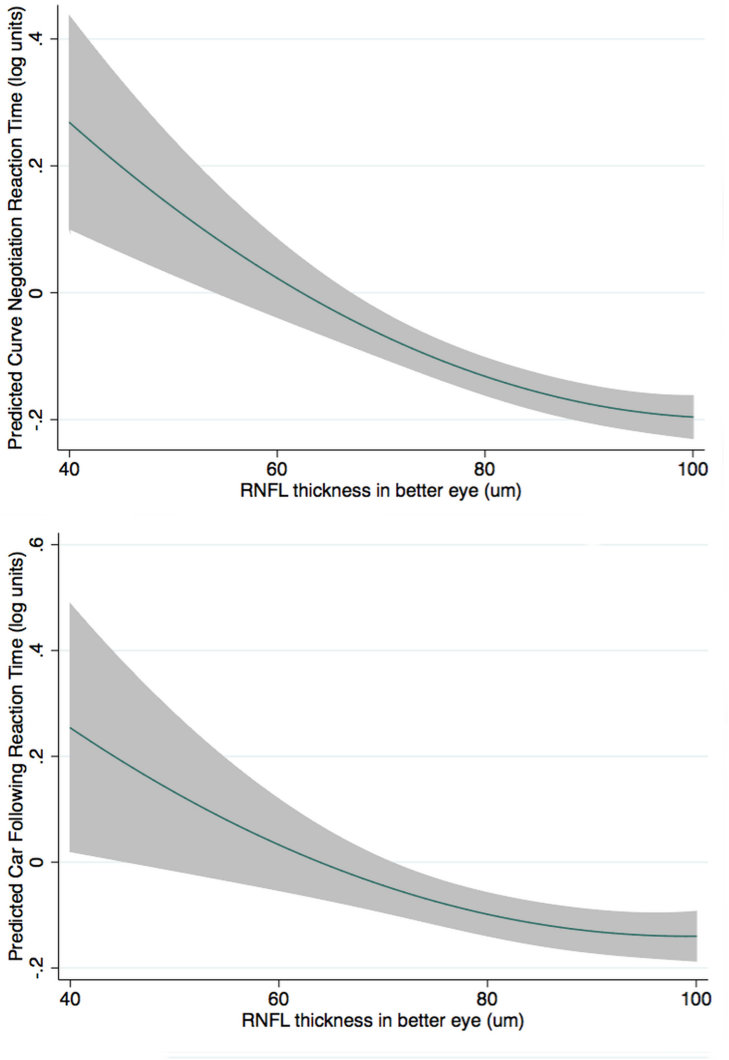

The difference between reaction times to the low and high contrast stimuli, calculated to minimise the contribution of the motor response to reaction times, was also related to RNFL thickness in the better eye for car following (spearman rank correlation ρ = -0.458; P <0.001) and curve negotiation tasks (spearman rank correlation ρ = -0.262; P <0.001), even accounting for confounding factors (Table 4-12).

Table 4-12. Results of multivariable regression analyses examining the relationship between RNFL thickness in the better eye and the difference in reaction times to the driving simulator divided attention tasks at high and low contrast.

Curve Negotiation Task **Driving simulator divided attention reaction time at low contrast minus reaction time at high contrast, adjusted R^2 = 0.327.**			
	Coefficient	**95% CI**	**P-Value**
RNFL thickness in better eye (per 10μm)	-0.78	-1.28 to -0.27	0.003
RNFL thickness in better eye squared (per 100μm^2)	0.04	0.01 to 0.07	0.010
Age (per 10 years)	0.06	-0.03 to 0.15	0.207
MD in best eye (dB)	-0.06	-0.09 to -0.02	0.001
Curve coherence	-1.10	-2.91 to 0.72	0.235
Montreal Cognitive Assessment score	-0.01	-0.05 to 0.03	0.759
Constant	4.78	1.54 to 8.03	0.004

Car Following Task **Driving simulator divided attention reaction time at low contrast minus reaction time at high contrast, adjusted R^2 = 0.256.**			
	Coefficient	**95% CI**	**P-Value**
RNFL thickness in better eye (per 10μm)	-0.85	-1.51 to -0.18	0.014
RNFL thickness in better eye squared (per 100μm^2)	0.04	0.01 to 0.08	0.026
Age (per 10 years)	0.05	-0.01 to 0.16	0.421
MD in best eye (dB)	-0.07	-0.12 to -0.03	0.002
Speed coherence	-0.41	-1.48 to 0.65	0.444
Montreal Cognitive Assessment score	0.01	-0.04 to 0.06	0.738
Constant	4.09	0.39 to 7.79	0.030

A 0.1 decrease in Michelson contrast was associated with 0.077 (95% CI 0.059 to 0.096) and 0.075 (95% CI 0.053 to 0.098) increases in curve negotiation and car following reaction times (in logarithmic units) in those with glaucoma, compared to increases of only 0.026 (95% CI 0.016 to 0.035) and 0.046 (95% CI 0.032 to 0.059) in controls.

4.4.5. Discussion

This phase of my research had several important findings. First, compared to similarly aged controls, drivers with glaucoma were found to have impaired ability to divide attention during the simulated driving tasks using low contrast stimuli. Impaired ability to divide attention has potentially serious consequences, as it is likely to affect the ability of a subject to perceive a dangerous situation in a timely manner.

The second important finding was that ability to divide attention was related to measures of glaucoma severity, with longer reaction times observed in patients with more severe disease. Therefore, whereas drivers with early glaucoma had reaction times to divided attention tasks like controls, those with advanced disease tended to have slower reaction times. There was a significant relationship between RNFL thinning and longer reaction times to the divided attention tasks (Figure 4-21), and a significant relationship between worse SAP MD and longer reaction times; however, RNFL thickness provided additional information (Table 4-11). This suggests that structural measurements might provide additional information compared to SAP in evaluating the likely impact of glaucoma on ability to perform tasks of daily living and therefore quality of life.

Although ophthalmologists tend to rely on SAP to assess functional losses in glaucoma, several studies have shown only a weak relationship between SAP and quality of life, or SAP and ability to perform daily activities (van Gestel et al 2010; Richman et al 2010; McKean-Cowdin et al 2007; Owsley, & McGwin 2010). It is possible that SAP may not fully capture changes in vision that are relevant to ability to perform some everyday tasks like driving such as motion perception or visual multi-tasking. Recent work has also indicated that significant neural losses may occur in the macular area of patients with glaucoma, which are likely to be relevant to daily tasks and may not be fully captured by SAP (Hood et al 2013).

As contrast has previously been shown to adversely affect driving performance, (Richman et al 2010) we decided to evaluate ability to divide attention using low, medium and high contrast stimuli. This methodology also allowed us to calculate the difference in reaction times to high and low contrast stimuli ('motor response corrected' reaction time), to minimise the contribution of the motor response to reaction times. Although divided attention reaction times increased with decreasing contrast for drivers with glaucoma and controls, drivers with glaucoma were worse affected. For example, drivers with glaucoma had a 3-fold greater increase in reaction times (in logarithmic units) compared to controls with decreasing contrast during the curve negotiation task, a finding consistent with previous studies showing patients with glaucoma to be more affected by low contrast than controls (Burton et al 2012; Richman et al 2010). For example, Burton and colleagues recently reported that patients with glaucoma have more difficulty reading at low contrast compared to healthy individuals (Burton et al 2012).

Thinner RNFL in the better eye was also associated with larger differences in reaction time to low and high contrast stimuli suggesting the relationship between RNFL thickness and reaction time during simulated driving was not due to differences in motor response (Table 4-12). Although the difference in reaction time between low and high contrast stimuli was not significantly different between patients with glaucoma and controls (Table 4-10), this is likely due to the relatively large number of patients with early and moderate glaucoma, as there was a significant association between MD and RNFL thickness and the 'motor-response corrected reaction time'. Average distance driven per week was recorded but was not significantly associated with reaction times to the divided attention tasks. There was also no evidence of difference in speed-accuracy trade-offs between glaucomatous and healthy individuals as indicated by similar rates of false-positive responses.

Although this phase of my research project fulfilled the objective to evaluate the relationship between a structural measure of glaucomatous neural loss and ability to perform a task relevant to daily living, the study has some limitations. Driving is a complex task, influenced by many factors and so it is important to emphasise that RNFL thinning and worsening SAP MD account for only some of the variability in ability to divide attention during driving simulation. I did not assess the relationship between RNFL thickness and motor vehicle collisions directly, as collisions are rare and difficult to predict. I instead focused on measures of ability to divide attention that have previously been shown to be related to collision risk (Owsley, & McGwin 2010; Medeiros et al 2012; Owsley et al 1998). Also, divided attention was assessed using a driving simulator rather than during on-road driving and it is possible that drivers may show differences in

behaviour in real world driving, when the risks to safety are also real. A further limitation is that the study included relatively few patients with moderate to advanced visual field loss. Had we included more patients with worse field loss, the relationship between perimetry and simulated driving performance may have been stronger.

A further potential limitation is that driving is a binocular task, whereas SAP assesses vision in each eye separately and I examined the relationship between ability to divide attention and SAP MD in the better and worse eyes, rather than using a binocular visual field. I have subsequently re-run the analysis using integrated binocular visual field sensitivities calculated from monocular SAP sensitivities using the binocular summation method described by Nelson-Quigg and colleagues (Nelson-Quigg et al 2000).

There was slightly correlation between reaction times to the simulated driving tasks and binocular SAP sensitivity than between reaction times and SAP MD in the better or worse eyes alone (Figure 4-26) ($\rho = -0.559$; $P<0.001$ for the relationship between binocular SAP sensitivity and $\log_{10}$ reaction times for the curve negotiation task (compared to $\rho = -0.480$ and $\rho = -0.480$ for SAP MD and RNFL thickness in the better eye) and $\rho = -0.319$; $P<0.001$ for the relationship between binocular SAP sensitivity and $\log_{10}$ reaction times for the car following task (compared to $\rho = -0.315$ and $\rho =-0.280$ for SAP MD and RNFL thickness in the better eye). Although binocular SAP sensitivity had the strongest relationship with reaction times to the peripheral divided attention stimuli, RNFL thickness still provided additional information for predicting ability to divide attention when binocular SAP sensitivity was included in the multivariable model.

Figure 4-26. Scatter and LOWESS plots showing the relationship between integrated binocular visual field sensitivity and reaction times to low contrast divided attention stimuli during the curve negotiation and car following simulated driving tasks.

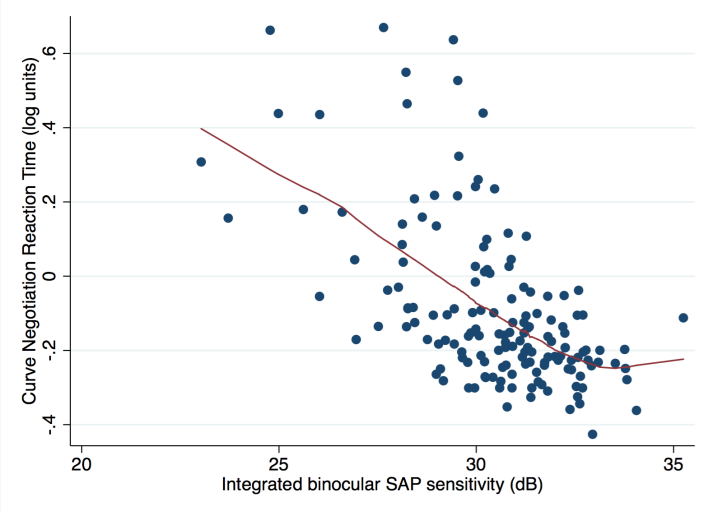

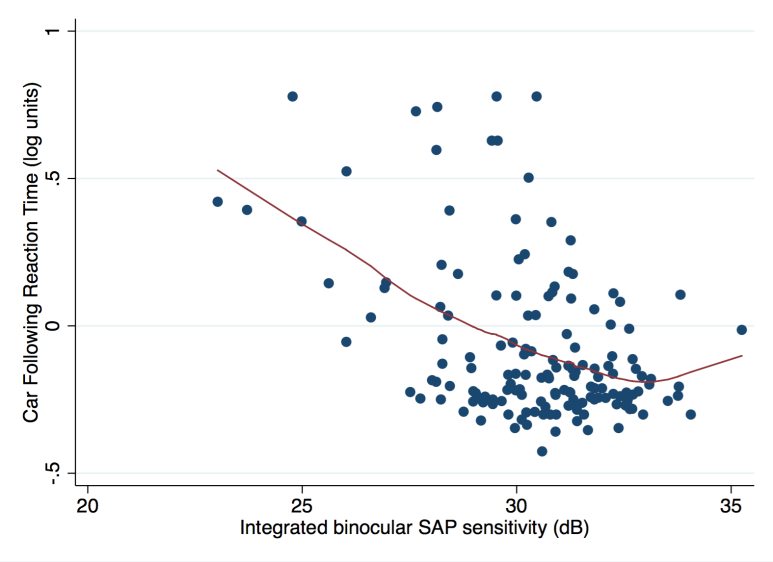

Univariable regression analysis revealed a 0.064 log unit increase in reaction time to the curve negotiation divided attention task for each 1dB decrease in integrated binocular SAP sensitivity (95% CI 0.049 to 0.078,

P<0.001, R^2 = 0.343). There was a 0.058 log unit increase in reaction time for each 1 dB decrease in binocular SAP sensitivity (95% CI 0.039 to 0.077, P<0.001, R^2 = 0.189). The correlation between binocular SAP sensitivity and reaction times to the divided attention tasks was similar to the correlation between RNFL thickness in the better eye (converted to log units) and reaction times (R^2 = 0.332, P<0.001 for RNFL thickness in the better eye and reaction time to the curve negotiation divided attention task and R^2 = 0.184, P<0.001 for the car following divided attention task).

Recently, David Crabb's group have explored the utility of binocular and monocular visual field tests for assessing fitness to drive. They found that SAP MD in the better eye is strongly related to legal fitness to drive criteria (Saunders et al 2012). Their study, which included 2,604 patients with glaucoma and visual field damage in both eyes, found SAP MD in the better eye to achieve an AUC of 0.962 for discriminating patients meeting and failing the UK visual field criteria assessed using the surrogate of integrated binocular visual field. Using SAP MD from both eyes offered no additional information. The results of my work suggest slightly better correlation between binocular SAP sensitivity and performance on a simulated driving task than SAP MD in the better eye, however inclusion of information from structural tests may further improve the ability to determine ability to safely drive. It is however possible that functional tests that employ different test strategies to the 24-2 used in this study, may negate the additive predictive ability of structural measures.

Although I did not examine whether the location of visual field loss was related to driving task performance, a recent study has shown loss of the superior visual field to have a larger impact on ability to detect hazards when viewing

driving scenes than loss of the inferior visual field (Glen et al 2015). It has also been shown that drivers with glaucoma may exhibit different eye movement behaviour compared to healthy subjects, which is likely to vary depending on the location of field loss (Zhu et al 2014; Crabb et al 2010). It is also important to acknowledge that I did not examine whether drivers met the visual criteria for legal fitness to drive, which in the UK includes the Esterman binocular visual field. However, it has previously been shown that integrated binocular visual fields and Esterman visual fields have good agreement for classifying patients as pass or fail for UK visual field component of fitness to drive (Crabb et al 2004). In a study of 65 patients, Crabb and colleagues found 44 (68%) were classified as pass by both integrated binocular and Esterman visual fields, 13 failed both tests, and 8 failed the integrated visual field but not Esterman.

Despite the limitations of this phase of my research, this study furthers understanding of the relationship between structural and functional changes in glaucoma, and helps provide evidence that structural changes are relevant to the patient. I found drivers with glaucoma to have slower reaction times to low contrast divided attention tasks during simulated driving, which is likely to indicate increased risk of collision. Although worse performance on SAP was also associated with worse ability to divide attention, RNFL thinning on OCT provided additional information. These findings help explain why drivers with glaucoma are at increased risk of collisions and help validate the use of structural measurements to quantify glaucomatous changes, however it is important to emphasise that structural measurements complement functional testing and do not replace it. The study also suggest that combining information from structural

and functional tests may improve our ability to determine which patients might have problems performing daily activities, such as driving.

5 SECTION IV: CONCLUSIONS

5.1. Summary

The results of this body of work can be summarised as follows:

1. Various models have demonstrated good correlation between structural and functional parameters in glaucoma as long as appropriate measurement scales are used. However, some discordance between structure and function is to be expected, for example, functional changes may be noted in the absence of detectable structural change due to RGCs becoming dysfunctional prior to changes in their axonal diameter measurable as a reduction in RNFL thickness on OCT. Conversely, due to factors such as incomplete spatial summation, high test-retest variability, and differences in dynamic range between instruments, in some patients, structural changes may be detectable prior to functional changes. The result is that for optimal detection of glaucoma and glaucoma progression there is a continued need to test both domains.

2. Correlation between results of structural and functional tests suggests that detection of change to the ONH or RNFL is clinically relevant for patients, i.e., structural changes are related to the clinically relevant outcome of deterioration in visual field. Though the structure-function models which helped elucidate this relationship are cross-sectional, longitudinal studies have also shown a relationship between progressive structural changes and worsening visual field. For example, faster rates of RNFL loss detected by OCT, or faster rate of rim loss detected by CSLO, are associated with increased future risk of worsening visual field. These studies should not be

interpreted as proof that structural changes always precede functional losses though as, in some patients, a reduction in DLS on SAP is detected before changes to the ONH are apparent.

3. Structural changes in glaucoma include localised loss of the RNFL, a feature traditionally considered an early manifestation of disease. The current body of work has suggested that rather than be an early manifestation of disease, localised RNFL defects visible on photographs may be associated with large neural losses. On average, eyes with RNFL defects had an estimated 39% fewer RGCs compared to similarly aged healthy eyes, despite an average SAP MD of only -3.3 dB. As part of this body of work I attempted to estimate RGC losses in eyes with localised RNFL defects but found major flaws in the formulae proposed for RGC estimation. Harwerth's method for RGC estimation has been cited in many peer review articles as a useful tool, however I would recommend it is not used before further histological validation. The formulae were derived from experiments in non-human primates by examining the relationship between OCT RNFL thickness, SAP sensitivity and histological counts of RGC number. However, there was wide disparity in RGC counts for a given RNFL thickness or SAP sensitivity and the formulae include several incorrect assumptions, not least use of the wrong axonal diameter. During the course of my study, as I became aware of these limitations, I decided to abandon use of this method of RGC estimation.

4. Glaucomatous damage often occurs at different rates in each eye leading to asymmetry. If glaucoma is sufficiently asymmetric, asymmetry of the pupillary response can be detected as a RAPD. The results of my work revealed strong correlation between magnitude of RAPD and inter-eye differences in RNFL thickness and SAP MD. A larger magnitude RAPD is therefore likely to indicate greater asymmetry of each of these parameters. The swinging flashlight test, the most common method of identifying a RAPD in clinical practice can detect a RAPD of approximately 0.3 log units, which equated to an inter-eye difference in RNFL thickness of 6 μm or an inter-eye difference in SAP MD of 3.5dB if the average MD is -5dB or 6dB if the average MD in -15dB.

5. Finally, this body of work has demonstrated an association between glaucomatous structural change and impaired performance on simulated driving, to the best of my knowledge the first study to reveal such an association. I found drivers with glaucoma had impaired ability to divide attention during simulated driving, particularly under low contrast conditions. Patients with thinner RNFL in the better eye tended to have worse ability to divide attention. Worse SAP sensitivity in the better eye and worse binocular SAP sensitivity were also strongly correlated with worse driving simulator performance, however, structural information was of additional predictive value, even when results of SAP were taken into account. The results should not be interpreted that structural measurements are superior to SAP, but rather that they provide complimentary information that, when used with

SAP, may improve our ability to gauge the impact of glaucoma on at least one important activity of daily living.

5.2. Impact

The results of this body of work suggest that information from structural measurements could be combined with information from functional tests to improve predictions of the impact of glaucoma on the ability to perform tasks of daily living. Driving was the sole task examined in this work, however, it is probable that combining information from structural and functional tests may be a useful strategy for predicting the impact of glaucoma on other activities; an important area for further study.

Together with previous experiments that have demonstrated progressive structural changes to be predictive of future decline in visual function, the current work provides evidence that structural measurements are relevant to patients. This may help decisions regarding whether structural measurements could be valid surrogates as endpoints for clinical trials. As structural changes often precede detectable changes on perimetry and as psychophysical tests are often subject to considerable test-rest variability, the use of structural endpoints, or endpoints consisting of a combination of information from structural and functional tests, may allow the length of trials to be shortened.

It should however be noted that patients enrolled in the current studies performed only a 24-2 visual field. Although SAP remains the gold standard for assessing functional loss in glaucoma, this work suggests that conventional 24-2 perimetry fails to fully capture the impact of glaucomatous neural losses. This may be because the 24-2 samples only 24 degrees of the retina and has relatively few test points in the central field, or be due to the inherent variability of

psychophysical testing reducing the association between metrics. It is possible that the additional value of the measurements from OCT may have diminished if information from alternative functional tests had been included. For example, incorporation of data from 10-2 visual fields may have reduced the additional value of OCT. Nevertheless, multiple studies have shown that structural and functional changes are rarely detected simultaneously.

It is conceivable that a driving risk prediction tool might be developed that combines information from SAP and OCT to identify patients with impaired ability to divide attention. Impaired ability to divide attention whilst driving has potentially serious consequences, as it is likely to affect the ability of a subject to perceive a dangerous situation in a timely manner and is associated with increased risk of collision. Patients identified as high risk could then undergo more detailed scrutiny of their driving, for example, with a simulated or on-road assessment. By monitoring changes on OCT and SAP it may also be possible to estimate the lifetime risk of losing one's driving licence, similar to current visual field trend-analyses used to predict lifetime risk of visual loss. Such a tool could help identify those who might benefit from escalation in treatment at an earlier stage and avoid unnecessary treatments for those at low risk. By incorporating structural measurements into predictions of glaucoma progression, it may also be possible to improve predictions of the impact of disease on ability to perform other tasks. Put simply, improved understanding of the relationship between commonly measured clinical metrics and activities of daily living may allow clinicians to better appreciate the significance of changes in SAP and OCT to patients.

My conclusion is that both structural and functional tests are important and that rather debate which test is best, future research should focus on developing methods of integrating the results from both domains to better understand the impact of glaucoma on patients.

5.3. Future Work

Since returning to clinical practice I have been fortunate to secure funded research time from NHS Research Scotland, which has enabled me to continue the collaboration with UCSD and begin to develop my own research programme. In collaboration with UCSD I have continued to investigate the impact of glaucoma on driving and the next stage of this work is to conduct a longitudinal study to examine the relationship between change in structural and functional parameters and driving performance over time. Further validity would also be gained by examining whether objective measures of glaucomatous damage are related to real-world on-road driving metrics. In the UK, the current visual field standard for driving is assessed using the Esterman visual field test, which was not designed for this task, and has a lack of evidence to support its use. It is conceivable that a battery of tests, including SAP and OCT may be a better discriminator of whether a person has sufficient sight to safely drive, and further research comparing Esterman to other clinical tests is needed.

Dr Medeiros' team have also begun evaluating the relationship between conventional measures of glaucoma and the ability to perform other common tasks such as walking and searching for objects. This has involved building computer simulations displayed using a virtual reality headset, which allows development of a set of standardised scenarios, with eye tracking used to measure response times and examine search strategies. We have established that a combination of information from structural and functional tests is required; therefore, an important area of future study should be the development of better methods of integrating measurements. For example, using Bayesian statistical

methods to modify predictions of decline in SAP using prior information from OCT, with the possibility of also adding information regarding other risk factors to the model.

Arguably the most important structure-function relationship is the relationship between structural changes and quality of life. In collaboration with Carolina Gracitelli, a PhD student at UCSD, have recently conducted a study examining this issue (Gracitelli et al 2015). 260 subjects with glaucoma were followed for an average of 2.5 years. All were asked to complete the 25-item National Eye Institute Visual Function Questionnaire (NEI VFQ-25) and changes in visual field and structural measurements were compared to changes in self-reported quality of life. We found patients experiencing faster rates of RNFL loss, measured using OCT, had faster rates of decline in quality of life and in agreement with the results of my investigation of driving simulation, information from structural testing provided additional information explaining patient-reported outcomes even after adjusting for the contribution of SAP. This study was limited by the potential bias introduced by patient's knowledge of their progression status; in other words, patients' perceptions regarding quality of life may have been influenced by being told they were progressing rather than by deterioration in quality of life due to the disease process. Nevertheless, it adds to the evidence that information from structural tests can provide additional value to conventional measures of visual function alone when assessing the impact of disease on patients.

During the course of my research, I became more aware of the limitations of the current tests available in clinical practice, in particular the limitations of the 24-2 SAP testing strategy. A major focus of my current work is the attempt to develop an improved psychophysical test. Together with engineers from University of Edinburgh we have been designing a new perimetric test that, rather than require the patient to press a button, uses eye-tracking to assess responses to seen stimuli. The patient is permitted to move their head during testing and does not need to keep their chin on a rest. Preliminary results suggest that patients prefer eye tracking perimetry to conventional SAP and we have received funding from the International Glaucoma Association to develop the test further. It is conceivable that as the test more closely reflects the real world environment, where patients are free to move their head and eyes to detect visual stimuli, the results from this test might be better correlated to ability to perform vision-related tasks of daily living than SAP.

A final further interesting area of study is the importance of macular changes in glaucoma. Until recently imaging in glaucoma has primarily focused on assessment of the ONH and RNFL, however, as the macula contains approximately 50% of RGCs, imaging the macula may provide additional information in the assessment of glaucomatous damage. Glaucomatous changes in the macula are also likely to have particularly serious consequences for quality of life given the importance of central vision. As the macula is largely devoid of large vessels and has a readily identifiable centre, assessment of this region may also overcome some limitations of circumpapillary measurements, such as interference from retinal and optic nerve head vasculature, parapapillary atrophy, and variable placement of the measurement circle around the disc. Future

studies should assess whether combining information from OCT of the macula, RNFL or ONH, and SAP further improves our ability to measure and understand the consequences of glaucoma for our patients.

6 SECTION VI: REFERENCES

Anderson, D.R., Drance, S.M., Schulzer, M., Collaborative Normal-Tension Glaucoma Study Group, 2001, Natural history of normal-tension glaucoma, *Ophthalmology*, 108, 247-253.

Anton, A., Yamagishi, N., Zangwill, L., Sample, P.A., Weinreb, R.N., 1998, Mapping structural to functional damage in glaucoma with standard automated perimetry and confocal scanning laser ophthalmoscopy, *American Journal of Ophthalmology*, 125, 436-446.

Armaly, M.F., 1969, Cup-disc ratio in early open-angle glaucoma, *Documenta ophthalmologica. Advances in Ophthalmology*, 26, 526-533.

Aydin, A., Wollstein, G., Price, L.L., Fujimoto, J.G., Schuman, J.S., 2003, Optical coherence tomography assessment of retinal nerve fibre layer thickness changes after glaucoma surgery, *Ophthalmology*, 110, 1506-1511.

Azuara-Blanco, A., Katz, L.J., Spaeth, G.L., Vernon, S.A., Spencer, F., Lanzl, I.M., 2003, Clinical agreement among glaucoma experts in the detection of glaucomatous changes of the optic disk using simultaneous stereoscopic photographs, *American Journal of Ophthalmology*, 136, 949-950.

Ball, K., Owsley, C., 1993, The useful field of view test: a new technique for evaluating age-related declines in visual function, *Journal of the American Optometric Association*, 64, 71-79.

Banister, K., Boachie, C., Bourne, R., Cook, J., Burr, J.M., Ramsay, C., Garway-Heath, D., Gray, J., McMeekin, P., Hernández, R., Azuara-Blanco, A., 2016, Can

Automated Imaging for Optic Disc and Retinal Nerve Fibre Layer Analysis Aid Glaucoma Detection? *Ophthalmology*, 123, 930-938.

Banitt, M.R., Ventura, L.M., Feuer, W.J., Savatovsky, E., Luna, G., Shif, O., Bosse, B., Porciatti, V., 2013, Progressive loss of retinal ganglion cell function precedes structural loss by several years in glaucoma suspects, *Investigative Ophthalmology & Visual Science*, 54, 2346-2352.

Bengtsson, B., Heijl, A., 2006, Diagnostic sensitivity of fast blue-yellow and standard automated perimetry in early glaucoma: a comparison between different test programs, *Ophthalmology*, 113, 1092-1097.

Bengtsson, B., Heijl, A., 2008, A visual field index for calculation of glaucoma rate of progression, *American Journal of Ophthalmology*, 145, 343-353.

Bengtsson, B., Andersson, S., Heijl, A., 2012, Performance of time-domain and spectral-domain Optical Coherence Tomography for glaucoma screening, *Acta Ophthalmologica*, 90, 310-315.

Boodhna, T., Saunders, L.J., Crabb, D.P., 2015, Are rates of vision loss in patients in English glaucoma clinics slowing down over time? Trends from a decade of data, *Eye*, 29, 1613-1619.

Broman, A.T., West, S.K., Muñoz, B., Bandeen-Roche, K., Rubin, G.S., Turano, K.A., 2004, Divided visual attention as a predictor of bumping while walking: the Salisbury Eye Evaluation, *Investigative Ophthalmology & Visual Science*, 45, 2955-2960.

Brookhuis, K., de Waard, D., Mulder, B., 1994, Measuring driving performance by car-following in traffic, *Ergonomics*, 37, 427-434.

Brouwer, W.H., Waterink, W., Van Wolffelaar, P.C., Rothengatter, T., 1991, Divided attention in experienced young and older drivers: lane tracking and visual analysis in a dynamic driving simulator, *Human Factors: The Journal of the Human Factors and Ergonomics Society*, 33, 573-582.

Budenz, D.L., Barton, K., Whiteside-de Vos, J., Schiffman, J., Bandi, J., Nolan, W., Herndon, L., Kim, H., Hay-Smith, G., Tielsch, J.M., 2013, Prevalence of glaucoma in an urban west African population: the Tema Eye Survey, *JAMA Ophthalmology*, 131, 651-658.

Budenz, D.L., Michael, A., Chang, R.T., McSoley, J., Katz, J., 2005, Sensitivity and specificity of the Stratus OCT for perimetric glaucoma, *Ophthalmology*, 112, 3-9.

Burgoyne, C.F., Downs, J.C., Bellezza, A.J., Suh, J.K., Hart, R.T., 2005, The optic nerve head as a biomechanical structure: a new paradigm for understanding the role of IOP-related stress and strain in the pathophysiology of glaucomatous optic nerve head damage, *Progress in Retinal and Eye Research*, 24, 39-73.

Burr, J.M., Mowatt, G., Hernandez, R., Siddiqui, M.A., Cook, J., Lourenco, T., Ramsay, C., Vae, L., Fraser, C., Azuara-Blanco, A., Deeks J., Cairns, J., Wormald, R., McPherson, S., Rabindranath, K., Grant, A., 2007, The clinical effectiveness and cost-effectiveness of screening for open angle glaucoma: a

systematic review and economic evaluation. *Health Technology Assessment*, 11:1-190.

Burton, R., Crabb, D.P., Smith, N.D., Glen, F.C., Garway-Heath, D.F., 2012, Glaucoma and reading: exploring the effects of contrast lowering of text, *Optometry and Vision Science*, 89, 1282-1287.

Celebi, A.R., Mirza, G.E., 2013, Age-related change in retinal nerve fibre layer thickness measured with spectral domain optical coherence tomography, *Investigative Ophthalmology & Visual Science*, 54, 8095-8103.

Cello, K.E., Nelson-Quigg, J.M., Johnson, C.A., 2000, Frequency doubling technology perimetry for detection of glaucomatous visual field loss, *American Journal of Ophthalmology*, 129, 314-322.

Chang, D.S., Boland, M.V., Arora, K.S., Supakontanasan, W., Chen, B.B., Friedman, D.S., 2013a, Symmetry of the pupillary light reflex and its relationship to retinal nerve fibre layer thickness and visual field defect, *Investigative Ophthalmology & Visual Science*, 54, 5596-5601.

Chang, D.S., Xu, L., Boland, M.V., Friedman, D.S., 2013b, Accuracy of pupil assessment for the detection of glaucoma: a systematic review and meta-analysis, *Ophthalmology*, 120, 2217-2225.

Chang, R.T., Knight, O.J., Feuer, W.J., Budenz, D.L., 2009, Sensitivity and specificity of time-domain versus spectral-domain optical coherence tomography in diagnosing early to moderate glaucoma, *Ophthalmology*, 116, 2294-2299.

Charalel, R.A., Lin, H.S., Singh, K., 2014, Glaucoma screening using relative afferent pupillary defect, *Journal of Glaucoma*, 23, 169-173.

Chauhan, B.C., Garway-Heath, D.F., Goñi, F.J., Rossetti, L., Bengtsson, B., Viswanathan, A.C., Heijl, A., 2008, Practical recommendations for measuring rates of visual field change in glaucoma, *The British Journal of Ophthalmology*, 92, 569-573.

Chauhan, B.C., Malik, R., Shuba, L.M., Rafuse, P.E., Nicolela, M.T., Artes, P.H., 2014, Rates of glaucomatous visual field change in a large clinical population, *Investigative Ophthalmology & Visual Science*, 55, 4135-4143.

Chauhan, B.C., Nicolela, M.T., Artes, P.H., 2009, Incidence and rates of visual field progression after longitudinally measured optic disc change in glaucoma, *Ophthalmology*, 116, 2110-2118.

Chauhan, B.C., O'Leary, N., Almobarak, F.A., Reis, A.S., Yang, H., Sharpe, G.P., Hutchison, D.M., Nicolela, M.T., Burgoyne, C.F., 2013, Enhanced Detection of Open-angle Glaucoma with an Anatomically Accurate Optical Coherence Tomography-Derived Neuroretinal Rim Parameter, *Ophthalmology*, 120, 535-543.

Chew, S.S., Cunnningham, W.J., Gamble, G.D., Danesh-Meyer, H.V., 2010, Retinal nerve fibre layer loss in glaucoma patients with a relative afferent pupillary defect, *Investigative Ophthalmology & Visual Science*, 51, 5049-5053.

Chew, S.S., Kerr, N.M., Wong, A.B., Craig, J.P., Chou, C.Y., Danesh-Meyer, H.V., 2016, Anxiety in visual field testing, *The British Journal of Ophthalmology*, 100, 1128-1133.

Crabb, D.P., Fitzke, F.W., Hitchings, R.A., Viswanathan, A.C., 2004, A practical approach to measuring the visual field component of fitness to drive, *The British Journal of Ophthalmology*, 88, 1191-1196.

Crabb, D.P., Smith, N.D., Rauscher, F.G., Chisholm, C.M., Barbur, J.L., Edgar, D.F., Garway-Heath, D.F., 2010, Exploring eye movements in patients with glaucoma when viewing a driving scene, *PloS one*, 5, e9710.

Crowston, J.G., Fahy, E.T., Fry, L., Trounce, I.A., van Wijngaarden, P., Petou, S., Chrysostomou, V., 2017. Targeting retinal ganglion cell recovery, Eye, 31,196-198.

Cull, G.A., Reynaud, J., Wang, L., Cioffi, G.A., Burgoyne, C.F., Fortune, B., 2012, Relationship between orbital optic nerve axon counts and retinal nerve fibre layer thickness measured by spectral domain optical coherence tomography, *Investigative Ophthalmology & Visual Science*, 53, 7766-7773.

Curcio, C.A., Allen, K.A., 1990, Topography of ganglion cells in human retina, *Journal of Comparative Neurology*, 300, 5-25.

Curcio, C.A., Drucker, D.N., 1993, Retinal ganglion cells in Alzheimer's disease and aging, *Annals of Neurology*, 33, 248-257.

Dacey, D.M., Lee, B.B., 1994, The 'blue-on' opponent pathway in primate retina originates from a distinct bistratified ganglion cell type, *Nature*, 367, 731-735.

Deleón-Ortega, J.E., Arthur, S.N., McGwin, G., Xie, A., Monheit, B.E., Girkin, C.A., 2006, Discrimination between glaucomatous and nonglaucomatous eyes using quantitative imaging devices and subjective optic nerve head assessment, *Investigative Ophthalmology & Visual Science*, 47, 3374-3380.

Drasdo, N., Millican, C.L., Katholi, C.R., Curcio, C.A., 2007, The length of Henle fibres in the human retina and a model of ganglion receptive field density in the visual field, *Vision Research*, 47, 2901-2911.

Drasdo, N., Mortlock, K.E., North, R.V., 2008, Ganglion cell loss and dysfunction: relationship to perimetric sensitivity, *Optometry and Vision Science*, 85, 1036-1042.

Ferreras, A., Pablo, L.E., Garway-Heath, D.F., Fogagnolo, P., García-Feijoo, J., 2008, Mapping standard automated perimetry to the peripapillary retinal nerve fibre layer in glaucoma, *Investigative Ophthalmology & Visual Science*, 49, 3018-3025.

Fonda, S.J., Wallace, R.B., Herzog, A.R., 2001, Changes in driving patterns and worsening depressive symptoms among older adults, *The Journals of Gerontology. Series B, Psychological sciences and social sciences*, 56, S343-351.

Fortune, B., Burgoyne, C.F., Cull, G., Reynaud, J., Wang, L., 2013a, Onset and progression of peripapillary retinal nerve fibre layer (RNFL) retardance changes occur earlier than RNFL thickness changes in experimental glaucoma, *Investigative Ophthalmology & Visual Science*, 54, 5653-5661.

Fortune, B., Reynaud, J., Wang, L., Burgoyne, C.F., 2013b, Does optic nerve head surface topography change prior to loss of retinal nerve fibre layer thickness: a test of the site of injury hypothesis in experimental glaucoma, *PloS one*, 8, e77831.

Garas, A., Vargha, P., Holló, G., 2011, Diagnostic accuracy of nerve fibre layer, macular thickness and optic disc measurements made with the RTVue-100 optical coherence tomograph to detect glaucoma, *Eye*, 25, 57-65.

Garway-Heath, D.F., Caprioli, J., Fitzke, F.W., Hitchings, R.A., 2000, Scaling the hill of vision: the physiological relationship between light sensitivity and ganglion cell numbers, *Investigative Ophthalmology & Visual Science*, 41, 1774-1782.

Garway-Heath, D.F., Holder, G.E., Fitzke, F.W., Hitchings, R.A., 2002, Relationship between electrophysiological, psychophysical, and anatomical measurements in glaucoma, *Investigative Ophthalmology & Visual Science*, 43, 2213-2220.

Garway-Heath, D.F., Poinoosawmy, D., Fitzke, F.W., Hitchings, R.A., 2000, Mapping the visual field to the optic disc in normal tension glaucoma eyes, *Ophthalmology*, 107, 1809-1815.

Glen, F.C., Baker, H., Crabb, D.P., 2014, A qualitative investigation into patients' views on visual field testing for glaucoma monitoring, *BMJ open*, 4, e003996.

Glen, F.C., Crabb, D.P., Garway-Heath, D.F., 2011, The direction of research into visual disability and quality of life in glaucoma, *BMC Ophthalmology*, 11, 19.

Glen, F.C., Smith, N.D., Crabb, D.P., 2015, Impact of superior and inferior visual field loss on hazard detection in a computer-based driving test, *British Journal of Ophthalmology*, 99, 613-617.

Gordon, M.O., Beiser, J.A., Brandt, J.D., Heuer, D.K., Higginbotham, E.J., Johnson, C.A., Keltner, J.L., Miller, J.P., Parrish, R.K., Wilson, M.R., Kass, M.A., 2002, The Ocular Hypertension Treatment Study: baseline factors that predict the onset of primary open-angle glaucoma, *Archives of Ophthalmology*, 120, 714-720.

Gracitelli, C.P., Abe, R.Y., Tatham, A.J., Rosen, P.N., Zangwill, L.M., Boer, E.R., Weinreb, R.N. Medeiros, F.A., 2015, Association between progressive retinal nerve fibre layer loss and longitudinal change in quality of life in glaucoma, *JAMA Ophthalmology*, 133, 384-390.

Greaney, M.J., Hoffman, D.C., Garway-Heath, D.F., Nakla, M., Coleman, A.L., Caprioli, J., 2002, Comparison of optic nerve imaging methods to distinguish normal eyes from those with glaucoma, *Investigative Ophthalmology & Visual Science*, 43, 140-145.

Greenfield, D.S., Liebmann, J.M., Ritch, R., Krupin, T., Low-Pressure Glaucoma Study Group, 2007, Visual field and intraocular pressure asymmetry in the low-pressure glaucoma treatment study, *Ophthalmology*, 114, 460-465.

Hadwin, S.E., Redmond, T., Garway-Heath, D.F., Lemij, H.G., Reus, N.J., Ward, G., Anderson, R.S., 2013, Assessment of optic disc photographs for glaucoma by UK optometrists: the Moorfields Optic Disc Assessment Study (MODAS), *Ophthalmic & Physiological Optics,* 33, 618-624.

Harman, A., Abrahams, B., Moore, S., Hoskins, R., 2000, Neuronal density in the human retinal ganglion cell layer from 16--77 years, *The Anatomical Record*, 260, 124-131.

Harwerth, R.S., Carter-Dawson, L., Smith, E.L., Barnes, G., Holt, W.F., Crawford, M.L., 2004, Neural losses correlated with visual losses in clinical perimetry, *Investigative Ophthalmology & Visual Science*, 45, 3152-3160.

Harwerth, R.S., Vilupuru, A.S., Rangaswamy, N.V., Smith, E.L., 2007, The relationship between nerve fibre layer and perimetry measurements, *Investigative Ophthalmology & Visual Science*, 48, 763-773.

Harwerth, R.S., Wheat, J.L., Fredette, M.J., Anderson, D.R., 2010, Linking structure and function in glaucoma, *Progress in Retinal and Eye Research*, 29, 249-271.

Haymes, S.A., Leblanc, R.P., Nicolela, M.T., Chiasson, L.A., Chauhan, B.C., 2007, Risk of falls and motor vehicle collisions in glaucoma, *Investigative Ophthalmology & Visual Science*, 48, 1149-1155.

He, L., Yang, H., Gardiner, S.K., Williams, G., Hardin, C., Strouthidis, N.G., Fortune, B., Burgoyne, C.F., 2014, Longitudinal detection of optic nerve head changes by spectral domain optical coherence tomography in early experimental glaucoma, *Investigative Ophthalmology & Visual Science*, 55, 574-586.

Heijl, A., Bengtsson, B., Hyman, L., Leske, M.C., Early Manifest Glaucoma Trial Group, 2009, Natural history of open-angle glaucoma, *Ophthalmology*, 116, 2271-2276.

Heijl, A., Buchholz, P., Norrgren, G. & Bengtsson, B., 2013, Rates of visual field progression in clinical glaucoma care, *Acta Ophthalmologica*, 91, 406-412.

Heijl, A., Lindgren, G. & Olsson, J., 1987, Normal variability of static perimetric threshold values across the central visual field, *Archives of Ophthalmology*, 105, 1544-1549.

Hennis, A., Wu, S.-Y., Nemesure, B., Honkanen, R., Leske, M.C., 2007, Awareness of incident open-angle glaucoma in a population study: the Barbados Eye Studies, *Ophthalmology*, 114, 1816-1821.

Henson, D.B., Artes, P.H., Chauhan, B.C., 1999, Diffuse loss of sensitivity in early glaucoma, *Investigative Ophthalmology & Visual Science*, 40, 3147-3151.

Hood, D.C., Kardon, R.H., 2007, A framework for comparing structural and functional measures of glaucomatous damage, *Progress in Retinal and Eye research*, 26, 688-710.

Hood, D.C., Greenstein, V.C., Odel, J.G., Zhang, X., Ritch, R., Liebmann, J.M., Hong, J.E., Chen, C.S., Thienprasiddhi, P., 2002, Visual field defects and multifocal visual evoked potentials: evidence of a linear relationship, *Archives of Ophthalmology*, 120, 1672-1681.

Hood, D.C., Raza, A.S., de Moraes, C.G., Liebmann, J.M., Ritch, R., 2013, Glaucomatous damage of the macula, *Progress in Retinal and Eye Research*, 32, 1-21.

Horn, F.K., Tornow, R.P., Jünemann, A.G., Laemmer, R., Kremers, J., 2014, Perimetric measurements with flicker-defined form stimulation in comparison with

conventional perimetry and retinal nerve fibre measurements, *Investigative Ophthalmology & Visual Science*, 55, 2317-2323.

Horn, F.K., Wakili, N., Jünemann, A.M. & Korth, M., 2002, Testing for glaucoma with frequency-doubling perimetry in normals, ocular hypertensives, and glaucoma patients, *Graefe's Archive for Clinical and Experimental Ophthalmology,* 240, 658-665.

Huang, D., Swanson, E.A., Lin, C.P., Schuman, J.S., Stinson, W.G., Chang, W., Hee, M.R., Flottee, T., Gregory, K., Puliafito, C.A., et al. 1991, Optical coherence tomography, *Science,* 254, 1178-1181.

Hultsch, D.F., MacDonald, S.W., Dixon, R.A., 2002, Variability in reaction time performance of younger and older adults, *The Journals of Gerontology Series B: Psychological Sciences and Social Sciences*, 57, 101-115.

Jampel, H.D., Friedman, D., Quigley, H., Vitale, S., Miller, R., Knezevich, F. & Ding, Y., 2009, Agreement among glaucoma specialists in assessing progressive disc changes from photographs in open-angle glaucoma patients, *American Journal of Ophthalmology*, 147, 39-44.

Johnson, C.A., Samuels, S.J., 1997, Screening for glaucomatous visual field loss with frequency-doubling perimetry, *Investigative Ophthalmology & Visual Science*, 38, 413-425.

Johnson, C.A., Adams, A.J., Casson, E.J., Brandt, J.D., 1993, Progression of early glaucomatous visual field loss as detected by blue-on-yellow and standard white-on-white automated perimetry, *Archives of Ophthalmology*, 111, 651-656.

Johnson, L.N., Hill, R.A., Bartholomew, M.J., 1988, Correlation of afferent pupillary defect with visual field loss on automated perimetry, *Ophthalmology*, 95, 1649-1655.

Jonas, J.B., Schiro, D., 1994a, Localised wedge shaped defects of the retinal nerve fibre layer in glaucoma, *The British Journal of Ophthalmology*, 78, 285-290.

Jonas, J.B., Schiro, D., 1994b, Localized retinal nerve fibre layer defects in nonglaucomatous optic nerve atrophy, *Graefe's Archive for Clinical and Experimental Ophthalmology*, 232, 759-60.

Jonas, J.B., Budde, W.M., Panda-Jonas, S., 1999, Ophthalmoscopic evaluation of the optic nerve head, *Survey of Ophthalmology*, 43, 293-320.

Jonas, J.B., Nguyen, N.X., Naumann, G.O., 1989, The retinal nerve fibre layer in normal eyes, *Ophthalmology*, 96, 627-632.

Jonas, J.B., Zäch, F.M., Naumann, G.O., 1990, Quantitative pupillometry of relative afferent defects in glaucoma, *Archives of Ophthalmology*, 108, 479-480.

Kankipati, L., Girkin, C.A., Gamlin, P.D., 2011, The post-illumination pupil response is reduced in glaucoma patients, *Investigative Ophthalmology & Visual Science*, 52, 2287-2292.

Kass, M.A., Heuer, D.K., Higginbotham, E.J., Johnson, C.A., Keltner, J.L., Miller, J.P., Parrish, I.I., Richard, K., Wilson, M.R., Gordon, M.O., 2002, The Ocular Hypertension Treatment Study: a randomized trial determines that topical ocular hypotensive medication delays or prevents the onset of primary open-angle glaucoma, *Archives of ophthalmology*, 120, 701-713.

Kawasaki, A., Kardon, R.H., 2007, Intrinsically photosensitive retinal ganglion cells, *Journal of Neuro-ophthalmology*, 27, 195-204.

Kerrigan-Baumrind, L.A., Quigley, H.A., Pease, M.E., Kerrigan, D.F., Mitchell, R.S., 2000, Number of ganglion cells in glaucoma eyes compared with threshold visual field tests in the same persons, *Investigative Ophthalmology & Visual Science*, 41, 741-748.

Kerrison, J.B., Buchanan, K., Rosenberg, M.L., Clark, R., Andreason, K., Alfaro, D.V., Grossniklaus, H.E., Kerrigan-Baumrind, L.A., Kerrigan, D.F., Miller, N.R., Quigley, H.A., 2001, Quantification of optic nerve axon loss associated with a relative afferent pupillary defect in the monkey, *Archives of Ophthalmology*, 119, 1333-1341.

Klauer, S.G., Dingus, T.A., Neale, V.L., Sudweeks, J.D., Ramsey, D.J., 2006, *The impact of driver inattention on near-crash/crash risk: An analysis using the 100-car naturalistic driving study data*. US Department of Transportation, National Highway Traffic Safety Administration, Springfield, Virginia, DOT HA 810 595.

Lagrèze, W.D., Kardon, R.H., 1998, Correlation of relative afferent pupillary defect and estimated retinal ganglion cell loss, *Graefe's Archive for Clinical and Experimental Ophthalmology*, 236, 401-404.

Lalezary, M., Medeiros, F.A., Weinreb, R.N., Bowd, C., Sample, P.A., Tavares, I.M., Tafreshi, A., Zangwill, L.M., 2006, Baseline optical coherence tomography predicts the development of glaucomatous change in glaucoma suspects, *American Journal of Ophthalmology*, 142, 576-582.

Lamparter, J., Russell, R.A., Schulze, A., Schuff, A.C., Pfeiffer, N., Hoffmann, E.M., 2012, Structure-function relationship between FDF, FDT, SAP, and scanning laser ophthalmoscopy in glaucoma patients, *Investigative Ophthalmology & Visual Science*, 53, 7553-9.

Landers, J.A., Goldberg, I., Graham, S.L., 2003, Detection of early visual field loss in glaucoma using frequency-doubling perimetry and short-wavelength automated perimetry, *Archives of Ophthalmology*, 121, 1705-1710.

Lankaranian, D., Altangerel, U., Spaeth, G.L., Leavitt, J.A., Steinmann, W.C., 2005, The usefulness of a new method of testing for a relative afferent pupillary defect in patients with ocular hypertension and glaucoma, *Transactions of the American Ophthalmological Society*, 103, 200-207.

Lee, A.J., Wang, J.J., Rochtchina, E., Healey, P., Chia, E., M., Mitchell, P., 2003, Patterns of glaucomatous visual field defects in an older population: the Blue Mountains Eye Study, *Clinical & Experimental Ophthalmology*, 31, 331-335.

Leite, M.T., Zangwill, L.M., Weinreb, R.N., Rao, H.L., Alencar, L.M., Sample, P.A., Medeiros, F.A., 2010, Effect of disease severity on the performance of Cirrus spectral-domain OCT for glaucoma diagnosis, *Investigative Ophthalmology & Visual Science*, 51, 4104-4109.

Leske, M.C., Heijl, A., Hyman, L., Bengtsson, B., 1999, Early Manifest Glaucoma Trial: design and baseline data, *Ophthalmology*, 106, 2144-2153.

Leung, C.K., Cheung, C.Y., Weinreb, R.N., Qiu, K., Liu, S., Li, H., Xu, G., Fan, N., Pang, C.P., Tse, K.K., Lam, D.S., 2010, Evaluation of retinal nerve fibre layer

progression in glaucoma: a study on optical coherence tomography guided progression analysis, *Investigative Ophthalmology & Visual Science*, 51, 217-222.

Leung, C.K., Cheung, C.Y., Weinreb, R.N., Qiu, Q., Liu, S., Li, H., Xu, G., Fan, N., Huang, L., Pang, C.P., Lam, D.S., 2009, Retinal nerve fibre layer imaging with spectral-domain optical coherence tomography: a variability and diagnostic performance study, *Ophthalmology*, 116, 1257-1263.

Leung, C.K., Chiu, V., Weinreb, R.N., Liu, S., Ye, C., Yu, M., Cheung, C.Y., Lai, G., Lam, D.S., 2011, Evaluation of retinal nerve fibre layer progression in glaucoma: a comparison between spectral-domain and time-domain optical coherence tomography, *Ophthalmology*, 118, 1558-1562.

Leung, C.K., Ye, C., Weinreb, R.N., Yu, M., Lai, G., Lam, D.S., 2013, Impact of age-related change of retinal nerve fibre layer and macular thicknesses on evaluation of glaucoma progression, *Ophthalmology*, 120, 2485-2492.

Leung, C.K., Yu, M., Weinreb, R.N., Ye, C., Liu, S., Lai, G., Lam, D.S., 2012, Retinal nerve fibre layer imaging with spectral-domain optical coherence tomography: a prospective analysis of age-related loss, *Ophthalmology*, 119, 731-737.

Leung, C.K.S., 2014, Diagnosing glaucoma progression with optical coherence tomography, *Current Opinion in Ophthalmology*, 25, 104-111.

Levatin, P., 1959, Pupillary escape in disease of the retina or optic nerve, *Archives of Ophthalmology*, 62, 768-779.

Levine, R.A., Demirel, S., Fan, J., Keltner, J.L., Johnson, C.A., Kass, M.A., Ocular Hypertension Treatment Study Group, 2006, Asymmetries and visual field summaries as predictors of glaucoma in the ocular hypertension treatment study, *Investigative Ophthalmology & Visual Science*, 47, 3896-3903.

Lisboa, R., Leite, M.T., Zangwill, L.M., Tafreshi, A., Weinreb, R.N., Medeiros, F.A., 2012, Diagnosing preperimetric glaucoma with spectral domain optical coherence tomography, *Ophthalmology*, 119, 2261-2269.

Lisboa, R., Weinreb, R.N., Medeiros, F.A., 2013, Combining structure and function to evaluate glaucomatous progression: implications for the design of clinical trials, *Current Opinion in Pharmacology*, 13, 115-122.

Liu, S., Lam, S., Weinreb, R.N., Ye, C., Cheung, C.Y., Lai, G., Lam, D.S., Leung, C.K., 2011, Comparison of standard automated perimetry, frequency-doubling technology perimetry, and short-wavelength automated perimetry for detection of glaucoma, *Investigative Ophthalmology & Visual Science*, 52, 7325-7331.

Malik, R., Swanson, W.H., Garway-Heath, D.F., 2006, Development and evaluation of a linear staircase strategy for the measurement of perimetric sensitivity, *Vision Research*, 46, 2956-2967.

Malik, R., Swanson, W.H., Garway-Heath, D.F., 2012, 'Structure-function relationship' in glaucoma: past thinking and current concepts, *Clinical & Experimental Ophthalmology*, 40, 369-380.

Marín-Franch, I., Malik, R., Crabb, D.P., Swanson, W.H., 2013, Choice of statistical method influences apparent association between structure and function in glaucoma, *Investigative Ophthalmology & Visual Science*, 54, 4189-96.

Marottoli, R.A., Mendes de Leon, C.F., Glass, T.A., Williams, C.S., Cooney, L.M., Berkman, L.F., Tinetti, M.E., 1997, Driving cessation and increased depressive symptoms: prospective evidence from the New Haven EPESE. Established Populations for Epidemiologic Studies of the Elderly, *Journal of the American Geriatrics Society*, 45, 202-6.

Marsden, G., McDonald, M., Brackstone, M., 2001, Towards an understanding of adaptive cruise control, *Transportation Research Part C: Emerging Technologies*, 9, 33-51.

McGwin, G., Xie, A., Mays, A., Joiner, W., DeCarlo, D.K., Hall, T.A., Owsley, C., 2005, Visual field defects and the risk of motor vehicle collisions among patients with glaucoma, *Investigative Ophthalmology & Visual Science*, 46, 4437-41.

McKean-Cowdin, R., Varma, R., Wu, J., Hays, R.D., Azen, S.P., Los Angeles Latino Eye Study Group, 2007, Severity of visual field loss and health-related quality of life, *American Journal of Ophthalmology*, 143, 1013-23.

Medeiros, F.A., Alencar, L.M., Zangwill, L.M., Bowd, C., Sample, P.A., Weinreb, R.N., 2009, Prediction of functional loss in glaucoma from progressive optic disc damage, *Archives of Ophthalmology*, 127, 1250-6.

Medeiros, F.A., Lisboa, R., Weinreb, R.N., Girkin, C.A., Liebmann, J.M., Zangwill, L.M., 2012, A combined index of structure and function for staging glaucomatous damage, *Archives of Ophthalmology*, 130, 1107-1116.

Medeiros, F.A., Lisboa, R., Zangwill, L.M., Liebmann, J.M., Girkin, C.A., Bowd, C., Weinreb, R.N., 2013, Evaluation of progressive neuroretinal rim loss as a surrogate end-point for development of visual field loss in glaucoma, *Ophthalmology*, 121, 100-109.

Medeiros, F.A., Sample, P.A., Zangwill, L.M., Liebmann, J.M., Girkin, C.A., Weinreb, R.N., 2006, A statistical approach to the evaluation of covariate effects on the receiver operating characteristic curves of diagnostic tests in glaucoma, *Investigative Ophthalmology & Visual Science*, 47, 2520-2527.

Medeiros, F.A., Vizzeri, G., Zangwill, L.M., Alencar, L.M., Sample, P.A., Weinreb, R.N., 2008, Comparison of retinal nerve fibre layer and optic disc imaging for diagnosing glaucoma in patients suspected of having the disease, *Ophthalmology*, 115, 1340-1346.

Medeiros, F.A., Weinreb, R.N., R Boer, E., Rosen, P.N., 2012, Driving simulation as a performance-based test of visual impairment in glaucoma, *Journal of Glaucoma*, 21, 221-227.

Medeiros, F.A., Zangwill, L.M., Alencar, L.M., Bowd, C., Sample, P.A., Susanna, R., Weinreb, R.N., 2009, Detection of glaucoma progression with stratus OCT retinal nerve fibre layer, optic nerve head, and macular thickness measurements, *Investigative Ophthalmology & Visual Science*, 50, 5741-5748.

Medeiros, F.A., Zangwill, L.M., Bowd, C., Weinreb, R.N., 2004, Comparison of the GDx VCC scanning laser polarimeter, HRT II confocal scanning laser ophthalmoscope, and stratus OCT optical coherence tomograph for the detection of glaucoma, *Archives of Ophthalmology*, 122, 827-837.

Medeiros, F.A., Zangwill, L.M., Bowd, C., Mansouri, K., Weinreb, R.N., 2012, The structure and function relationship in glaucoma: implications for detection of progression and measurement of rates of change, *Investigative Ophthalmology & Visual Science*, 53, 6939-6946.

Medeiros, F.A., Zangwill, L.M., Bowd, C., Vessani, R.M., Susanna, R. & Weinreb, R.N., 2005, Evaluation of retinal nerve fibre layer, optic nerve head, and macular thickness measurements for glaucoma detection using optical coherence tomography, *American Journal of Ophthalmology*, 139, 44-55.

Medeiros, F.A., Tatham, A.J., 2016. Structure versus Function: the debate that doesn't need to be, Ophthalmology, 2016, 123, 1170-1172.

Miki, A., Medeiros, F.A., Weinreb, R.N., Jain, S., He, F., Sharpsten, L., Khachatryan, N., Hammel, N., Liebmann, J.M., Girkin, C.A., Sample, P.A., Zangwill, L.M., 2014, Rates of retinal nerve fibre layer thinning in glaucoma suspect eyes, *Ophthalmology*, 121, 1350-8.

Morgan, J.E., 2002, Retinal ganglion cell shrinkage in glaucoma, *Journal of Glaucoma*, 11, 365-70.

Mulak, M., Szumny, D., Sieja-Bujewska, A., Kubrak, M., 2012, Heidelberg edge perimeter employment in glaucoma diagnosis--preliminary report, *Advances in Clinical and Experimental Medicine*, 21, 665-670.

Mwanza, J.C., Chang, R.T., Budenz, D.L., Durbin, M.K., Gendy, M.G., Shi, W., Feuer, W.J., 2010, Reproducibility of peripapillary retinal nerve fibre layer thickness and optic nerve head parameters measured with cirrus HD-OCT in glaucomatous eyes, *Investigative Ophthalmology & Visual Science*, 51, 5724-5730.

Mwanza, J.C., Durbin, M.K., Budenz, D.L., Sayyad, F.E., Chang, R.T., Neelakantan, A., Godfrey, D.G., Carter, R. & Crandall, A.S., 2012, Glaucoma diagnostic accuracy of ganglion cell-inner plexiform layer thickness: comparison with nerve fibre layer and optic nerve head, *Ophthalmology*, 119, 1151-1158.

Nasreddine, Z.S., Phillips, N.A., Bédirian, V., Charbonneau, S., Whitehead, V., Collin, I., Cummings, J.L., Chertkow, H., 2005, The Montreal Cognitive Assessment, MoCA: a brief screening tool for mild cognitive impairment, *Journal of the American Geriatrics Society*, 53, 695-699.

Nelson-Quigg, J.M., Cello, K., Johnson, C.A., 2000, Predicting binocular visual field sensitivity from monocular visual field results, *Investigative Ophthalmology & Visual Science*, 41, 2212-21.

National institute for Health and Clinical Excellence (NICE), Glaucoma: diagnosis and management, 2009.

O'Leary, N., Chauhan, B.C., Artes, P.H., 2012, Visual field progression in glaucoma: estimating the overall significance of deterioration with permutation analyses of pointwise linear regression (PoPLR), *Investigative Ophthalmology & Visual Science*, 53, 6776-6784.

Ong, L.S., Mitchell, P., Healey, P.R., Cumming, R.G., 1999, Asymmetry in optic disc parameters: The Blue Mountains Eye Study, *Investigative Ophthalmology & Visual Science*, 40, 849-857.

Owsley, C., McGwin, G., 2010, Vision and driving, *Vision Research*, 50, 2348-2361.

Owsley, C., Ball, K., McGwin, G., Sloane, M.E., Roenker, D.L., White, M.F. & Overley, E.T., 1998, Visual processing impairment and risk of motor vehicle crash among older adults, *JAMA,* 279, 1083-1088.

Park, S.B., Sung, K.R., Kang, S.Y., Kim, K.R., Kook, M.S., 2009, Comparison of glaucoma diagnostic Capabilities of Cirrus HD and Stratus optical coherence tomography, *Archives of Ophthalmology*, 127, 1603-1609.

Pathak, M., Demirel, S. & Gardiner, S.K., 2013, Nonlinear, multilevel mixed-effects approach for modeling longitudinal standard automated perimetry data in glaucoma, *Investigative Ophthalmology & Visual Science*, 54, 5505-5513.

Pirenne, M.H., 1943, Binocular and uniocular threshold of vision, *Nature*, 152, 698-699.

Quigley, H.A., 1986, Examination of the retinal nerve fibre layer in the recognition of early glaucoma damage, *Transactions of the American Ophthalmological Society*, 84, 920-966.

Quigley, H.A., 1998, Identification of glaucoma-related visual field abnormality with the screening protocol of frequency doubling technology, *American Journal of Ophthalmology*, 125, 819-829.

Quigley, H.A., Addicks, E.M., 1982, Quantitative studies of retinal nerve fibre layer defects, *Archives of Ophthalmology*, 100, 807-814.

Quigley, H.A., Broman, A.T., 2006, The number of people with glaucoma worldwide in 2010 and 2020, *The British Journal of Ophthalmology*, 90, 262-267.

Quigley, H.A., Sommer, A., 1987, How to use nerve fibre layer examination in the management of glaucoma, *Transactions of the American Ophthalmological Society*, 85, 254-272.

Quigley, H.A., Dunkelberger, G.R., Green, W.R., 1989, Retinal ganglion cell atrophy correlated with automated perimetry in human eyes with glaucoma, *American Journal of Ophthalmology*, 107, 453-464.

Racette, L., Medeiros, F.A., Zangwill, L.M., Ng, D., Weinreb, R.N., Sample, P.A., 2008, Diagnostic accuracy of the Matrix 24-2 and original N-30 frequency-doubling technology tests compared with standard automated perimetry, *Investigative Ophthalmology & Visual Science*, 49, 954-960.

Radius, R.L., Anderson, D.R., 1979, The histology of retinal nerve fibre layer bundles and bundle defects, *Archives of Ophthalmology*, 97, 948-950.

Ragland, D.R., Satariano, W.A., MacLeod, K.E., 2005, Driving cessation and increased depressive symptoms, *The Journals of Gerontology Series A: Biological Sciences and Medical Sciences*, 60, 399-403.

Rao, H.L., Leite, M.T., Weinreb, R.N., Zangwill, L.M., Alencar, L.M., Sample, P.A., Medeiros, F.A., 2011, Effect of disease severity and optic disc size on diagnostic accuracy of RTVue spectral domain optical coherence tomograph in glaucoma, *Investigative Ophthalmology & Visual Science*, 52, 1290-1296.

Realini, T., Zangwill, L.M., Flanagan, J.G., Garway-Heath, D., Patella, V.M., Johnson, C.A., Artes, P.H., Gaddie, I.B., Fingeret, M., 2014, Normative Databases for Imaging Instrumentation, *Journal of Glaucoma*, 24, 480-483.

Redmond, T., Anderson, R.S., Russell, R.A., Garway-Heath, D.F., 2013, Relating retinal nerve fibre layer thickness and functional estimates of ganglion cell sampling density in healthy eyes and in early glaucoma, *Investigative Ophthalmology & Visual Science*, 54, 2153-2162.

Redmond, T., Zlatkova, M.B., Garway-Heath, D.F., Anderson, R.S., 2010, The effect of age on the area of complete spatial summation for chromatic and achromatic stimuli, *Investigative Ophthalmology & Visual Science*, 51, 6533-6539.

Reus, N.J., Lemij, H.G., Garway-Heath, D.F., Airaksinen, P.J., Anton, A., Bron, A.M., Faschinger, C., Holló, G., Iester, M., Jonas, J.B., Mistlberger, A., Topouzis, F., Zeyen, T.G., 2010, Clinical assessment of stereoscopic optic disc photographs for glaucoma: the European Optic Disc Assessment Trial, *Ophthalmology*, 117, 717-723.

Richman, J., Lorenzana, L.L., Lankaranian, D., Dugar, J., Mayer, J.R., Wizov, S.S., Spaeth, G.L., 2010, Relationships in glaucoma patients between standard vision tests, quality of life, and ability to perform daily activities, *Ophthalmic Epidemiology*, 17, 144-151.

Rotchford, A.P., Kirwan, J.F., Muller, M.A., Johnson, G.J., Roux, P., 2003, Temba glaucoma study: a population-based cross-sectional survey in urban South Africa, *Ophthalmology*, 110, 376-382.

Rubin, G.S., Ng, E.S., Bandeen-Roche, K., Keyl, P.M., Freeman, E.E., West, S.K., 2007, A prospective, population-based study of the role of visual impairment in motor vehicle crashes among older drivers: the SEE study, *Investigative Ophthalmology & Visual Science*, 48, 1483-1491.

Russell, R.A., Malik, R., Chauhan, B.C., Crabb, D.P., Garway-Heath, D.F., 2012, Improved estimates of visual field progression using Bayesian linear regression to integrate structural information in patients with ocular hypertension, *Investigative Ophthalmology & Visual Science*, 53, 2760-2769.

Sample, P.A., Weinreb, R.N., 1990, Colour perimetry for assessment of primary open-angle glaucoma, *Investigative Ophthalmology & Visual Science*, 31, 1869-75.

Sample, P.A., Girkin, C.A., Zangwill, L.M., Jain, S., Racette, L., Becerra, L.M., Weinreb, R.N., Medeiros, F.A., Wilson, M.R., De León-Ortega, J., Tello, C., Bowd, C., Liebmann, J.M., African Descent and Glaucoma Evaluation Study Group, 2009, The African Descent and Glaucoma Evaluation Study (ADAGES): design and baseline data, *Archives of Ophthalmology*, 127, 1136-1145.

Sample, P.A., Medeiros, F.A., Racette, L., Pascual, J.P., Boden, C., Zangwill, L.M., Bowd, C., Weinreb, R.N., 2006, Identifying glaucomatous vision loss with visual-function--specific perimetry in the diagnostic innovations in glaucoma study, *Investigative Ophthalmology & Visual Science*, 47, 3381-3389.

Sarezky, D., Krupin, T., Cohen, A., Stewart, C.W., Volpe, N.J., Tanna, A.P., 2014, Correlation between intereye difference in visual field mean deviation values and relative afferent pupillary response as measured by an automated pupillometer in subjects with glaucoma, *Journal of Glaucoma*, 23, 419-423.

Saunders, L.J., Russell, R.A. & Crabb, D.P., 2012, Practical landmarks for visual field disability in glaucoma, *The British Journal of Ophthalmology*, 96, 1185-1189.

Saunders, L.J., Russell, R.A., Kirwan, J.F., McNaught, A.I., Crabb, D.P., 2014, Examining visual field loss in patients in glaucoma clinics during their predicted remaining lifetime, *Investigative Ophthalmology & Visual Science*, 55, 102-109.

Shabana, N., Cornilleau Pérès, V., Carkeet, A., Chew, P.T., 2003, Motion perception in glaucoma patients: a review, *Survey of Ophthalmology*, 48, 92-106.

Skorkovská, K., Wilhelm, H., Lüdtke, H., Wilhelm, B., 2011, [Relative afferent pupillary defect in glaucoma], *Klinische Monatsblätter für Augenheilkunde*, 228, 979-983.

Sommer, A., Katz, J., Quigley, H.A., Miller, N.R., Robin, A.L., Richter, R.C., Witt, K.A., 1991, Clinically detectable nerve fibre atrophy precedes the onset of glaucomatous field loss, *Archives of Ophthalmology*, 109, 77-83.

Sommer, A., Miller, N.R., Pollack, I., Maumenee, A.E., George, T., 1977, The nerve fibre layer in the diagnosis of glaucoma, *Archives of Ophthalmology*, 95, 2149-2156.

Spry, P.G., Hussin, H.M. & Sparrow, J.M., 2005, Clinical evaluation of frequency doubling technology perimetry using the Humphrey Matrix 24-2 threshold strategy, *The British Journal of Ophthalmology*, 89, 1031-1035.

Strouthidis, N.G., Gardiner, S.K., Owen, V.M., Zuniga, C., Garway-Heath, D.F., 2010, Predicting progression to glaucoma in ocular hypertensive patients, *Journal of Glaucoma*, 19, 304-309.

Strouthidis, N.G., Scott, A., Peter, N.M., Garway-Heath, D.F., 2006, Optic disc and visual field progression in ocular hypertensive subjects: detection rates, specificity, and agreement, *Investigative Ophthalmology & Visual Science*, 47, 2904-2910.

Sullivan-Mee, M., Ruegg, C.C., Pensyl, D., Halverson, K., Qualls, C., 2013, Diagnostic precision of retinal nerve fibre layer and macular thickness asymmetry parameters for identifying early primary open-angle glaucoma, *American Journal of Ophthalmology*, 156, 567-577.

Sung, K.R., Na, J.H., Lee, Y., 2012, Glaucoma diagnostic capabilities of optic nerve head parameters as determined by Cirrus HD optical coherence tomography, *Journal of Glaucoma*, 21, 498-504.

Swanson, W.H., Horner, D.G., 2015, Assessing assumptions of a combined structure-function index, *Ophthalmic & Physiological Optics,* 35, 186-193.

Swanson, W.H., Felius, J., Pan, F., 2004, Perimetric defects and ganglion cell damage: interpreting linear relations using a two-stage neural model, *Investigative Ophthalmology & Visual Science*, 45, 466-472.

Tafreshi, A., Sample, P.A., Liebmann, J.M., Girkin, C.A., Zangwill, L.M., Weinreb, R.N., Lalezary, M., Racette, L., 2009, Visual function-specific perimetry to identify glaucomatous visual loss using three different definitions of visual field abnormality, *Investigative Ophthalmology & Visual Science*, 50, 1234-1240.

Tan, O., Chopra, V., Lu, A.T., Schuman, J.S., Ishikawa, H., Wollstein, G., Varma, R., Huang, D., 2009, Detection of macular ganglion cell loss in glaucoma by Fourier-domain optical coherence tomography, *Ophthalmology*, 116, 2305-2314.

Tanabe, S., Yuki, K., Ozeki, N., Shiba, D., Abe, T., Kouyama, K., Tsubota, K., 2011, The association between primary open-angle glaucoma and motor vehicle collisions, *Investigative Ophthalmology & Visual Science*, 52, 4177-4181.

Tatham, A.J., Boer, E.R., Rosen, P.N., Della Penna, M., Meira-Freitas, D., Weinreb, R.N., Zangwill, L.M., Medeiros, F.A., 2014a, Glaucomatous retinal nerve fibre layer thickness loss is associated with slower reaction times under a divided attention task, *American Journal of Ophthalmology*, 158, 1008-1017.

Tatham, A.J., Meira-Freitas, D., Weinreb, R.N., Marvasti, A.H., Zangwill, L.M., Medeiros, F.A., 2014b, Estimation of retinal ganglion cell loss in glaucomatous eyes with a relative afferent pupillary defect, *Investigative Ophthalmology & Visual Science*, 55, 513-522.

Tatham, A.J., Weinreb, R.N., Zangwill, L.M., Liebmann, J.M., Girkin, C.A., Medeiros, F.A., 2013, Estimated retinal ganglion cell counts in glaucomatous eyes with localized retinal nerve fibre layer defects, *American Journal of Ophthalmology*, 156, 578-587.

Tatsumi, Y., Nakamura, M., Fujioka, M., Nakanishi, Y., Kusuhara, A., Maeda, H. Negi, A., 2007, Quantification of retinal nerve fibre layer thickness reduction associated with a relative afferent pupillary defect in asymmetric glaucoma, *The British Journal of Ophthalmology*, 91, 633-637.

Thompson, H.S., Corbett, J.J., Cox, T.A., 1981, How to measure the relative afferent pupillary defect, *Survey of Ophthalmology*, 26, 39-42.

Thompson, H.S., Montague, P., Cox, T.A., Corbett, J.J., 1982, The relationship between visual acuity, pupillary defect, and visual field loss, *American Journal of Ophthalmology*, 93, 681-688.

van Gestel, A., Webers, C.A., Beckers, H.J., van Dongen, M.C., Severens, J.L., Hendrikse, F., Schouten, J.S., 2010, The relationship between visual field loss in glaucoma and health-related quality-of-life, *Eye*, 24, 1759-1769.

Viswanathan, A.C., Crabb, D.P., McNaught, A.I., Westcott, M.C., Kamal, D., Garway-Heath, D.F., Fitzke, F.W., Hitchings, R.A., 2003, Interobserver agreement on visual field progression in glaucoma: a comparison of methods, *The British Journal of Ophthalmology*, 87, 726-730.

Viswanathan, A.C., Fitzke, F.W. & Hitchings, R.A., 1997, Early detection of visual field progression in glaucoma: a comparison of PROGRESSOR and STATPAC 2, *The British Journal of Ophthalmology*, 81, 1037-1042.

Wang, L., Dong, J., Cull, G., Fortune, B., Cioffi, G.A., 2003, Varicosities of intraretinal ganglion cell axons in human and nonhuman primates, *Investigative Ophthalmology & Visual Science*, 44, 2-9.

Weber, J., Dannheim, F. & Dannheim, D., 1990, The topographical relationship between optic disc and visual field in glaucoma, *Acta ophthalmologica*, 68, 568-574.

Weinreb, R.N., Aung, T., Medeiros, F.A., 2014, The pathophysiology and treatment of glaucoma: a review, *JAMA*, 311, 1901-1911.

White, A.J., Sun, H., Swanson, W.H., Lee, B.B., 2002, An examination of physiological mechanisms underlying the frequency-doubling illusion, *Investigative Ophthalmology & Visual Science*, 43, 3590-3599.

Wilhelm, H. & Wilhelm, B., 2003, Clinical applications of pupillography, *Journal of Neuro-ophthalmology*, 23, 42-49.

Wilhelm, H., Peters, T., Lüdtke, H., Wilhelm, B., 2007, The prevalence of relative afferent pupillary defects in normal subjects, *Journal of Neuro-ophthalmology*, 27, 263-267.

Williams, A.L., Gatla, S., Leiby, B.E., Fahmy, I., Biswas, A., de Barros, D.M., Ramakrishnan, R., Bhardwaj, S., Wright, C., Dubey, S., Lynch, J.F., Bayer, A., Khandelwal, R., Ichhpujani, P., Gheith, M., Siam, G., Feldman, R.M., Henderer,

J.D., Spaeth, G.L., 2013, The value of intraocular pressure asymmetry in diagnosing glaucoma, *Journal of Glaucoma*, 22, 215-218.

Wirtschafter, J.D., Becker, W.L., Howe, J.B., Younge, B.R., 1982, Glaucoma visual field analysis by computed profile of nerve fibre function in optic disc sectors, *Ophthalmology*, 89, 255-267.

Wollstein, G., Garway-Heath, D.F., Hitchings, R.A., 1998, Identification of early glaucoma cases with the scanning laser ophthalmoscope, *Ophthalmology*, 105, 1557-1563.

Wollstein, G., Garway-Heath, D.F., Fontana, L., Hitchings, R.A., 2000, Identifying early glaucomatous changes. Comparison between expert clinical assessment of optic disc photographs and confocal scanning ophthalmoscopy, *Ophthalmology*, 107, 2272-2277.

Wollstein, G., Schuman, J.S., Price, L.L., Aydin, A., Stark, P.C., Hertzmark, E., Lai, E., Ishikawa, H., Mattox, C., Fujimoto, J.G., 2005, Optical coherence tomography longitudinal evaluation of retinal nerve fibre layer thickness in glaucoma, *Archives of Ophthalmology*, 123, 464-470.

Wood, J.M., Black, A.A., Mallon, K., Thomas, R., Owsley, C., 2016, Glaucoma and Driving: On-Road Driving Characteristics, *PloS one*, 11, e0158318.

Xu, J., Ishikawa, H., Wollstein, G., Bilonick, R.A., Folio, L.S., Nadler, Z., Kagemann, L., Schuman, J.S., 2013, Three-dimensional spectral-domain optical coherence tomography data analysis for glaucoma detection, *PloS one*, 8, e55476.

Yamagishi, N., Anton, A., Sample, P.A., Zangwill, L., Lopez, A., Weinreb, R.N., 1997, Mapping structural damage of the optic disk to visual field defect in glaucoma, *American Journal of Ophthalmology*, 123, 667-676.

Yücel, Y.H., Zhang, Q., Weinreb, R.N., Kaufman, P.L. & Gupta, N., 2003, Effects of retinal ganglion cell loss on magno-, parvo-, koniocellular pathways in the lateral geniculate nucleus and visual cortex in glaucoma, *Progress in Retinal and Eye Research*, 22, 465-481.

Zangwill, L.M., Bowd, C., Berry, C.C., Williams, J., Blumenthal, E.Z., Sánchez-Galeana, C.A., Vasile, C., Weinreb, R.N., 2001, Discriminating between normal and glaucomatous eyes using the Heidelberg retina tomograph, GDx nerve fibre analyzer, and optical coherence tomograph, *Archives of Ophthalmology*, 119, 985-993.

Zangwill, L.M., Weinreb, R.N., Beiser, J.A., Berry, C.C., Cioffi, G.A., Coleman, A.L., Trick, G., Liebmann, J.M., Brandt, J.D., Piltz-Seymour, J.R., Dirkes, K.A., Vega, S., Kass, M.A., Gordon, M.O., 2005, Baseline topographic optic disc measurements are associated with the development of primary open-angle glaucoma: The Confocal Scanning Laser Ophthalmoscopy Ancillary Study to the Ocular Hypertension Treatment Study, *Archives of Ophthalmology*, 123, 1188-1197.

Zhu, H., Crabb, D.P., Ho, T., Garway-Heath, D.F., 2015, More Accurate Modeling of Visual Field Progression in Glaucoma: ANSWERS, *Investigative Ophthalmology & Visual Science*, 56, 6077-6083.

Zhu, H., Crabb, D.P., Schlottmann, P.G., Lemij, H.G., Reus, N.J., Healey, P.R., Mitchell, P., Ho, T., Garway-Heath, D.F., 2010, Predicting visual function from the measurements of retinal nerve fibre layer structure, *Investigative Ophthalmology & Visual Science*, 51, 5657-5666.

Zhu, H., Russell, R.A., Saunders, L.J., Ceccon, S., Garway-Heath, D.F., Crabb, D.P., 2014, Detecting changes in retinal function: Analysis with Non-Stationary Weibull Error Regression and Spatial enhancement (ANSWERS), *PloS one*, 9, e85654.